

Clearing Things Up: A Vertical Mucus Clearance Assay to Investigate Rheological and Biochemical Parameters Governing Mucociliary Clearance.

Jerome Carpenter

A dissertation submitted to the faculty of the University of North Carolina at Chapel Hill in partial fulfillment of the requirements for the degree of Doctor of Philosophy in the Curriculum in Applied Sciences and Engineering.

Chapel Hill
2013

Approved by

Richard Superfine

Al Banes

Greg Forrest

Scott Randell

Sean Washburn

© 2013
Jerome Carpenter
All Rights Reserved

ABSTRACT

JEROME CARPENTER: Clearing Things Up: A Vertical Mucus Clearance Assay to Investigate Rheological and Biochemical Parameters Governing Mucociliary Clearance.
(Under the direction of Richard Superfine)

Mucociliary clearance (MCC) plays an essential role to protect the airways from pathogens and pollutants. Impaired MCC leads to a host of diseases and initiates a cascade of chronic infection, inflammation, and reduced lung function. Understanding the mechanisms of clearance is a critical step in preventing and ultimately treating disease. The fundamental mechanisms guiding clearance are still poorly understood. Existing models have focused on fluid rheology, but haven't reached a consensus on which parameters govern the system. In this work I build an *in vitro* model capable of evaluating rheological and biochemical parameters and their effect on clearance.

My model integrates the air-liquid interface (ALI) bronchial epithelial cell culture model with microfluidics to create a mucus clearance assay (MCA). Growing well-ciliated cells inside of a fluidics channel allows me to use external flow to investigate cilia-ASL interactions. I use external flow to build and validate a model of cilia hydrodynamics. Then I demonstrate external flow can be used as a force probe to investigate adhesion on the epithelial surface.

Next I integrate the MCA with a tilting microscope to explore the effects of gravity on mucociliary clearance. Gravity has been largely ignored in mucus clearance experiments despite vertical transport *in vivo* and therapies exploiting gravitational drainage. I observe fluids transporting horizontally, but failing to transport when the cilia driven flow is opposed by gravity. This establishes gravitational effects as a necessary requirement for evaluating the parameters that govern MCC. Next I tested a 4.5% 1MDa PEG solution that matched the apparent viscosity of mucus and observed that unlike mucus, the PEG solution didn't transport vertically. This experiment demonstrates that viscosity alone is not a predictor of vertical transport. Finally I suggest that the inability to transport vertically is a result of the system dehydrating and posit that mucus' ability to transport vertically is the result of biochemical adhesion with the cilia.

Acknowledgements

I would like to thank my advisor, Rich Superfine. Thanks for your guidance, your patience, but above all else teaching me how to be a scientist. I don't know how many times the light bulb has come on for me hours later, days, or even months later when I finally realized where you were steering me. Beyond teaching, thank you for creating such a great environment for science and the exchange of ideas. Your passion and enthusiasm for science is contagious. Also I think I probably still owe you a few bags of peanut M&Ms.

Sean thanks for the guidance and support that you've given me. It doesn't seem that long ago that I was a TA for your electronics lab. I'm pretty sure that I still use the fire hose approach to communicate. You've played a major role in my growth as a scientist. I learned so much in device meeting and while I still have a ways to go, I at least cringe when I look at the first few iterations of a plot or figure.

Thanks to others in NSRG. Tim thanks for you bio and microscopy expertise. Mike thanks for the guidance. Russ thanks for the amazing tools that enabled my project. Cassandra thank you for all of the POs, the emergency gas cylinders and supplies so that my cells would live another day. David thanks for being my mucus supplier.

To everyone at the UNC CF Tissue Procurement and Cell Culture Core, but especially Leslie, thank you! Thanks for not only teaching me how to do cell culture

with a tricky cell type, but also being there whenever there was a contamination scare or other cell related crisis.

Everyone else in the Physics department, again too many to name, but thanks Sallie, Jean, Bev and everyone else. Thanks to the machine shop for not only getting me through the shop class with all my digits intact, but helping to build and consult on several key pieces of equipment in my project. Thanks to the BME lab for access to the 3D printer and laser cutter: equipment which without I couldn't have built my system. Thanks to everyone in CHANL for all of the help with microscopy and fabrication.

To all of my fellow graduate students past and present thank you for making my time here amazing. Whether in Phillips Hall or the Chapman fishbowl it's been a great honor to work with so many wonderful people whose talent is only exceeded by their character. I hesitate in trying to name everyone (I have the dubious distinction of overlapping with the most students in the group), but I'm going to give it a shot. Thanks Adam H., Adam S., Ben, Briana, Kwan, Lamar, Nathan, Kris, Jeremy, Suzy, Rob, Luke, Nadira, Kellie, Ricky, Jay, Sreeja, Michael, Cory and Vinay. (I roughly tried alphabetical order, but that quickly fell apart.) I apologize for any omissions and could easily write a couple of pages thanking all of you specifically, but I'll save that for the academy speech, also I think I hear the orchestra beginning to play me off stage. Suzy thanks for helping to push me over the finish line. Also I couldn't have done it with your help along with Evan, John, Mike, Vishal and Schuyler.

Finally I would like to thank my parents. Mom and Dad thanks for, well everything. Thanks for nurturing curiosity, giving me support, and working so hard to give me opportunities. I don't say it enough and I'm not sure if it'd be possible to say it enough, but thank you. And yes mom, now I'm done.

Table of Contents

List of Figures	xiii
Abbreviations	xvi
Chapter 1 Introduction	1
1.1 Motivation	1
1.2 Thesis Statement and contributions	2
1.3 Outline for the document	4
Chapter 2 Mechanisms of Mucociliary Clearance	6
2.1 Lung physiology and airway defense	6
2.2 Epithelium	9
2.2.1 Cells of the epithelium	9
2.2.2 Epithelial Cross-Section	14
2.3 Cilia	16
2.3.1 Cilia Primer	17
2.3.2 Cilia Organization and Entrainment	19
2.3.3 Beyond Cilia: Cilium Surface and the PCL	24
2.4 Airway Surface Liquid	25
2.4.1 Mucins and Mucus	26
2.4.2 Properties of the Mucus Gel	33
2.4.3 Mucociliary Transport and Viscoelasticity	38
2.4.4 Fluid Regulation	40
2.4.5 Mucus and cilia adhesion	41

2.4.6 Other Forces acting on the ASL	42
2.5 Model Systems	43
2.5.1 Animal MCC studies	44
2.5.2 <i>In vitro</i> MCC studies	45
Chapter 3 Building the Mucus Clearance Assay	50
3.1 Design Considerations	50
3.1.1 Designing the chamber: Physiological Considerations.....	52
3.1.2 Cell perfusion rate to determine basolateral volume	59
3.1.3 Experimental Requirements	60
3.1.3.1 Controlling the Airway Surface Liquid.....	61
3.1.3.2 Optimizing optics: integrating the MCA with a microscope.....	62
3.2 Channel Fabrication and Assembly.....	65
3.2.1 Mold Fabrication	66
3.2.2 Channel Fabrication	67
3.3 Ciliated, transporting cultures in the Mucus Clearance Assay.....	70
3.3.1 Cells span the MCA chamber and can be patterned.....	70
3.3.2 MCAs differentiate and produce regions of long range transport.....	72
3.4 Conclusion	75
3.5 Methods	75
3.5.1 Channel Sterilization.....	75
3.5.2 Growing cells in the Clearance Assay	76
3.5.3 Cell viability and confluence	77
3.5.4 Measuring Ciliation	77
3.5.5 Measuring ASL flow with PIV	80
Chapter 4 Cilia and Fluid Flow: Building a model for the bilayer channel	82

4.1 Fluid Mechanics Primer	83
4.1.1 Navier-Stokes	83
4.1.2 Poiseuille flow	87
4.1.3 Couette Flow	88
4.1.4 Couette + Poiseuille Flow	89
4.2 Initial Channel Fluid Characterization (no external flow)	89
4.2.1 Lateral Heterogeneity of particle velocity due to variations in cilia diminish as a function of height	90
4.2.3 Channels take on a Couette-Poiseuille flow profile in the absence of external flow	92
4.3 External Flow	95
4.3.1 Syringe pump driven Poiseuille profile.	96
4.3.2 Verifying negligible CBF change with applied shear stresses	97
4.3.3 Couette + Poiseuille revisited with an external fluid flow	99
4.3.4 Future flow experiments	101
4.4 Adhesion Assay.....	102
4.4.1 Forces on the bead.....	103
4.4.2 Releasing the bead.....	108
4.4.3 WGA beads demonstrate stronger adhesion than PEG beads on an untreated epithelial surface	110
4.4.4 WGA beads demonstrate similar adhesion as PEG beads on an epithelium incubated with free WGA.....	112
4.4.5 Future Direction for the Adhesion Assay	115
4.5 Conclusions	117
4.6 Experimental Methods	117
4.6.1 Preparing channels for flow experiments	117
4.6.2 Performing experiments with an external fluid flow	119
4.6.3 Experiment to test CBF response to shear-stress	119

4.6.4 Modifying the chamber for adhesion assay experiments	120
4.6.5 Functionalizing beads with Wheat Germ Agglutinin and PEG.....	121
4.6.6 Performing the Adhesion Assay experiments.....	122
Chapter 5 Clearing against gravity	125
5.1 Gravity and Clearance.....	126
5.2 Tilting the clearance assays	127
5.2.1 Submerged Zone	129
5.2.2 Meniscal Zone	130
5.2.3 Air-Liquid Interface	131
5.3 Adding Drainage to the model	132
5.4 Vertical Air-Liquid Interface (VALI) transport	138
5.4.1 Mucus Transports at VALI while Buffer does not	139
5.4.2 Vertical Hurricanes	142
5.5.1 A True Clearance Assay	145
5.5.2 Developing a Methodology	145
5.5.3 Choosing Simulants	147
5.5.4 DTT treated mucus: A direct assault on rheology	147
5.5.5 Matching mucus' apparent viscosity with PEG	155
5.6 Conclusions	163
5.7 Future Directions	165
5.7.1 Clearance isn't the same as transport	165
5.7.2 DTT Revisited	166
5.7.3 Mucin covered particles	167
5.8 Experimental Methods	167
5.8.1 Transport vs. Tilt Angle experiments	167

5.8.2 Clearance Assay Experiment Protocol	168
References	170

List of Figures

Figure 2.1 Lung branching structure and the characteristic epithelium	7
Figure 2.2 Epithelial profile with various cell types	14
Figure 2.3 SEM image showing a side view of cilia.....	17
Figure 2.4 Sialyl Lewis X capping mucins	28
Figure 2.5 Structure and sizes of Membrane bound mucins	30
Figure 2.6 Organization and structure of the gel forming mucins.....	32
Figure 2.7 Distribution of different mucin types in the ASL.....	33
Figure 3.1 Cross section of the bilayer design	51
Figure 3.2 Diagram showing the cellular microenvironmen.....	53
Figure 3.3 Left: SEM image of scaffolds.....	56
Figure 3.4 H&E stains of HBE cells grown on custom scaffolds.	57
Figure 3.5 Left: Elastin-Collagen Scaffold	57
Figure 3.6 Tilting microscope "Ixion"..	64
Figure 3.7 Custom built stage.....	65
Figure 3.8 MCA mold design	66
Figure 3.9 MCA molds.....	67
Figure 3.10 Apical chamber fabrication	68
Figure 3.11 Basolater chamber fabrication and final assembly.....	69
Figure 3. 12 Mucus Clearance Assay Device.....	70
Figure 3.13 Live/dead assay of an entire channel.....	71
Figure 3.14 Live/dead assay of HBE cells forming a Y junction.	72
Figure 3.15 Streaklines showing long range transport in the MCA	74

Figure 3.16 Processing used to measure Cilia Beat Frequency (CBF).....	80
Figure 4.1 Correlative microscopy showing lateral heterogeneity	92
Figure 4.2 Flow profile of 2um beads in a ciliated fluidics channel.....	95
Figure 4.3 Poiseuille flow profiles at several volumetric flow rates.....	97
Figure 4.4 Cilia beat frequency vs. flow.....	99
Figure 4.5 Flow profiles of opposed cilia driven fluid flow.....	100
Figure 4.6 Free body diagram of an adhered bead undergoing fluid flow.....	104
Figure 4.7: Diagram showing the mechanism of bead rolling.....	110
Figure 4.8 Adhesion of PEG beads and WGA beads on HBE16 cells	111
Figure 4.9 HBE 16 cell surface decorated with FITC-WGAs	114
Figure 4.10 Adhesion of beads to an untreated surface.....	115
Figure 4.11 Adhesion of beads to a WGA treated surface	116
Figure 4.12 Bubble trap diagram	121
Figure 4.13 Bead functionalization protocol.	122
Figure 4.14 WGA functionalized microbeads (16um) on HBE 16 cells layer.	123
Figure 5. 1 The custom built microscope IXION.....	128
Figure 5. 2 Different fluid regimes in a partially filled channel	129
Figure 5. 3 The velocity profile for vertical liquid films	135
Figure 5. 4 Draining buffer and mucus velocity profiles.....	136
Figure 5. 5 The velocity profile for a 1um film of buffer on a vertical surface.	137
Figure 5.6 Field of view showing the meniscal and ALI zones of a tilted channel.....	139

Figure 5. 7 Buffer transport vs tilt angle.....	141
Figure 5. 8 Particle transport for buffer and mucus at a 60° tilt	142
Figure 5. 9 Mucus hurricane streaklines.....	143
Figure 5. 10 Mucus hurricane vs tilt angle	144
Figure 5.11 DTT reduction.....	148
Figure 5.12 Effective viscosity of normal and DTT treated mucus	149
Figure 5.13 Mucus and DTT Mucus streaklines	151
Figure 5.14 Mucus/DTT Mucus velocity field.....	152
Figure 5.15 Buffer/Mucus velocity vs distance from meniscus.....	153
Figure 5.16 Loss and Storage modulus of 4.5% 1MD PEG	156
Figure 5.17 Apparent viscosity of 4.5% 1MD Dalton PEG	157
Figure 5.18 Flow profile of a vertical 10um film of 4.5% 1MD Dalton PEG.....	158
Figure 5.19 Velocity field for 4.5% 1 MD PEG solution at a 60° incline.....	159

Abbreviations

ABS	Acrylonitrile Butadiene Styrene
ALI	Air-liquid Interface
ASL	Airway Surface Liquid
ATI	Alveolar Type I
ATII	Alveolar Type II
ATP	Adenosine Triphosphate
CBF	Cilia Beat Frequency
CCSP	Clara Cell Secretory Protein
CF	Cystic Fibrosis
CFTR	Cystic Fibrosis Transmembrane Conductance Regulator
CISMM	Computer Integrated Systems for Microscopy and Manipulation
Con A	Concanavalin A
COPD	Chronic Obstructive Pulmonary Disease
DMEM	Dulbecco's Modified Eagle Medium
DMT	Derjaguin-Muller-Toporov
DTT	Dithiothreitol
ECM	Extracellular Matrix
EDAC	1-Ethyl-3-[3-dimethylaminopropyl]carbodiimide hydrochloride
EGF	Epithelial Growth Factor
ENaC	Epithelial Sodium Channel
FITC	Fluorescein isothiocyanate

HBE	Human Bronchial Epithelial
HBE16	Human Bronchial Epithelial 16
IgA	Immunoglobulin A
MCA	Mucus Clearance Assay
MCC	Mucociliary Clearance
MIP	Maximum/Minimum Intensity Projection
NA	Numerical Aperture
PA	Pseudomonas Aeruginosa
PBS	Phosphate Buffer Saline
PCD	Primary Cilia Dyskinesia
PCL	Periciliary Liquid
PCP	Planar Cellular Polarity
PDMS	Polydimethylsiloxane
PEG	Polyethylene Glycol
PIV	Particle Image Velocimetry
PTFE	Polytetrafluoroethylene
PU	Polyurethane
PVC	Polyvinyl Chloride
RA	Retinoic Acid
SEM	Scanning Electron Microscope
TRIS	tris(hydroxymethyl)aminomethane
UV	Ultraviolet
VALI	Vertical Air Liquid Interface

Vangl2	Van gogh like 2
VNTR	Variable Number Tandem Repeats
VWD	Von Willebrand Factor Type D
WGA	Wheat Germ Agglutinin

Chapter 1 Introduction

1.1 Motivation

Breathing is important. It shouldn't come as a surprise that diseases that affect breathing take a huge toll on human health and life. Respiratory infections and chronic obstructive pulmonary disease (COPD) are the 3rd and 4th leading killers worldwide: combined they are responsible for over 7 million deaths a year (Mathers et al., 2008) How do these diseases sicken and kill? Ultimately it comes down to the ability of the lung to clear pathogens and toxins. Impaired clearance obstructs the airways, but long term it triggers a cascade that changes the fabric of the lung itself. Impaired clearance leads to infection, inflammation and ultimately remodeling of the lung. Treating and ultimately curing these diseases relies on restoring effective clearance.

How do we fix clearance? The first step is to understand the mechanisms of clearance. At its essence mucociliary clearance seems a rather simple concept. Cells secrete an assortment of molecules in an effort to impede or ensnare potential invaders and irritants. Ciliated cells transport the resulting detritus out of the airway. The simplicity of the system quickly disappears when trying to understand all of the parameters involved in clearance. "Ciliated cell transport" is a complicated process that pushes our understanding of fluid dynamics, rheology, biochemistry, and cell signaling. Furthermore these questions span from the organ level down to the

protein level. As a result, work in answering these questions has spawned clearance treatments ranging from using body posture to enhance clearance down to drugs that correct misshapen proteins. Furthering our understanding of mucociliary clearance will advance the development of treatments for these awful pulmonary diseases.

1.2 Thesis Statement and contributions

This thesis argues that *in vivo* mucociliary clearance is a product of both the biophysical and biochemical properties of the airway surface liquid. Specifically, mucociliary clearance relies on the viscoelastic properties of mucus and biochemical interactions between mucus and cilia to successfully transport mucus against gravity. One of the key contributions of this work is the development of a mucus clearance assay (MCA). The MCA integrates cell culture techniques with a microfluidics platform to provide the first *in vitro* system capable of

- 1) Probing adhesion interactions between the epithelium and ligands found in the airway surface liquid (ASL), and
- 2) Challenging mucociliary clearance with external fluid flows (including breathing regimens), and
- 3) Evaluating the ability of mucus simulants (rheological and biochemical mimics) to transport against gravity.

Furthermore as a clearance assay the system can be used to explore clearance of diseased states and the efficacy of pharmaceuticals in treating those states.

The primary goal of this work and primary use of the MCA is to elucidate the mechanism of clearance. The mechanisms of mucociliary clearance are still very much an open question. An important unsolved aspect of mucociliary clearance is the interaction between the cilium and the overlying mucus gel. Is the cilium merely an actuator pushing the gel forward, or is there a biochemical connection that provides a transient adhesion between the cilium and the gel? Prior *in vitro* systems have always had the airway surface liquid normal to gravity, this orientation forces the liquid to self-level over the epithelial surface. The MCA makes it possible to orient the culture at varying degrees, including parallel to gravity. The vertical surface orientation removes the artifact of self-leveling as the liquid height is determined by the surface energy between the luminal surface and liquid along with cilia driven transport of the liquid. By using fluids with varying rheological and biochemical profiles, it makes it possible to probe for and to isolate the properties required for vertical mucociliary clearance. Experiments from the system have demonstrated that fluids transporting horizontally aren't necessarily capable of transporting against gravity. Also the system has demonstrated that viscosity as a rheological parameter isn't sufficient in predicting clearance. Finally the system can be modified to test for adhesion interactions between ASL species and the epithelium. Results from this system make it possible to form a clearer model of the interaction between mucus and cilia.

1.3 Outline for the document

Chapter 2 starts with a brief overview of the mucociliary system. The chapter starts by examining the different elements involved with mucociliary clearance MCC: the epithelium, cilia, mucus and assorted miscellaneous factors. The goal is to familiarize the reader with the mechanisms of MCC while building a “requirements list” for a clearance model; this requirements list is important in evaluating existing model systems and the model system described in this work. The chapter then explores current model systems. A literature survey describes notable model systems that have been used to advance the knowledge of lung clearance and discusses findings as well as shortcomings and remaining questions.

Chapter 3 focuses on the model system, the MCA, which I developed during the course of my dissertation work. The chapter starts by compiling the design requirements from chapter 2 and adding specifications relating to cell culture and intended experiments. These requirements and specs are then weighed and used to make design decisions. Next the chapter details the fabrication process, sterilization procedure and associated cell culture. Finally, the chapter closes by looking at data demonstrating that not only can cells be grown in the system, but also they are well differentiated, well-ciliated and demonstrate long range ciliary entrainment. Example measurements of CBF, %ciliation, and flow are shown as well as discussion of the techniques.

Chapter 4 starts building a simple hydrodynamic model. Initially the goal of the model is to demonstrate that the beating cilia can be coarse-grained into a shear boundary. I demonstrate that using this boundary condition produces flow profiles in

agreement with canonical solutions to the Navier-Stokes equations. Ultimately this model will resurface in chapter 5 to demonstrate that hydrodynamics alone aren't enough to describe transport (or lack thereof) in the tilted conformation. I then use the fluidics aspect of the channel as a force probe to measure the adhesion between functionalized beads and the epithelial surface. I demonstrate that the clearance assay can also be used as an adhesion assay to identify and quantify adhesion of moieties attached to the beads and the epithelial surface.

Chapter 5 extends the model developed in chapter 4 and includes gravitational drainage. Using this model I determine that if the boundary condition holds, then buffer, mucus, and pathological mucus would all be able to transport up a vertical surface. I test this with buffer and mucus and discover that while buffer transports horizontally, it failed to transport vertically. Next I develop the system into a mucus clearance assay; I developed a methodology to test which properties (biochemical or rheological) enable transport against gravity. Finally I test viscosity with a Polyethylene Glycol solution and determine that viscosity alone doesn't enable transport. I'm able to conclude that the boundary condition developed in chapter 4 changes when the system is in a vertical conformation; gravitational drainage changes the interaction between the cilia and the ASL. I suggest that mucus is able to transport vertically in spite of drainage because of biochemical interactions.

Chapter 2 Mechanisms of Mucociliary Clearance

In this chapter I present an overview of mucociliary clearance. The first part of the chapter introduces different aspects of the mucociliary clearance system. The goal of these sections is to familiarize the reader with clearance and to discuss key parameters that potentially govern clearance. Current literature and models suggest that the major guiding parameters are cilia behavior (beat frequency and distribution) as well as the ASL's properties (rheology, hydration). In working towards my hypothesis that there is a biochemical interaction that plays a role in clearance, I also present potential binding interactions between cilia and the ASL that could potentially play a role in ASL transport. The end of the chapter is a survey of existing animal and *in vitro* model systems. The goal of this section is to understand the successes of current model systems, but also their limitations. Finally I close the chapter by reviewing the key parameters and current model systems to generate requirements for the model system that I design and build in chapter 3.

2.1 Lung physiology and airway defense

The lungs handle gas exchange for the entire body; the cellular respiration of trillions of cells depends on the ability of the lungs to take in oxygen and dump carbon dioxide back into the atmosphere. Meeting the demands of the entire body

requires that the lungs have a large surface area available for gas exchange, a surface area that ranges from 24-69m² (Hasleton, 1972).

The lungs achieve a large surface area through a bifurcating tree structure (Fig. 2.1). Air enters (and exits) the trachea where it splits into two main bronchi that deliver air to each lung. These bronchi further split into another generation of bronchi that feed the different lobes of the lung. This branching continues on for a total of approximately 23 generations (Weibel & Gomez, 1962), at which point the path ends at alveolar sacs. In general these generations can be classified into two zones. The conducting zone consists of the approximately the first 14 generations and is responsible for filtering and conditioning inhaled air. Beyond lies the acinar zone. The acinar zone makes up about 90% of the lung volume (Weibel & Gomez, 1962) and is responsible for gas exchange in the lung.

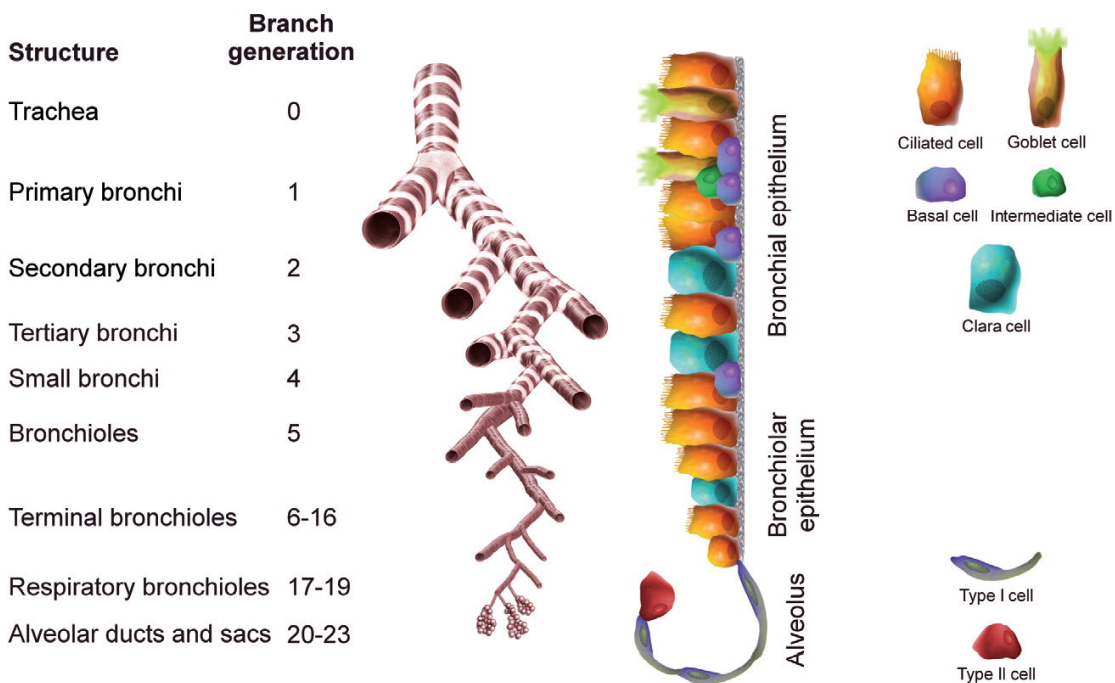


Figure 2.1 Lung branching structure and the characteristic epithelium at each level. Taken from Scotton 2011(Scotton, 2011).

The large surface area, however, acts as a double-edged sword. Every additional square foot available for gas exchange also represents an area that has to be fortified against potential pathogens. Furthermore this fortification has to protect the airway, while having minimal impact on breathing. In meeting this challenge of a large, yet unobtrusive defense system, the airway employs several different lines of defense. The epithelium itself represents a line of defense: the epithelial cells form a barrier and can control what crosses the epithelial barrier. In the conducting airways, mucociliary clearance acts as a large moving filter: pathogens are trapped in a mucus gel and then transported via cilia out of the airway. Additionally the mucus gel contains agents such as secretory IgA, lactoferrin, lysozyme, and defensins that have anti-microbial properties (Goldman et al., 1997; Wanner et al., 1996). Finally macrophages act as a final line of defense: they actively seek and destroy any pathogens that are able to penetrate the airway tree.

Amongst these mechanisms, mucus clearance seems to be the primary defense mechanism (Knowles & Boucher, 2002). The work in this dissertation will focus exclusively on the mucociliary apparatus. As a consequence the model system developed for this work will attempt to recreate the environment of the conducting airways. Specifically my model will attempt to match the geometry and structure of the bronchioles. While a more thorough discussion of scale and choice will appear in chapter 3, I should note an important physiological point regarding this choice. Typically the trachea and large bronchi have a large number of sub-mucosal glands (Tos, 1966), a feature that I won't be able to recreate in my cell culture model.

In order to build a mucociliary clearance model, it's necessary to have a strong background of the different components. The next few sections will detail the different components of the mucociliary apparatus: the epithelium, cilia, and the airway surface liquid (ASL).

2.2 Epithelium

In discussing MCC in the airways, understanding the pulmonary epithelium is of vital importance. Mucociliary clearance *is* an epithelial process. The epithelium's importance lies in both the generation of cilia and the airway surface liquid, but also the regulation of the two. To get a better sense of the epithelium and its involvement in the MCC process, I will first talk about the most common cells found in the airway epithelium and the roles as they relate to mucociliary clearance and model systems. Next I'll discuss the epithelial structure; how the cells assemble and how that assembly shapes the epithelial surface. Finally I'll discuss epithelial secretions as well as how the epithelium regulates fluids.

2.2.1 Cells of the epithelium

The epithelium is filled with a variety of cells that serve a variety of purposes. The cells of the airway epithelium include

- Serous cells
- Clara cells
- Mucous cells
- Brush cells
- Columnar Ciliated cells

Additionally in the acinar zone there are

- Alveolar Type I pneumocytes
- Alveolar Type II pneumocytes

While there are several other types of cells in the airway, I'll limit discussion to those above, as they are the cells found superficially and/or directly contribute to the epithelial environment. The cells mentioned above can be categorized as secretory cells, brush and ciliated cells, and alveolar cells. The secretory cells produce several key components of the ASL and thus play a major role in the physical and chemical properties of the liquid. The ciliated cells play a vital role in transport, but their contribution to the epithelial surface structures along with brush cells may also play a role in mucus dynamics. The *in vitro* model on which I base my clearance assay produces well-differentiated cells including secretory and ciliated cells (Fulcher et al., 2005). Furthermore the secreted products of these cells are highly similar to induced sputum samples. The major differences being saliva, plasma exudate, immune cells, and surfactant produced by alveolar cells (Kesimer et al., 2008). My model will not include alveolar cells, but future iterations may incorporate them to study their effects on clearance and host defense.

2.2.1.1 Secretory Cells

Serous cells

In a 1990 Annual Review of Physiology paper Basbaum et al. compare the serous cell to “an immobilized neutrophil” because of the cell’s role in secreting anti-

microbial products. Serous cells are the origin of most of the non-mucin protein found in the ASL (Basbaum, Jany, & Finkbeiner, 1990). Secretory products of these cells include lysozyme, lactoferrin, peroxidases, secretory IgA, as well as protease inhibitors, albumin, and high molecular weight glycoproteins. In humans, serous cells are found only in submucosal glands, and occupy 60% of the gland volume (Takizawa & Thurlbeck, 1971). *In vitro*, serous cells have also been grown by isolating submucosal glands (Finkbeiner, Zlock, Mehdi, & Widdicombe, 2009). The presence of lactoferrin and lysozyme suggests that serous cells are present in cultures generated from general tracheal/bronchial isolations. Interestingly the proportion of serous cells to mucous cells seems to decrease as retinoic acid (RA), an additive used to promote mucociliary-differentiation, concentration is increased in media (Gray, Guzman, Davis, Abdullah, & Nettesheim, 1996; Mammoto, Montoya-Zavala, Hsin, & Ingber, 2010).

Clara cells

Clara cells are found in the terminal bronchioles of the airway where they perform diverse tasks (Jeffery & Li, 1997). One function is that of a precursor cell; Clara cells have the ability to differentiate into both mucous and ciliated cells (Ayers & Jeffery, 1988). Clara cells also have a diverse array of secretory products. Clara cell secretory protein (CCSP) has been shown to act as an anti-inflammatory by regulating macrophage behavior (Snyder et al., 2010). Cytochrome P450 helps metabolize toxins (Devereux et al., 1981). Clara cells also produce surfactant protein D, a C-type lectin (Crouch, Parghi, Kuan, & Persson, 1992).

Mucous/Goblet cells

Mucous cells, also known as goblet cells are found in both the surface epithelium and in sub-mucosal glands. In the trachea there are ~6,500 mucous cells per mm² (Ellefsen & Tos, 1972), but this number decreases further down the airway tree (Wanner et al., 1996). Mucous cells are often referred to as goblet cells because of their characteristic shape. Histology sections show that they resemble a goblet: the nucleus is towards the bottom of the cell while a large secretory granule dominates the top half of the cell (Rhodin, 1966). Goblet cells are the major source of the gel forming mucins that form the mucus layer, which I'll discuss later in this chapter. Functionally the cells can store large mucin reserves and secrete those reserves into the ASL. The stored mucus capacity for the lung has been estimated at 4ml (Reid, 1965) and it takes between 2-4 hours for a goblet cell to synthesize and secrete Muc5AC (Sheehan et al., 2004).

2.2.1.2 Brush and Ciliated Cells

Brush Cells

Brush cells are found throughout the airway and feature a tuft of microvilli on their surface. Their function isn't well understood but the following roles have been speculated (Reid et al., 2005).

1. Absorptive
2. Chemoreceptors
3. Immune surveillance
4. Detoxification

Ciliated Cells

Ciliated Cells are terminally differentiated cells, each of which is covered with an average of 200 hair like projections called cilia(Rhodin, 1966). Cilia drive the mucociliary system; understanding their movement, organization, and interaction with mucus is a critical step in understanding mucociliary clearance and an area in which I will go into greater detail in subsequent sections. In addition to cilia, these cells also have microvilli and glycocalyx on their apical surface(Rhodin, 1966). The number of ciliated cells varies with the location in the airway tree. In the human trachea ciliated cells outnumber mucous cells by a ratio of 5:1, but the numbers decrease in more distal generations (Wanner et al., 1996).

2.2.1.3 Alveolar cells

Alveolar Type I

Alveolar Type I (ATI) pneumocytes are found in the respiratory zone of the lung and are the main constituents of the alveoli; they make up 90% of the alveolar surface (Haies, Gil, & Weibel, 1981). Structurally ATI cells are ideal for diffusion; they are extremely thin with a large surface area. Each cell has a surface area of $5100\mu\text{m}^2$ (Crapo, Barry, Gehr, Bachofen, & Weibel, 1982) and an average thickness of only 200nm (Weibel, Gehr, Haies, & GIL, 1976)

Alveolar Type II

Alveolar Type II (ATII) pneumocytes make up 10% of the alveolar epithelial surface (Haies et al., 1981). They produce surfactant proteins A, B, C,D lysozyme, and lysosomal enzymes. (Voorhout, Weaver, Haagsman, Geuze, & Van Golde, 1993) (Madsen et al., 2000)

2.2.2 Epithelial Cross-Section

As shown in figure 2.1, the airway epithelium changes dramatically depending on the location in the lung. Figure 2.2 further illustrates the degree to which the epithelial profile changes. The thickness of the epithelium transitions from a ~60µm pseudostratified columnar profile in the proximal lung to a 100nm single cell layer in the alveoli (Patton & Byron, 2007). In addition to the thickness, the airway structure and distribution of cell types changes. The percentage of ciliated and mucous cells decrease distally as do the number of sub-mucosal glands (Whimster, 1986), which are mainly absent after the 10th generation (Wanner et al., 1996).

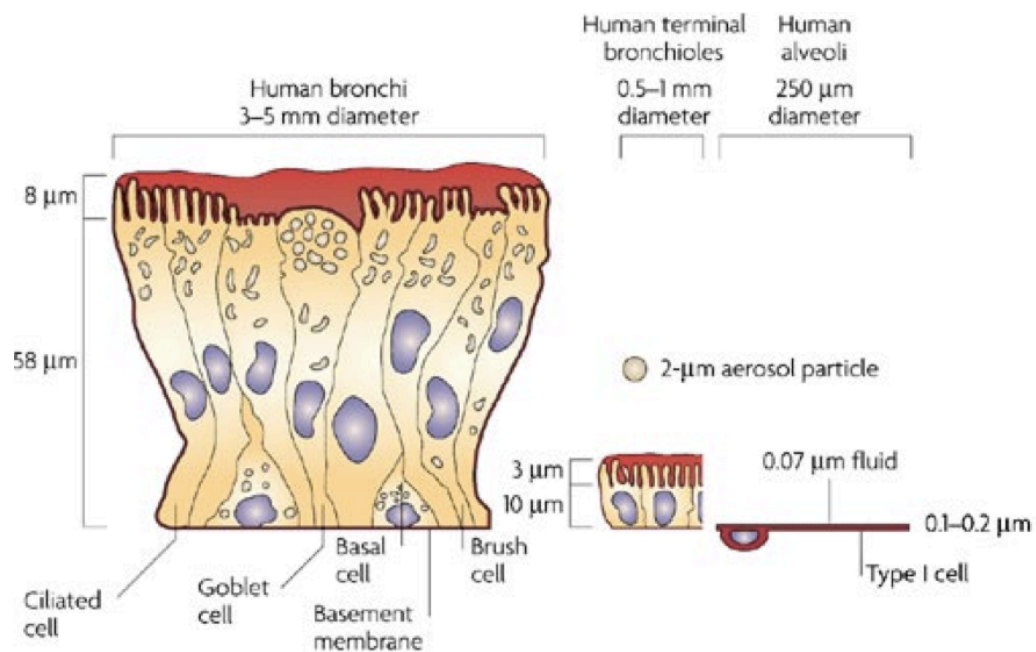


Figure 2.2 Epithelial profile with various cell types. The epithelial profile transitions from a 60µm thickness down to a 100 nanometer thickness in the distal airways. Taken from Patton 2007

The epithelium serves as a barrier itself; cells of the epithelium are bound together by tight junctions. The tight junctions form a seal that separates the airway

lumen from the rest of the body. This seal allows the epithelial cells to function as gatekeepers. This regulation extends down to the ion level; ions can only cross the epithelium through ion channels on the plasma membrane of epithelial cells. Using this mechanism the epithelium is able to regulate the ASL volume via osmotic pressure (J. Widdicombe, Bastacky, & Wu, 1997), a mechanism that I'll revisit in section 2.4.4.

The epithelial surface is covered by a variety of surface structures, which range in size from nanometers to microns. Understanding these structures and their biochemistry is important for eliciting any potential interactions with mucins.

2.2.2.1 Glycocalyx

Closest to the cell membrane is the glycocalyx. The glycocalyx is a collection of various polysaccharides extending 500-1500nm from the cell surface (Knowles & Boucher, 2002) and it covers all of the various cell types. The glycocalyx has many roles including cell adhesion, protection from pathogens, and signaling. A review by Martins et al. covers more of the specifics of the pulmonary glycocalyx (Martins & Bairos, 2002). The glycocalyx's ubiquity and large surface area make it a prime candidate for potential biochemical adhesion between cilia and the ASL.

Looking for these adhesions requires knowledge of the specific saccharides present in the bronchial epithelial glycocalyx. The bronchial epithelial glycocalyx is rich in sialic acid residues, MUC1 (discussed in section 2.4.1.1), and localized keratan sulfate. *In vitro* cultures express the same moieties as *in vivo*, but the density of the glycocalyx may be higher *in vivo* (Stonebraker et al., 2004).

Understanding the availability of these moieties will be important in developing the adhesion assay in chapter 4.

2.2.2.2 Microvilli

Microvilli are small ~1 micron tall protrusions coming from the cell surface, particularly brush cells and ciliated cells. Microvilli are themselves covered by the cell membrane and glycocalyx (Alexander, Ritchie, Maloney, & Hunter, 1975).

2.3 Cilia

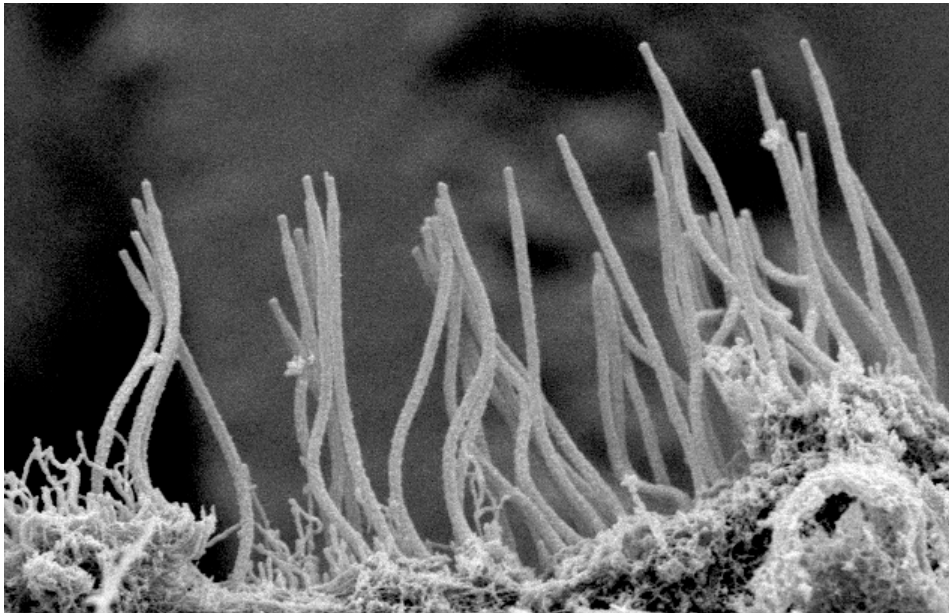


Figure 2.3 SEM image showing a side view of cilia. Cilia are about 6-7um long .

Cilia are small hair-like organelles expressed on the luminal side of the airway epithelium (fig 2.3). Through regular beating, cilia work in concert to transport mucus up the pulmonary tree. The mechanism of this interaction, however, is still very much an open question. Specifically this thesis investigates the nature of the interaction between cilia and the ASL. Do cilia simply act as actuators that push the overlying

mucus layer, or is there a biochemical interaction between cilia and mucus?

Exploring their role as actuators requires knowledge of cilia size, coverage, and cilia dynamics: the dynamics of individual cilia as well as their organization. Additionally in creating the cilia model discussed in chapters 4 and 5, it's important to know what external factors could change cilia behavior. Finally in exploring potential biochemical interactions an awareness of the cilia surface is necessary.

I'll start with a brief background on cilia structure and function. Next I'll review a couple of papers that discuss a particularly important aspect of cilia dynamics, cilia entrainment. Cilia entrainment, the alignment of cilia across the epithelial surface, is required for mucociliary clearance. It's of particular interest to my project because it is found *in vivo*, but the mechanisms of reproducing it *in vitro* are just starting to be understood. I'll conclude this section by discussing the cilia surface and its local environment.

2.3.1 Cilia Primer

The epithelial surface of the proximal conducting zone is dominated by cilia: as stated earlier ciliated cells outnumber mucous cells 5:1 in the trachea (Wanner et al., 1996). Each ciliated cell is home to approximately 100-200 cilia located on the apical surface. Each individual cilium has a length of about 6 microns and a diameter of 300 nanometers (Rhodin, 1966).

In order to propel mucus each cilium oscillates at a range of 10-20Hz, this large range being a product of normal variation, environmental conditions as well as location in the airway tree (Luk & Dulfano, 1983) (Rautiainen et al., 1992) (Rutland, Griffin, & Cole, 1982). During each oscillation the cilium demonstrates two separate

components; an effective stroke and a recovery stroke. The effective stroke is in the “forward” direction and occupies about 40% of the stroke cycle. During this phase the cilium stretches the farthest away from the cell, presumably to interact with the mucus gel. The recovery stroke occupies the remaining 60% of the cilia beat and travels in the “backwards” direction. During the recovery stroke the cilium travels closer to the surface of the cell, which presumably minimizes the interaction with the overlying gel (Sanderson, 1981) (Marino, 1982).

Several studies have examined external factors that influence cilia beat frequency. Clary-Meinesz et al. showed that CBF had a temperature dependence in nasal and tracheal brushings. They observed a 50% decrease in CBF when temperature was decreased from 20C to 9C (Clary-Meinesz, Cosson, & Huitorel, 1992). Additionally, several groups have also looked at mechanosensitivity of CBF. Lansley et al. showed CBF rapidly increased from an increase in intracellular calcium, an increase triggered by mechanical stimulation. Rabbit tracheal cilia at 37C increased their beat frequency from 17.2 to 26.7Hz with a corresponding rise intracellular calcium concentration of 100-650nM (Lansley & Sanderson, 1999). Winters et al. observed mouse tracheal CBF increase in response to an applied shear-stress(Winters, Davis, & Boucher, 2007). Button et al. observed an increase in CBF as a result of a cyclically applied trans-epithelial pressure(Button, Picher, & Boucher, 2007a).

Equally important to CBF is cilia coordination. In general the cilia of the lung are entrained in such a way that their effective strokes are all pointed in the cephalad direction, or “up” the airway tree(Wilson, Jahn, & Fonseca, 1975). They also

demonstrate temporal coordination; the beats of neighboring cilia are offset so that they produce a metachronal wave(Gheber & Priel, 1989). The origin of this coordination/entrainment is a heavily studied area, and rightly so. It represents a major element still poorly understood in *in vitro* cell cultures.

2.3.2 Cilia Organization and Entrainment

Cilia are coordinated at the cell level and on the tissue level. This coordination is an essential element of mucociliary clearance and highly desirable in a clearance assay. Starting at the cellular level, cilia are all “pointed” in the same direction. After a certain level of maturation, cilia are locked into a certain direction. Each cilium has an “anchor” in the cell called the basal foot, which locks into a certain direction as the cilium grows and matures (Lemullois, Klotz, & Sandoz, 1987). In healthy cells roughly all of the cilia are oriented such that their effective strokes are in the same direction. This coordination goes beyond the cellular level; in healthy *in vivo* systems neighboring ciliated cells also have their cilia pointing in the same direction. In fact this coordination spans the tissue, and is referred to as tissue polarization. Tissue polarization is essential to functional mucociliary clearance, it guarantees that all of the cilia have their effective strokes oriented to clear mucus out of the airway as opposed to deeper into the lung. Outside of the airway, the signaling that coordinates tissue polarization has been a hot field of study. Several groups are looking at the Planar Cellular Polarity (PCP) pathway and the proteins that regulate it in several organisms across several different types of tissue. Several studies have specifically tried to understand the role that the PCP signaling pathways and external mechanical forces play in shaping polarity amongst ciliated cells.

In a 2007 Nature paper, Mitchell et al. investigated the developmental mechanisms that polarize cilia on the skin of *Xenopus* embryos. Initially they looked at the basal body orientation in several cells *in vivo*. Basal feet were roughly aligned prior to cell differentiation. This alignment was present at the cell level as well as across several cells (clusters). The degree of alignment improved as the system matured. The cilia produced a strong directed flow, which Mitchell called the “Refinement Phase”. The initial alignment is created by a “Patterning Phase”. Next they looked at *in vitro* cells taken before and after the patterning phase. Explants taken prior to the patterning phase didn’t align the same way and were “chaotic”, explants taken after the patterning demonstrated alignment similar to *in vivo* results.

Next Mitchell et al. investigated the relationship between cilia function and polarization. They injected morpholinos to block expression of gene products required for cilia motility: essentially they gave the embryos the equivalent of Primary Cilia Dyskinesia (PCD), a genetic disease that disrupts normal cilia motility. The embryos still showed the rough alignment, but never experienced the refinement step. Again they looked at explants that were taken before the patterning stage. They exposed these to an external flow and saw an improvement in alignment, but the alignment wasn’t as good as the wild type. They also used a 1Hz oscillating flow and saw no alignment. Finally they exposed mutated PCD-like explants to flow and didn’t see alignment. Their major conclusions were

1. Most of the alignment takes place before differentiation/ciliation
2. *In vivo* flow serves as a further correction to initial patterning

3. In the absence of a patterning phase, external flow (with a shear-stress of 0.5 dynes/cm^2 , the same shear-stress applied to the ASL surface from breathing (Tarran et al., 2005)) will still lead to alignment, but not the same degree as seen *in vivo*.
4. Motile cilia are required for flow to affect alignment.

Guirao's 2010 Nature Cell Biology paper investigated cilia orientation in mouse brain ventricles (ependymal cells). They argue that this model, as well as other mammalian systems, requires a mechanism other than the 2-step patterning/refinement mechanism observed in *Xenopus*. Initially they looked at cilia coordination in *in vivo* models as a function of time. The immature cells had randomly aligned basal feet, which is opposite to the patterning that Mitchell et al. observed in *Xenopus*.

In their *in vitro* system, 60% of the ciliated cells formed in clusters surrounded by non-ciliated cells. They first concluded that isolated cells can align their own cilia, and that cell clusters align as well. They also cite their earlier theoretical work (Guirao & Joanny, 2007) for the mechanism by which cilia are aligned by an external force. If a cilium is not beating in the same orientation as the flow, then the flow will apply a torque to the cilium. If the basal body is free to rotate, the cilium will align itself with the flow. Next, they exposed *in vitro* cultures to an external flow via a rotating plate. The plate was situated atop the media above the cells. They rotated the plate so that the cell layer experienced a shear stress of 0.018 dynes/cm^2 . They found that cultures exposed during the right time window

aligned with the external flow, and that cultures exposed after this time period didn't realign. Cultures not exposed to flow showed "typical" cluster behavior. They then investigated the effect of PCP signaling, specifically the PCP protein Van Gogh-like 2 (Vangl2). In immature cultures they found Vangl localized at the apicocaudal borders of cells. More mature cultures showed asymmetric localization and that the protein localized along cilia from the tip to the base. They looked at Vangl2 mutants, which produced structurally normal cilia. In these mutants, the Vangl2 protein aggregated in the cytoplasm instead of localizing at the membrane. As a result, the cilia generated flow didn't affect each other at the cell or cluster level. They concluded that Vangl2 is required for cilia to be influenced by hydrodynamic forces. They explored this *in vivo* and found the same result. They then looked at a mutant that didn't have cilia. They found the asymmetric localization of Vangl2 even without cilia present; however, the basal bodies were still misaligned in mature cultures. So Vangl2 alone isn't enough for orientation. They conclude the following

1. There doesn't appear to be a patterning phase that aligns cilia in mouse ependymal cells and possibly mammalian cells in general.
2. Cilia will tend to align themselves in clusters.
3. Cilia can be aligned via an external force, but only during a small window
4. Not only are motile cilia required for flow-driven alignment, but also the Vangl2 protein.

5. Despite the lack of “patterning”, Vangl2 still localizes asymmetrically.
6. In mutants that prevent ciliogenesis, the basal bodies still misalign despite the Vangl2 localization.

Further studies have shown that both actin and microtubules play a large role in establishing PCP protein asymmetry across cells and orienting a basal body network (Vladar, Bayly, Sangoram, Scott, & Axelrod, 2012; Werner et al., 2011).

There are still many unanswered questions relating to cilia alignment particularly to lung epithelial cilia entrainment. What are the origins of entrainment *in vivo*? At what stage of cilia growth can cilia be entrained? Do airway cilia undergo a patterning step? Can airway cilia be entrained with an external force? The last question is of particular interest in designing the clearance system. By having a mechanism to deliver external flow, the mucus clearance assay could potentially be used to test this result in human bronchial epithelial (HBE) cell cultures.

In addition to spatial coordination, cilia are also coordinated temporally (Wanner et al., 1996). Neighboring cilia have an offset in their strokes so that there is a time lag. This time lag produces metachronal waves; a frequent example often cited is “the wave” that a crowd performs at a football stadium. The net effect of this is that there is a longer wavelength, slower frequency wave propagating along the ASL boundary. As I’ll discuss later, mucus’ viscoelasticity leads to a time-dependent mechanical response. For this reason it’s important to be aware of the metachronal wave and its associated time scale.

2.3.3 Beyond Cilia: Cilium Surface and the PCL

Understanding the cilium surface is important in identifying potential biochemical interactions with mucus in the ASL. The cilia membrane is similar to the cell membrane and it has recently been shown that MUC16 and MUC4 are present on the cilia membrane (Button et al., 2012). In attempting to identify a biochemical interaction, there are several examples of the cilia membrane having adhesive functions. *Chlamydomonas* uses adhesive cilia for motility (Bloodgood, 1990) and mating (Mesland & Ende, 1979). Cilia adhesion is used by mammalian oviduct cilia to help transport oocyte-cumulus complexes (Talbot, Shur, & Myles, 2003). I discuss cilia-mucin adhesion in greater detail in section 2.4.5. More examples of the adhesive functions of cilia and a more complete picture of the cilia membrane can be found in a 2008 Pazour chapter of *Current Topics in Developmental Biology* (Pazour, 2008).

The periciliary layer/periciliary environment (PCL) is the intermediate region that separates the epithelial surface from the overlying gel phase of the ASL. The PCL varies in height over different cell types: it ranges from 7 μ m over ciliated cells to 3 μ m over other non-ciliated cell types (Tarran et al., 2001). It's been hypothesized that the membrane-bound mucins and other glycolipids on the cell surface create a framework for the movement of water into this region (Randell, 2006). Button et al. further developed this into a "Gel-on-brush" model that proposed that membrane spanning mucins and mucopolysaccharides attached to cilia, microvilli and the epithelial surface sterically block large particles (large than 20-40nm) from penetrating the PCL (Button et al., 2012). Matsui et al. showed that cilia-driven

transport exists in the PCL, but that this transport is highly dependent on the overlying mucus layer. PCL transport is reduced by more than 80% without an overlying mucus layer (Matsui, Randell, Peretti, Davis, & Boucher, 1998b).

2.4 Airway Surface Liquid

The airway surface liquid (ASL) performs several important functions in maintaining pulmonary health and sterility. The first function is that of a barrier and trap: pathogens and toxicants are impeded and ensnared by the mucus gel. Throughout the pulmonary airway, the epithelial surface is normally covered by a liquid layer ranging from 5-20 μm in thickness (J. Widdicombe et al., 1997). Secondly, the ASL has a variety of antimicrobial agents that can disable potential invaders. Finally the ASL acts a cilia-driven transport vehicle to remove detritus from the airway (J. H. Widdicombe, 2002). This dissertation is chiefly concerned with the last point: understanding how the cilia interact with the mucus to remove it from the system. Knowledge of the other two functions, however, is still important in that their actions may have an effect on mucus transport and could potentially hint at biochemical interactions.

The ASL features a diverse collection of species that provide the aforementioned functions. A 1996 review of mucociliary clearance lists glycoproteins, proteoglycans, lipids, secretory IgA immunoglobulins, lysozyme, peroxidase, lactoferrin, DNA, actin as the constituents of the ASL (Wanner et al., 1996). A 2002 review further lists several additional polypeptides and defensins that act as antimicrobials in the ASL (Ganz, 2002). Finally, it's important to remember that electrolytes such as Na^+ , Cl^- , K^+ , Ca^{+2} , and HCO^{-3} are present in the ASL (R. C.

Boucher, Stutts, Bromberg, & Gatzky, 1981). Furthermore, these electrolytes have been implicated in defensin activation (J. Smith, Travis, & Greenberg, 1996), and ASL volume regulation/hydration (Matsui, Grubb, Tarran, Randell, Gatzky, Davis, et al., 1998a) (Mall, Grubb, Harkema, & O'Neal, 2004). In exploring potential biochemical interactions between the ASL and the cilia, it is important to realize that any of these species could act as potential intermediaries or catalyzing agents. In an effort to keep the problem somewhat tractable, I'll focus on the high molecular weight glycoproteins, the mucins, present in the ASL.

2.4.1 Mucins and Mucus

Mucins are high molecular weight glycoproteins that form the structure of the mucus gel (Verdugo, 1991). Structurally mucins have a central protein core that has at least one, and often times many, domains that are heavily glycosylated with oligosaccharide side chains. The heavily glycosylated regions, mucin-like domains, feature an abundance of serine and threonine, which serve as attachment points for O-glycans. These O-glycans attach to the serine/threonine through an N-acetylgalactosamine sugar. The rest of the O-glycan is composed of varying combinations of N-acetylgalactosamine, N-acetylglucosamine, galactose, fucose, sialic acid, and sulfate (Thornton, 2004). A more thorough review of the O-glycans and their assembly can be found in *Essentials of Glycobiology* (Varki, 1999).

The O-glycans in the mucin-like domain confer a couple of important properties to the mucins and by extension the mucus gel. Firstly the O-glycans play a major part in the conformation of the mucin. The high-concentration of carbohydrates in the mucin-like region (65-85% by weight) and the hydrophilic

nature of the carbohydrates heavily influence the shape of the mucin. The carbohydrates sterically prevent secondary and tertiary structures, which results in a linear extended conformation as compared to other proteins of the same contour length (Jentoft, 1990). Another important function of the O-glycans is their biochemical functionality. The oligosaccharides are biochemically similar to the glycocalyx, and thus they can intercept microorganisms that target the glycocalyx (Wanner et al., 1996) (Carnoy et al., 1994) (Lamblin et al., 1992; 1991). It's also important to note that there are oligosaccharide moieties present in mucins that are associated with known biochemical adhesions. Sialyl Lewis X (fig 2.4), for example, is present in mucins (Allahverdian, Wojcik, & Dorscheid, 2006), but also plays a major role in leukocyte tethering to the endothelium (Lawrence & Springer, 1991; McEver, 2005). Due to these interactions and the variation present in the O-glycans, they should be emphasized as potential sites of interaction with cilia.

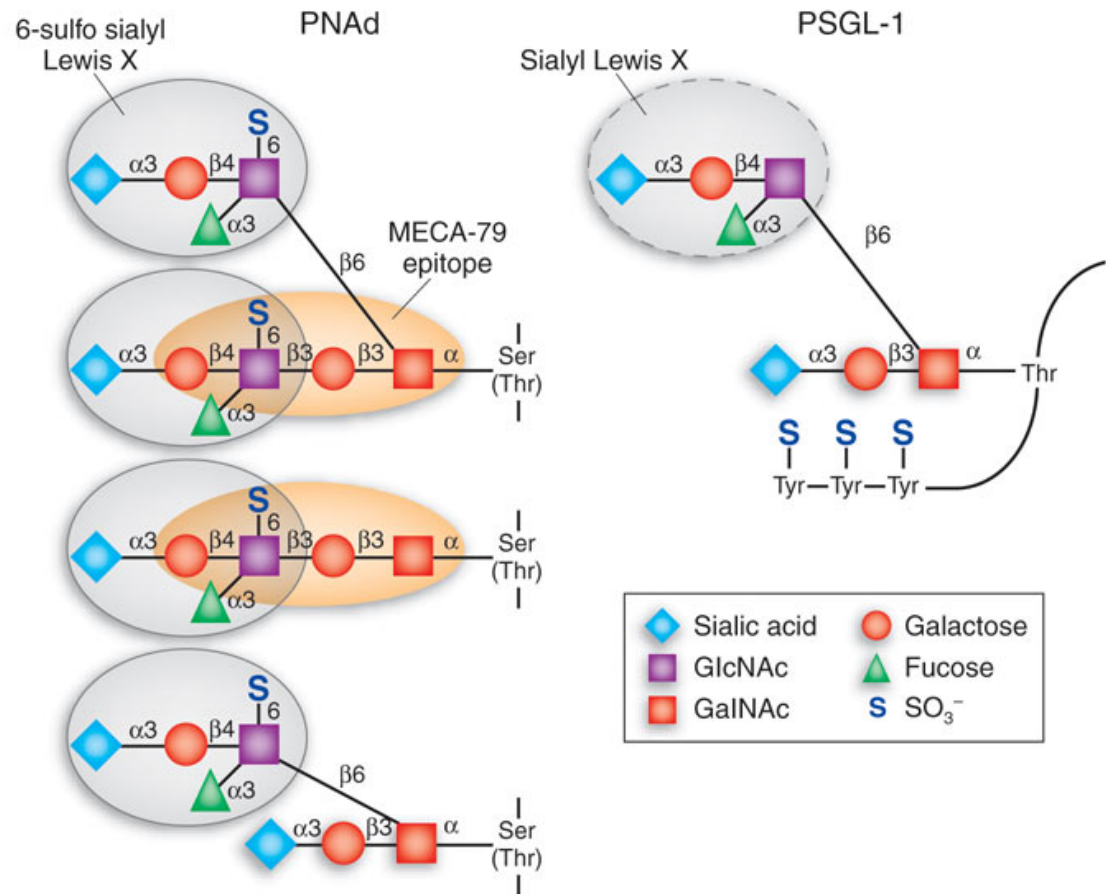


Figure 2.4 PNAd and PSGL-1, mucins expressed on endothelial cells and leukocytes respectively, are capped by Sialyl Lewis X. L-selectin binds to the sialic acid and fucose ends of Sialyl Lewis X. This bond plays a major role in leukocyte adhesion and rolling. (Taken from McEver 2005)

Structurally the mucin-like domains have a variable number of tandem repeats (VNTR) and thus these domains can vary in size between individuals (Hattrup & Gendler, 2008). The organization of these mucin-like domains into mucin monomers can be separated into two different families: membrane bound (tethered) mucins and gel forming (secretory) mucins.

2.4.1.1 Membrane Bound Mucins

Membrane bound mucins are named so because they are characteristically found near the cell surface and are tethered to the cell membrane. Structurally they are composed of two subunits. The larger of the subunits is dominated by a VNTR domain and located outside of the cell. The smaller subunit consists of a small extracellular region, a transmembrane domain, and a cytoplasmic tail. In the airway, the primary membrane bound mucins are MUC1, MUC4, and MUC16 (Fig 2.5). The structure of these mucins prevents them from polymerizing, so they are found in monomeric form. It should be noted that despite their name, they can also be found in the mucus layer and represent about 10% of the ASL mucins. A much deeper more detailed description of membrane bound mucins can be found in Hatstrup's 2008 review *Structure and Function of the Cell Surface (Tethered) Mucins* (Hatstrup & Gendler, 2008).

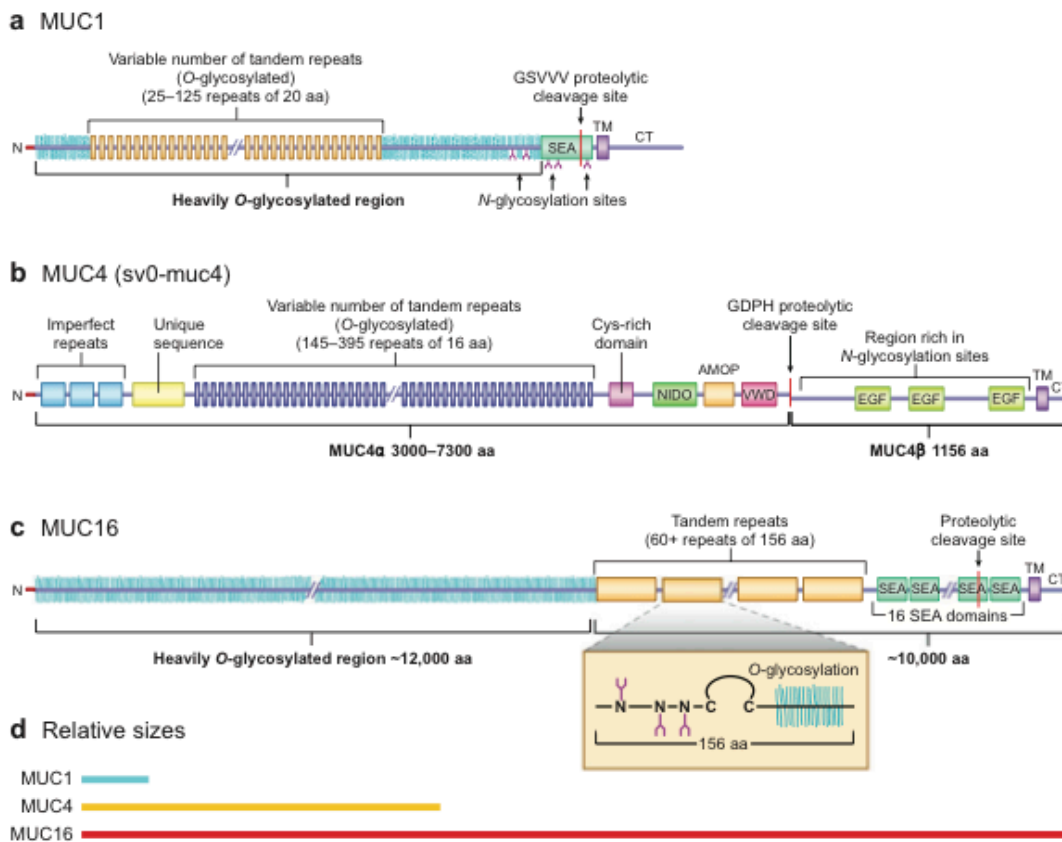


Figure 2.5 Structure and sizes of Membrane bound mucins. Hattrup 2008

2.4.1.2 Gel Forming Mucins

Unlike membrane bound mucins, gel-forming mucins linearly polymerize into polydisperse chains ranging in length from 0.5-10 μ m. This polymerization is enabled by structural differences in the mucin monomers. In gel-forming mucin monomers, the mucin-like domain is sandwiched between protein domains rich in cysteine residues (Fig 2.6). The monomers polymerize into linear chains through disulfide linkages between the cysteine rich, protein domains. The mucous gel is then formed by a combination of entanglement and reversible Ca⁺² dependent crosslinks (Thornton, Rousseau, & McGuckin, 2008). In the airway the dominant types of gel

forming mucins are MUC5AC and MUC5B, where together they make up 90% of the mucin raft (Fig 2.7)(Hatstrup & Gendler, 2008). These two species also have an interesting difference in their origins. MUC5AC is produced primarily by goblet cells on the surface of the epithelium, while MUC5B is typically produced in sub-mucosal glands. Thornton speculated that their differing origins and secretory control mechanisms could allow a mechanism for controlling the properties of the mucus gel by fine-tuning the ratio of MUC5AC to MUC5B (Thornton, 2004).

In creating a mucus clearance assay, it is important to have a solid understanding of differences between their presence and properties *in vivo* versus *in vitro*. In a 2009 paper, Kesimer et al. compared the apical secretions from ALI cultured HBE cells versus Induced Sputum. They found that overall the compositions were similar, but there were some important distinctions. MUC5B and MUC5AC appear at similar percentages 38% to 30% respectively in induced sputum vs. a 45% to 21% difference in cell culture respectively. Percentages were determined by looking at the non-glycosylated regions of the protein, so in essence it is the number of mucin monomers of a species expressed over all of the mucin monomers detected (Kesimer et al., 2009). Another interesting difference exists between the types of MUC5B expressed in cell cultures. *In vivo* MUC5B is produced in two different glycoforms: one is high charge and the other is low charge. MUC5B from cell culture, however, seems to be more homogeneous with only one glycoform appearing (MUC5AC is homogeneous in both cases) (Thornton, 2004). I would like to reemphasize that this section on the structure and components of the mucins barely scratches the surface and suggest Thornton's *Structure and Function of the*

Polymeric Mucins in Airway Mucus (Thornton et al., 2008) for more information about gel-forming mucins and their structure and Kesimer's *Tracheobronchial air-liquid interface cell culture: a model for innate mucosal defense of the upper airways?* (Kesimer et al., 2009) for an in depth comparison of *in vivo* versus. *in vitro* constituents of the ASL.

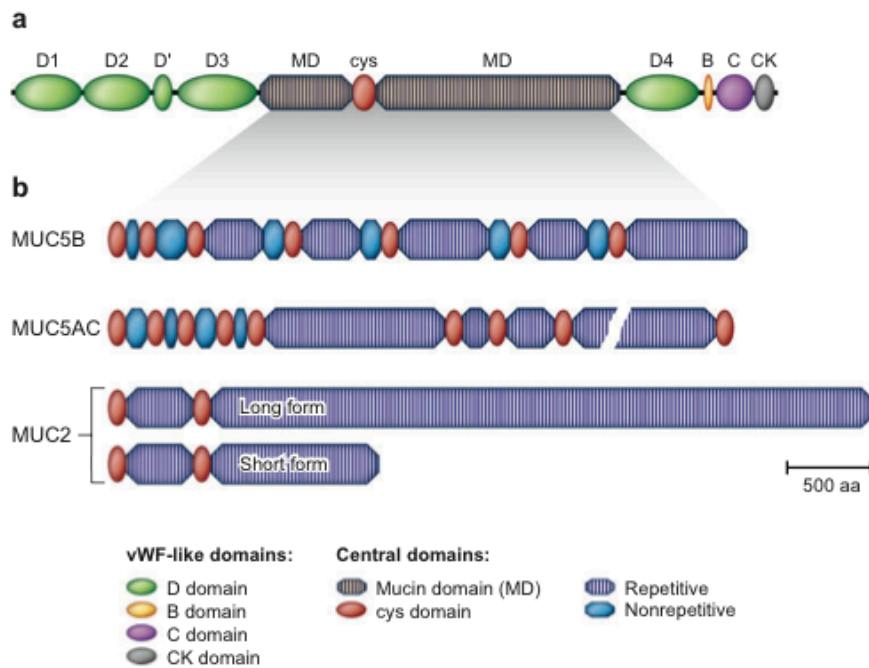


Figure 1

Cartoon of the major structural domains within polymeric airway mucins. (a) Generic representation of a polymeric mucin polypeptide. The N- and C-terminal von Willebrand factor (vWF)-like domains (D domains, the B domain, the C domain, and the CK domain) and the central region containing two mucin domains (MD) and one cys domain are highlighted. (b) The organization of the central domains of MUC5B, MUC5AC, and MUC2. Repetitive (*striped blue*) and nonrepetitive (*solid blue*) sequences within the mucin domains are shown. The central domains of MUC5B and MUC5AC show little length variation between individuals, but the fourth repetitive domain in MUC5AC shows a slight variation in length (30). In contrast, the second repetitive domain of MUC2 is variable in length, and the two extremes, with either 40 or 185 repeats, are depicted, illustrating the significant potential size difference for this mucin. aa denotes amino acid.

Figure 2.6 Organization and structure of the gel forming mucins found in the airway. (Thornton 2008)

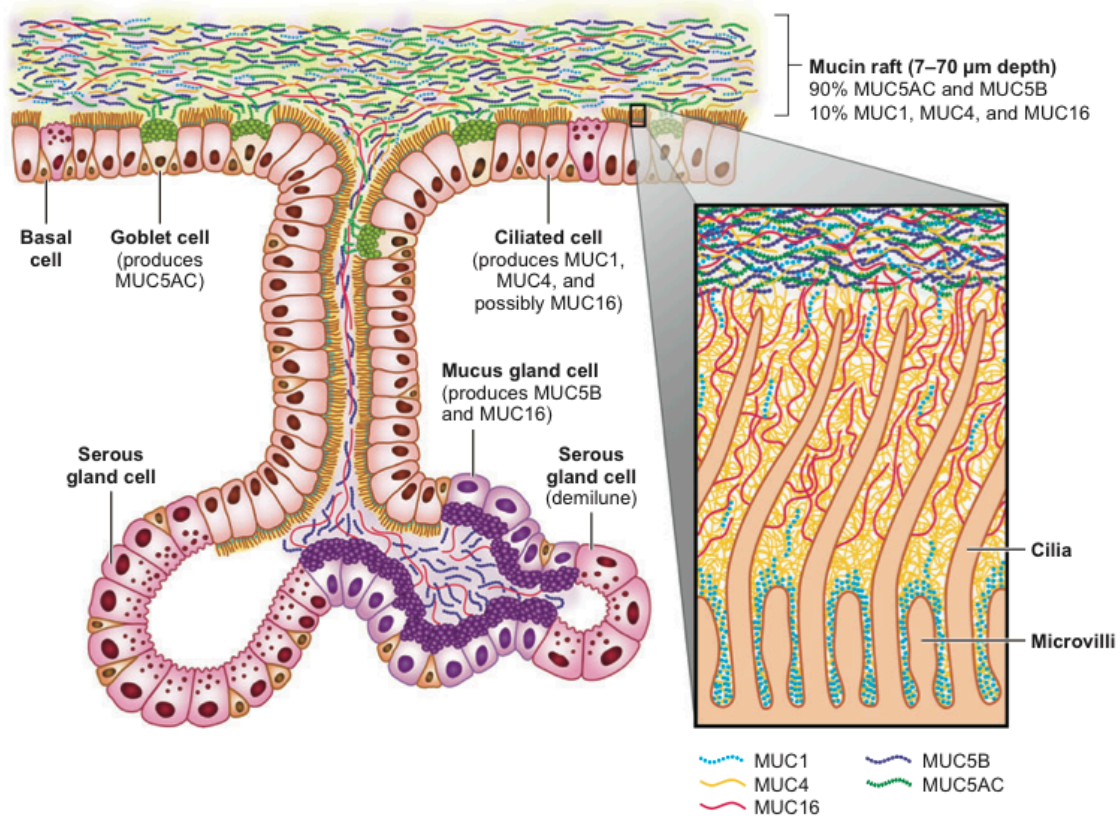


Figure 2.7 Distribution and origin of different mucin types in the airway surface liquid. Muc5B and Muc5AC make up 90% of the mucins on the epithelial surface, the remaining 10% are cleaved membrane bound mucins (from Hattrup 2008)

2.4.2 Properties of the Mucus Gel

The gel forming mucins account for the majority of the “structure” of mucus, and as a result they heavily influence the mechanical properties of the mucus gel. As discussed previously, the individual mucins are relatively stiff molecules that are crosslinked near their ends. The crosslinked mucus network behaves as a viscoelastic liquid. An understanding of mucus viscoelasticity is necessary to study how the mucus gel reacts to cilia, gravity, and ultimately clears out of the airway/model. Following is a quick aside on viscoelasticity, to provide the reader with

enough of a background to understand some basics of mucus behavior, but more importantly to understand the theories and experiments presented in sections 2.4.3 through 2.5.

2.4.2.1 Viscoelasticity

Viscoelastic materials exhibit viscous and elastic properties in response to an applied force. In modeling the elastic behavior, we fall back on Hooke's law and the concept of an ideal spring. If we displace the spring by distance x , we will have a restoring force that opposes that displacement by a spring constant k .

$$F = -kx \quad (2.1)$$

Which can also be expressed in terms of an applied stress (force per area) σ , an extensional strain ϵ and the elastic modulus E .

$$\sigma = E\epsilon \quad (2.2)$$

This equation is for extensional stress, a stress applied normal to the incident surface. If instead we apply a stress along a surface, we refer to it as a shear stress σ , the resulting displacement a shear strain γ , and the ratio of proportionality is the shear modulus.

$$\sigma = G\gamma \quad (2.3)$$

In dealing with viscoelastic fluid, our forces will be in the form of shear stresses, so we will primarily use equation 2.3. A quick point in regards to elasticity; fundamentally, elasticity is a function of bonds. Whether we are talking about a crystalline solid or a polymer network the bonds are at the heart of the elasticity. The

elastic relationship only holds true as long as the bonds are still intact. When a yield stress, a stress strong enough to irreversibly break the bonds is applied, the material no longer exhibits elastic behavior.

If elastic behavior is the mechanism by which a system stores energy from an applied stress, viscous behavior is the mechanism by which the system dissipates energy from an applied stress. Conceptually it helps to think of this dissipative loss as a friction between strata of a fluid. If a shear-stress is applied to the top stratum, that stratum will move at a certain velocity. Subsequent strata will also move, but the frictional force reduces the velocity. This can be expressed as

$$\sigma = \eta \dot{\gamma} \quad (2.4)$$

The applied shear-stress is proportional to the strain rate $\dot{\gamma}$ by the viscosity η . This equation follows our intuition; if we apply the same amount of shear to materials with different viscosities, the more viscous material will strain at a lower rate. In modeling material responses, simple mechanical schematics are useful in understanding the dynamics. Elasticity is represented by a spring, while viscosity is modeled as a dashpot. Viscoelastic materials are thus modeled as a combination of springs and dashpots. The Kelvin-Voigt model consists of a spring and dashpot in parallel and can be represented mathematically as the sum of the elastic and viscous responses

$$\sigma = G\gamma + \eta \dot{\gamma} \quad (2.5)$$

The Kelvin-Voigt model is often used for viscoelastic solids; the spring parallel to the dashpot implies that there will eventually be a complete recovery from

any displacement. The Maxwell model consists of a spring and dashpot in series and can be represented mathematically by

$$\dot{\gamma} = \frac{\dot{\sigma}}{G} + \frac{\sigma}{\eta} \quad (2.6)$$

This model is often used for viscoelastic fluids, and further components can be added to model more complicated fluid behavior.

We can extend these models to look at oscillating stresses or strains. G^* is the complex modulus and can be represented as

$$|G^*(\omega)| = \frac{\sigma_0}{\gamma_0} \quad (2.7)$$

Where σ_0 and γ_0 are the maximum shear and stress for a given frequency ω . Along with G^* , the phase lag between the stress and strain, δ , is useful in characterizing the mechanical response. It's also useful to express the complex shear modulus as a sum of the real and imaginary components. Expressing in this manner gives

$$G^*(\omega) = G'(\omega) + iG''(\omega) \quad (2.8)$$

Where G' is referred to as the storage modulus and G'' is referred to as the loss modulus. These quantities, along with the tangent of δ will be very useful in describing the rheological properties of mucus.

2.4.2.1 Mucus rheology parameters

Now that I've defined a few basic concepts about viscoelasticity, I'll briefly discuss some properties of mucus viscoelasticity. In a 1998 paper, King lists the following properties of mucus (King, 1998)

- viscosity, η , decreases with increased shear rate, $\dot{\sigma}$. (shear-thinning)
- Mucus responds to an applied stress in the following progression

solid-like -> viscoelastic deformation -> steady flow

- Mucus has only a partial strain recovery following the removal of an applied stress

In moving forward with understanding the interplay between mucus rheology and transport, it's clear that we need to pay very close attention to force response and time scale. When looking at mucus response we need to look at the "fast" 10Hz cilia oscillation, slower metachronal wave response, and the long scale gravity response. The following table (table 2.1) is a list of mucus rheological parameters that potentially govern mucociliary clearance. In the next section I discuss experiments that have attempted to draw a relationship between transport and some of these parameters.

Key Rheological Parameters

$G'(\omega = \text{low frequency})$	$G'(\omega = \text{CBF})$
$G''(\omega = \text{low frequency})$	$G''(\omega = \text{CBF})$
$G^*(\omega = \text{low frequency})$	$G^*(\omega = \text{CBF})$
$\text{Tan } \delta(\omega = \text{low frequency})$	$\text{Tan } \delta(\omega = \text{CBF})$

η (apparent viscosity long time scale)

Mesh size

Table 2.1 Several rheological parameters that may govern mucociliary clearance. Complex modulus, loss modulus, and storage modulus are measures of how the mucus strains in response to an applied shear

stress at a given frequency. $\tan \delta$ is the ratio of the loss modulus over the storage modulus for a given frequency. Apparent viscosity is the low frequency limit of the loss modulus. Mesh size may play an important role in cilia engaging the mucus and applying a shear.

2.4.3 Mucociliary Transport and Viscoelasticity

Several groups have used a variety of model systems to determine the governing parameters of mucociliary clearance. In particular several have focused on the relationship between the rheological properties of the mucus and the transport rate. Chen et al [1978] found that an optimal transport velocity occurred with an elasticity of 11-25 dynes/cm² and a viscosity of 1000-3000 poise using a frog palate model (Chen & Dulfano, 1978). Gelman et al [1979] looked at bovine cervical mucus on the frog palate system and found transport was essentially independent of G'' , but instead dependent on G' (Gelman & Meyer, 1979). King et al. used a similar system and found that the loss tangent, the ratio G''/G' , had a negative correlation with transport velocity. They also found that if the $\tan \delta$ remains constant, then transport rate decreases with elasticity (King, 1980). A later Puchelle paper looks at the transport of Xanthan Gum across frog palate and concludes that there is an optimum apparent viscosity of 12 Pa s for transport. Beyond this viscosity, Puchelle saw a decrease in transport rate, but also a correlated drop in cilia beat frequency (Puchelle, Zahm, & Quemada, 1987). The wide variety of results (summarized in table 2.2) and conclusions points to the complexity of directly correlating rheology to transport. This is further emphasized by a Shah paper that says that no one individual rheological property (G' , G'' , G^* , and $\tan \delta$) is sufficient in predicting the effect on transport rate (Shah & Donovan, 2007).

Rheological Parameter	Effect on Mucus Transport	Simulant/System
G' (~1Hz)	<p>Optimal at 2 Pa (Majima et al., 1986)</p> <p>Optimal at .16 Pa (Gelman & Meyer, 1979)</p> <p>Negative correlation if tan δ is held constant (King, 1980)</p>	<p>Mucus/Frog palate</p> <p>Mucus/Frog palate</p> <p>Guar/Frog palate</p>
G' (~16Hz)	<p>Optimal at 1 Pa (Shih, Litt, Khan, & Wolf, 1977)</p> <p>Negative correlation if tan δ is held constant (King, 1980)</p>	<p>Canine Mucus/Bovine Trachea</p> <p>Guar/Frog palate</p>
G''	<p>Independent(Gelman & Meyer, 1979)</p>	<p>Mucus/Frog palate</p>
G* (~.1hz)	<p>Negative correlation with log G* (Macchione et al., 1995)</p>	<p>Rat mucus/Frog palate</p>
tan δ (low)	<p>Negative correlation (King, 1980)</p>	<p>Guar/frog palate</p>
tan δ (high)	<p>Negative correlation (King, 1980)</p>	<p>Guar/frog palate</p>
η	<p>Optimal at 12 Pa s (Puchelle et al., 1987)</p>	<p>Xanthum gum/frog palate</p>
Spinability	<p>Positive correlation (Puchelle, Zahm, & Duvivier, 1983)</p>	<p>Mucus/frog palate</p>

Table 2.2 Summary of experimental results showing the relationship between rheological parameters and mucociliary transport. Spinability is a measurement of the length of mucus filaments.

2.4.4 Fluid Regulation

In examining the rheological properties of the ASL, it is important to understand how that rheology can change. While secretion of additional proteins/glycoproteins can change the rheology, hydration influences ASL rheology. As briefly mentioned before the epithelium is selectively permeable to several species. Localization of ion channels contributes to “electrical” properties of the epithelium. For example, Epithelium Sodium Channels (ENaC), are typically localized on the apical surface (and thus “above” the tight junctions) and control the absorption of Na^+ ions. Likewise, the Cystic Fibrosis Transmembrane Conductance Regulator (CFTR) channel is also localized apically and regulates the secretion of Cl^- ions into the ASL. The coordination of these ion channels (along with others) creates a potential across the epithelium.

An interesting extension of ion regulation is fluid regulation. Although most species are tightly regulated in crossing the plasma membrane, water is allowed to freely diffuse across. As the ion concentration inside and outside of the cells change, water crosses the plasma membrane in an effort to maintain osmotic balance. Using this mechanism, the epithelium can secrete an excess of ions into the ASL and increase the tonicity. In turn water crosses the epithelium to maintain osmolality and hydrates the ASL (Matsui, Davis, Tarran, & Boucher, 2000). Conversely if the epithelium absorbs an excess of ions, the water will cross into the cells and

dehydrate the ASL (Matsui, Grubb, Tarran, Randell, Gatzky, Davis, et al., 1998a). This mechanism plays prominently in the disease Cystic Fibrosis (CF). In CF a genetic defect causes a malformed or incorrectly localized CFTR channel (Riordan et al., 1989). This inhibits chloride ion secretion and interferes with the epithelium's ability to hydrate the ASL.

2.4.5 Mucus and cilia adhesion

In this dissertation I argue that mucociliary transport isn't solely determined by mucus rheology, but also a function of biochemical interactions. In this section I present three known adhesion mechanisms, of which all the necessary elements are present in the mucociliary system.

2.4.5.1 Gel forming mucins to membrane bound mucins

Knowles and Boucher's 2002 review of airway defense mentions a "Velcro effect" in which MUC5B and MUC5AC adhere to membrane bound MUC4 and MUC1 (Knowles & Boucher, 2002). Hattrup's 2008 review mentions that MUC4 is unique amongst the membrane bound mucins in that it has a von Willebrand factor type D (VWD) sequence, a sequence also found in the gel forming mucins. The VWD sequence may play a role in polymerization of gel forming mucins (Gum, Hicks, Toribara, Siddiki, & Kim, 1994) and likewise the tethering of gel forming mucins to membrane bound mucins. Combining this with the presence of MUC4 on the cilia membrane provides a mechanism for cilia-mucus adhesion (Button et al., 2012).

2.4.5.2 Membrane bound selectins and mucins

The tetrasaccharide Sialyl Lewis X, which I first brought up in section 2.4.1, plays an important role in leukocyte tethering (Lawrence & Springer, 1991). Furthermore it is present in the O-glycans expressed in airway mucins. The corresponding ligand, P-selectin, is also expressed in a subset of epithelium cells (Allahverdian et al., 2006). This lectin-saccharide interaction represents another known adhesion mechanism that could potentially adhere cilia to mucus.

2.4.5.2 Free lectins and mucins

One last interaction that I'll discuss is galectin-3. It's been hypothesized that galectin-3, which binds to galactose, can act as a cross-linking agent amongst O-glycans (Berry, McMaster, Corfield, & Miles, 2001). galectin-3 is present in both apical secretions and induced sputum samples, thus presenting another potential mucus-cilia adhesion interaction.

These examples are just a few potential adhesion interactions demonstrating that there are known adhesion mechanisms that exist in the ASL-cilia system. The adhesion assay developed in chapter 4 can serve to test and quantify these adhesions as well as discover new interactions. Finally the existence of these known adhesion mechanisms demonstrate that they are present and could be a part of mucociliary clearance.

2.4.6 Other Forces acting on the ASL

In addition to the elements that I've gone over, it's also important to remember the environment of the lung. First the act of breathing greatly influences

the epithelial environment. Lung expansion stretches the cells of the epithelium: the lung stretches about 4% during normal tidal breathing and up to 25% during sighs and deep inspirations (Gump, Haughney, & Fredberg, 2001). Furthermore, Espinosa and Kamm developed a mathematical model showing that non-uniform, periodic strain of a membrane could create directed flow in a thin liquid layer (Espinosa & Kamm, 1997). Closely related to stretch is the modulus of the substrate. In Janmey et al.'s review *The hard life of soft cells* the importance of matrix stiffness is ubiquitous element for mechanosensing, motility, and differentiation (Janmey, Winer, Murray, & Wen, 2009). Although there is more work to be done in ascertaining all of the physical properties of the pulmonary matrix, it is an important part in moving forward. In addition to substrate stretch, the act of breathing also applies a shear-stress to the ASL: airflow delivers a shear-stress between .4 and 2 dynes/cm² (Tarran et al., 2005).

Beyond this normal airflow is the much more forceful airflow that comes as a result of cough. Cough is often considered a mechanism aside from normal mucociliary clearance, but also play a role in removing mucus, especially in diseased states (King, Brock, & Lundell, 1985). Finally the effect of gravity on clearance will weigh heavily on the work contained in this dissertation.

2.5 Model Systems

In designing and implementing a biological model system the physiological relevance of the system is always a central question. How faithful is the model system to the *in vivo* system? Equally important, however, is access into the system; in trying to understand the system what dials can we turn and which gauges can we

read? The challenge of any model system lies in striking a balance between these questions: developing a system that has enough experimental access to understand underlying phenomena but still resembles the physical system. Before designing a new model system it's essential to understand the existing systems and how they address these two questions. The following sections examine the current body of model systems that have been employed to study mucociliary clearance. The models have been categorized into animal models, and *in vitro*.

2.5.1 Animal MCC studies

Animal models have been extremely useful in advancing understanding of the mucociliary apparatus; in fact many of the findings in the previous sections are a result of animal studies. That said it is important to remember that these are models and don't perfectly recreate the human pulmonary environment. There are a multitude of interspecies differences that could have an impact on mucociliary clearance mechanisms. In illustrating these differences, I'll primarily refer to the most popular animal models mice/rats and frogs, however, every animal model has key differences from human models.

In comparing animal models to human models, one of the first differences to jump out is that of structure and scale. Mouse lungs are 1/6000 the volume of human lungs, have fewer generations (13-17 as opposed to the 17-21 in humans), and don't follow a dichotomous branching system (Irvin & Bates, 2003). Another interesting difference is the pronograde mouse posture: mice lungs are mostly in a plane orthogonal to that of gravity. Beyond the gross structural differences, there are also important differences at the tissue and cellular level. Mice have a thinner

epithelium than humans, lack submucosal glands, and have a much higher percentage of Clara cells (Irvin & Bates, 2003). Frog mucosa exhibit a resting/quiescent stage where cilia did not beat (Spungin & Silberberg, 1984). Deeper yet are the differences at the protein and protein expression level. While mice and other animal types (including bovine, chimpanzee, rhesus monkey, equine, canine, chicken and tetraodon) have orthologs of human mucin genes (Thornton et al., 2008). The point of listing these differences isn't to eschew or denigrate animal models: these models have proven invaluable and are excellent experimental tools. The goal is to point out that they are fundamentally different types of experiments, and that it is important to always maintain an awareness that there are differences; demonstrating a concept in an animal model is not tantamount to demonstrating it in human.

2.5.2 *In vitro* MCC studies

In vitro models provide a unique advantage in that they enable excellent experimental access, far more accessibility than *in vivo* or animal models. This access, however, comes at the cost of physiological relevance: removing cells from their physiological environment greatly changes their behavior. Similar to animal models, it's important to remember that an *in vitro* experiment is not the same as an *in vivo* experiment; however, as the physiological mimicry improves and the *in vivo* environment is recreated, the *in vitro* experiment starts converging to the *in vivo* system.

In the interest of increasing physiological relevance for *in vitro* models, great attention has been paid in recreating elements of the *in vivo* system in the cell

culture system. Several key advances have been made in improving the physiological relevance of bronchial epithelial cells. Whitcutt et al. developed a biphasic chamber that only perfused the culture from the basal side. They observed that culturing guinea pig epithelial cells at an air liquid interface improved the differentiation of the cells as the cultures took on a phenotype reminiscent of the *in vivo* cells (Whitcutt, Adler, & Wu, 1988). Gray et al. experimented with the effects of retinoic acid (RA) and epithelial growth factor (EGF) on cultures. They found that retinoic acid increased the percentage of secretory cells by 10-20 times as well as promoting ciliation. They also found that decreasing the level of EGF improved the regularity of the epithelium and decreased cellular necrosis and cystic phenotypes. Moller et al. saw a huge improvement in cell growth, ciliation, and morphology by using a collagen coated Millicell filter as a growing substrate (Moller, Partridge, Cox, Pellegrini, & Ritchie, 1987). These advances, along with the tissue procurement, media composition, and cell culture techniques described in Fulcher et al. chapter *Well-differentiated human airway epithelial cells* have provided a strong foundation to create well-differentiated, human bronchial epithelial cells. It's from this foundation that the model in this dissertation will build from to incorporate the physical environment into an *in vitro* system.

To build upon the state of the art *in vitro* models, the first challenge is to determine what elements are essential to the mucociliary process. Whitcutt's work demonstrates the importance of the Air-liquid interface in promoting differentiation. Clary-Meinesz showed that temperature affects CBF, but additionally we know that temperature and humidity affect the rheological properties of the ASL. Simply

maintaining the cells will also require control over the cell media, maintaining appropriate gas concentrations in the system, as well as keeping the system contamination free.

The next challenge is determining the missing elements from the current systems; what can be added to the current systems to make them more physiologically relevant? The advances in the prior paragraph focused matching elements of the biochemical environment; while there is still much work to be done there, the biophysical environment of the cells have lagged far behind. In concluding my review of clearance, I mentioned several physical forces that may play an essential role in clearance, including stretching (which requires a compliant substrate) and shear-stress from breathing, as well as drainage from gravity. The cilia entrainment section also detailed that having an external fluid flow could help to ascertain the origin of ciliary alignment. While other groups have explored some of these phenomena, no one has made a comprehensive system to study all of them and their effects mucociliary clearance. Huh et al. designed a system that applied a cyclical stretch to alveolar cells (Mammoto et al., 2010). Even-Tzur have created systems that explored using a more compliant amniotic membrane (Even-Tzur et al., 2010) and the application of wall-shear stress to early stage HBE cells (Even-Tzur, Elad, Zaretsky, & Randell, 2006). Tarran et al. have developed systems that explore phasic shear-stress and mechanical stress applied to well-differentiated HBE cultures (Tarran et al., 2005) (Tarran & Button, 2006) (Button & Boucher, 2008) Although this dissertation will primarily focus on gravity, the model system was designed to ultimately incorporate all of the other elements. I have laid the

groundwork to incorporate stretch and “breathing” into the culture system. Finally the clearance assay will need the ability to measure clearance and explore the rheological and biochemical properties of the ASL. Particle Image Velocimetry (PIV) has been the main technique used to quantify transport in both animal and *in vitro* models. The exploration of rheological properties has been achieved through the use of simulants, which have been carefully chosen to represent a particular rheological, or biochemical property of the ASL. Table 2.3 catalogs the important features and requirements of clearance models and shows the progress that existing models possess. The last entry, the Mucus Clearance Assay (MCA) that I design and build in the next chapter, represents the most advanced *in vitro* system to study mucociliary clearance.

<i>In Vitro Model</i>	Differentiated	Well-Ciliated	External Fluid Flow	Particle Image Velocimetry (PIV)	Substrate Stretch	Tilted PIV
ALI cultures	✓	✓	✗	✓	✗	✗
Huh	✓ (Alveolar)	✗	✓	✓	✓	✗
Even-Tzur	✓	✗	✓	?	✗	✗
Tarran-Button Mechanical Stress ALI model	✓	✓	✓	✓	✗	✗
MCA	✓	✓	✓	✓	Developed (not implemented)	✓

Table 2.3 Features of existing clearance model systems. Checks in green squares denote the presence of a feature in a model; x's in red squares denotes the absence of a feature. The question mark in the Even-Tzur model denotes that the system is probably capable of PIV, but PIV experiments have not been reported

Chapter 3 Building the Mucus Clearance Assay

In this chapter I discuss my work in designing, fabricating, and evaluating the mucus clearance assay system. This device represents the first cell culture system to incorporate well-ciliated human bronchial epithelial cells into a fluidics channel. I demonstrate that the system is capable of “patterning” HBE cells into specific geometries and that the ciliated cells coordinate to produce long range flows in the channels. In chapter 4 I will use the ciliated fluidics channel to develop a simple model of the cilia-ASL boundary and use external flow to validate that model with well-known solutions of the Navier-Stokes equation. Another key feature of my mucus clearance assay is that the media is enclosed; this allows me to tilt the assay indefinitely. I also discuss the development of a unique tilting microscope. Incorporating the tilting mucus clearance assay along with the tilting microscope makes it possible to perform particle image velocimetry (PIV) experiments on a tilted system. In chapter 5 I use tilted PIV experiments to explore the effects of gravity on mucociliary clearance.

3.1 Design Considerations

My design strategy was to start with existing cell culture models as a baseline for both physiological relevance and experimental access: I didn't want to sacrifice any of the physiological relevance or capabilities found in existing models of well-

ciliated, well-differentiated cells. In prioritizing the items to incorporate, I considered that the overarching goal of my device was to probe the mucociliary process. Experiments would rely on varying the properties and dynamics of the ASL to examine their effect on mucus transport. This methodology places an emphasis on external fluid flow over the cultures and the ability to tilt the system.

Considering the importance of manipulating fluid flow, a bilayer system seemed the best starting point for a clearance assay design. Essentially the bilayer design consists of two channels separated by a porous membrane: in the most basic form it can be thought of as a compartmentalized Whitcutt chamber (Fig 3.1). This design has been used to perform flow studies on renal cells (Jang & Suh, 2010) and Caco-2 cells

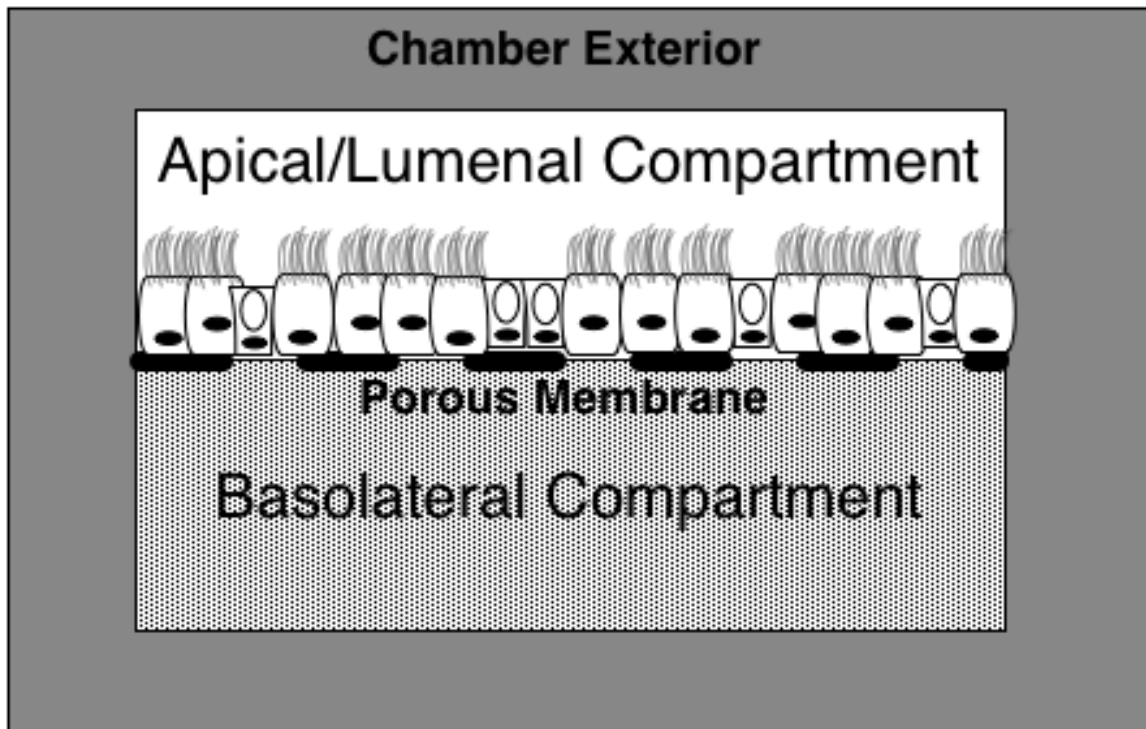


Figure 3.1 Cross section of the bilayer design. Cells are grown on a porous scaffold and are perfused by media in a basolateral compartment. The apical compartment is filled with air so that the cells are grown at an air-liquid interface.

(from the small intestine) (Kimura, Yamamoto, Sakai, Sakai, & Fujii, 2008). Additionally bilayer systems have been used in some capacity to study lung cells. Even-Tzur et al. have explored the effects of wall shear-stress on HBE cells (Even-Tzur et al., 2006) and Huh et al. used a bilayer design to study alveolar cells (Mammoto et al., 2010). Neither of these studies, however, explored using such a system with well-ciliated cultures and by extension mucociliary clearance. My challenge was to adapt the bilayer design so that I could successfully grow well-differentiated, well-ciliated cells; incorporate the external forces of gravity and fluid flow; and make sure that the new design had at least equal experimental access to existing HBE cell culture models.

Adapting the bilayer system

Choosing the bilayer system gave me a general blueprint for the Mucus Clearance Assay, but I still had to adapt the system to support growing well-differentiated, well-ciliated epithelial cultures as well as my planned experiments. Adaptation required making decisions regarding the dimensions, materials and the geometry of the device. The following sections examine the different requirements discussed earlier and use these requirements to inform decisions for the final device.

3.1.1 Designing the chamber: Physiological Considerations

In this section I discuss how physiological relevance influenced my design strategy in adapting the bilayer channel design. Growing well-differentiated HBE cells is a non-trivial task; it's easy to forget amongst the routine washing and feeding of cells that the end result is growing human tissue. Fortunately the advances in section 2.5.2 and the work from the UNC CF Center Tissue Procurement and Cell

Culture Core have given me a solid tissue engineering road map. In creating the MCA there are three key areas that I need to address to successfully grow and maintain physiologically relevant cultures

1. Scale
2. Cell Environment
3. Cell Perfusion

Young and Beebe wrote a review that addressed several of the issues in controlling the microenvironment of microfluidic cell cultures(Young & Beebe, 2010). Figure 3.2 shows several of the issues that they addressed, but applied to a bronchial epithelial culture.

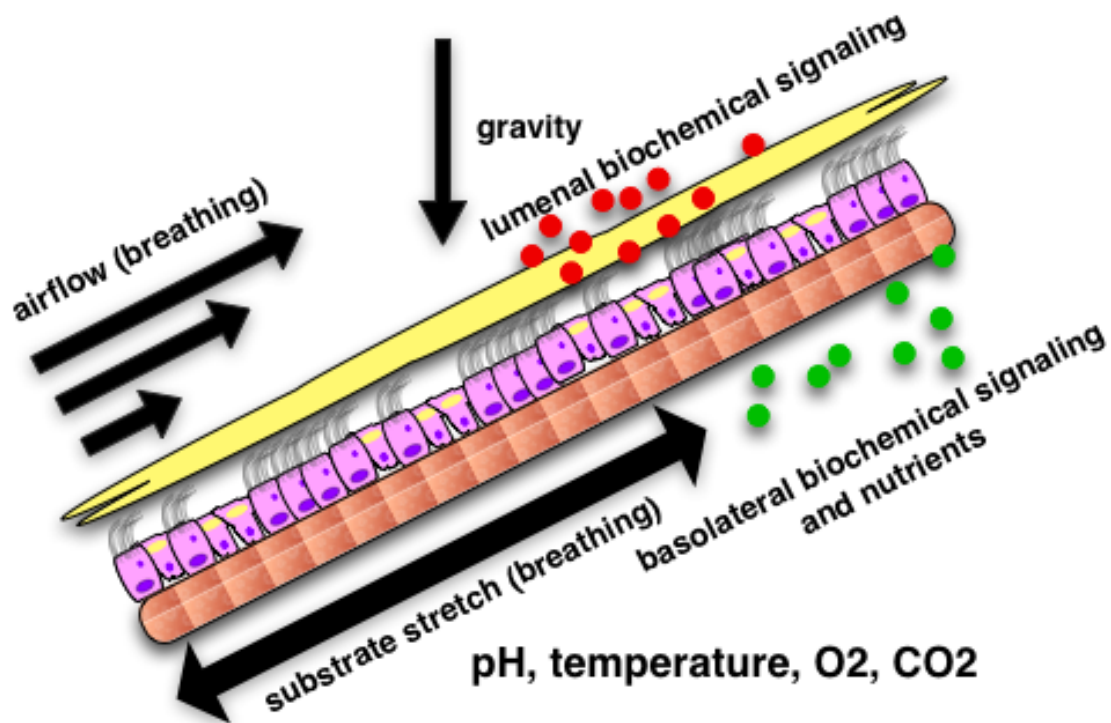


Figure 3.2 Diagram showing the cellular microenvironment for lung epithelial cells.

3.1.1.1 Scale

Designing a model system to explore the mucociliary phenomenon requires accurate scaling. The geometry and scale of the channel has a direct influence on how fluids behave in the channel and more importantly the shear-stress communicated to the epithelial cell surface. In particular matching the diameter of the channel to a specific segment of airway will ensure that

1. The channel has a similar Reynolds number and correspondingly similar fluid behavior as the *in vivo* system
2. That a specific fluid volumetric flow rate would map to a corresponding shear-stress at the cell surface as in the *in vivo* system.

The *in vivo* diameter of the trachea is in the neighborhood of 25mm (Breatnach, Abbott, & Fraser, 1984). The diameters of the conducting airways are fairly close to the power law,

$$d_z = d_0 \times 2^{\frac{-z}{3}} \quad (3.1)$$

where z represents the airway generation and d_0 is the trachea diameter (Weibel & Gomez, 1962). Using this equation yields an airway diameter of ~1mm for the distal end of the conducting zone. Broadly, to match the diameter of the conducting airway, the device should have a diameter between 1 and 25mm. In order to conserve cells and resources, as well as to have the opportunity to make more devices, I chose to make a device on the smaller end of this range, with dimensions on the order of 1mm.

3.1.1.2 Cell Environment

The clearance assay environment is a critical aspect in successful tissue growth. Designing a novel system requires not only maintaining the correct growing surface, temperature and humidity, but also making sure that no toxic agents are introduced into the system. Specifically the HBE cell cultures are going to require a porous scaffold, an air-liquid interface, and a humid environment.

Scaffolds

Over the past couple of decades, there's been an increased appreciation in the role that scaffolds play in cell behavior and development. There are plenty of examples of the mechanical and biochemical properties of scaffolds affecting cell behavior and phenotype. Lo et al. showed that fibroblast migrated up substrate stiffness gradients by sensing the substrate rigidity, a process coined durotaxis (Lo, Wang, Dembo, & Wang, 2000). Engler et al. demonstrated that mesenchymal stem cell differentiation has a strong dependence on substrate rigidity (Engler, Sen, Sweeney, & Discher, 2006). In pursuit of physiological relevance, I explored developing scaffolds that would be closer in composition and mechanical properties to the native ECM found *in vivo*. In addition to any potential direct mechanosensing of the substrate, the more physiologically relevant scaffold would enable stretching, as well as potential substrate remodeling by the cells.

In my first scaffold creation attempt I developed an electrospinning protocol based on work performed by Demir (Demir, Yilgor, Yilgor, & Erman, 2002). Without knowing the optimal scaffold parameters (porosity and fiber size) I attempted to recreate the structure of the commercially available millicell membranes (EMD

Millipore, PICM03050), but using polyurethane (PU) instead of Polytetrafluoroethylene (PTFE). Polyurethane was chosen primarily for the anticipated mechanical properties of the network, but also because of the success that other groups had with cell growth on porous PU (Ramrattan et al., 2005). I was able to match the fiber size of my PU scaffolds to that of the millicell scaffold (Fig. 3.3).

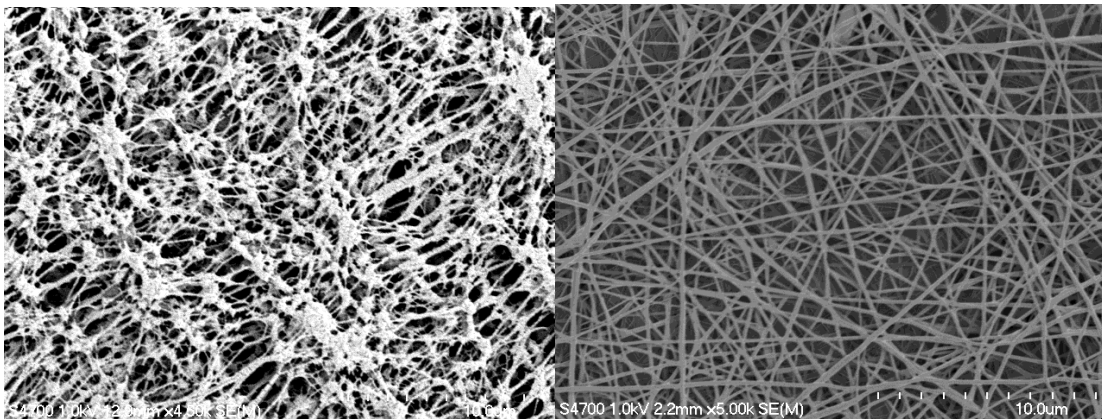
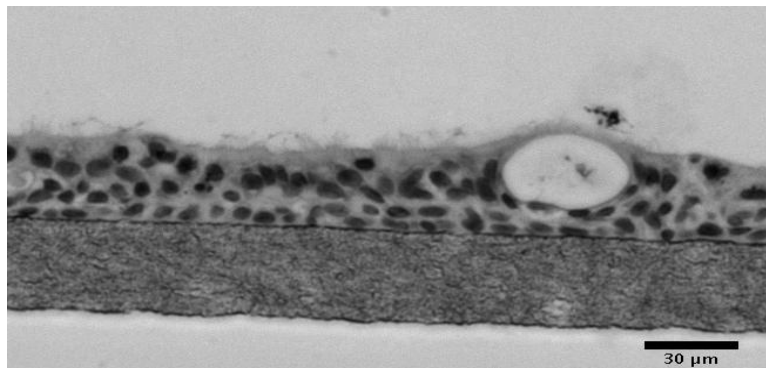


Figure 3.3 Left: SEM image of a commercially available millicell membrane. Right: Similarly scaled image of an electrospun polyurethane scaffold. The fiber diameters and porosity of the synthesized membrane on the right were designed to approximate the properties of the commercially available scaffold.

Furthermore I was able to grow well-differentiated, well-ciliated cells on polyurethane scaffolds (Fig. 3.4).



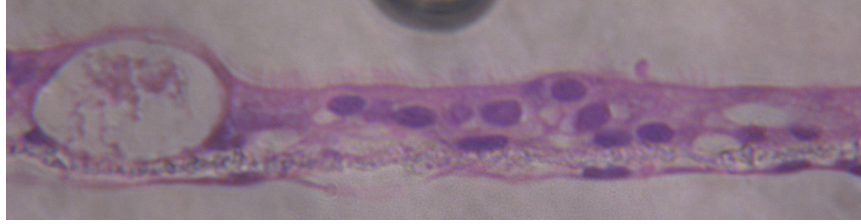


Figure 3.4 Hematoxylin and eosin stains of HBE cells grown on scaffolds. Both scaffolds show evidence of ciliated cells along the apical surface. Top: Millicell scaffold Bottom: Electrospun polyurethane scaffold

The polyurethane membranes seemed promising except for one fatal flaw: they had abysmal optical properties. The scaffolds scattered so much light that it made transmission bright field microscopy almost impossible. I also used a similar technique to develop elastin-collagen scaffolds.

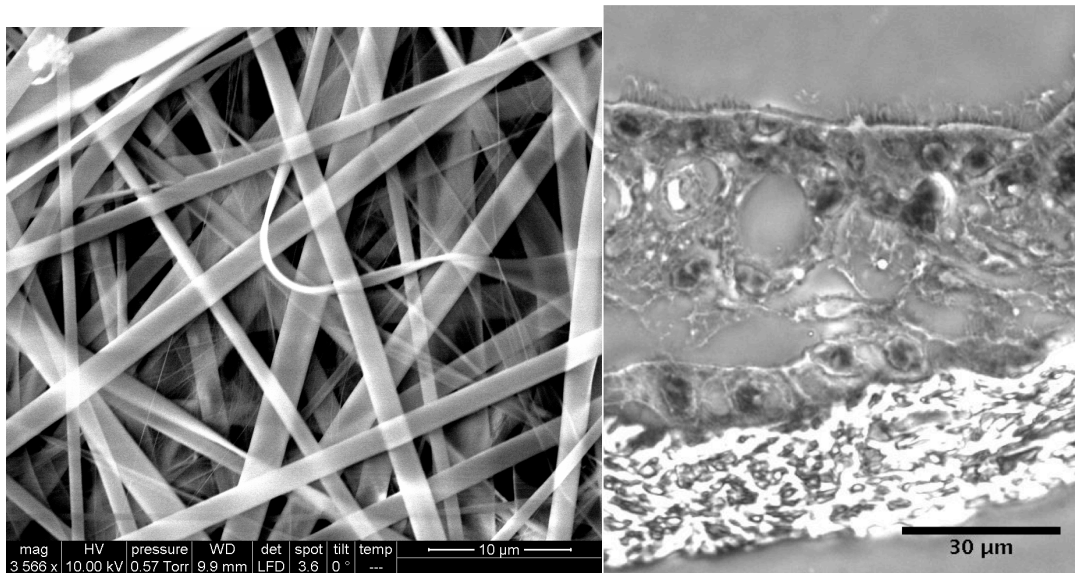


Figure 3.5 Left: SEM of an electrospun elastin-collagen scaffold. Right: Human Bronchial Epithelial cells grown on an electrospun elastin-collagen scaffold. Cilia are present on the cells, however, the cell layer shows evidence of delaminating.

These elastin-collagen scaffolds also supported HBE cell growth and differentiation (Fig. 3.5), but also suffered from the diminished optical properties. Additionally there were issues with long-term scaffold integrity and cohesiveness. Primarily due to the inferior optical properties, I decided to use the commercially available Millicell scaffolds for the mucus clearance assay. While this decision sacrifices the ability to stretch the system and to more closely match the modulus/properties of the substrate, the decision doesn't reduce the physiological relevance below that of existing models. Furthermore the system is designed in such a way that should a more appropriate substrate be developed, it can easily be incorporated into the existing system. As a final point, the choice to use the commercial membranes also set a size limitation on the device. The largest available membrane had a diameter of 30mm. Due to this constraint I decided on a channel width of 3mm and a length of about 15 mm.

Chamber

The chamber material is a key contributor to the cell microenvironment. First and foremost is the chamber's biocompatibility: the chamber will come into direct contact with the cell media and cell products. The material will also play a major role in determining the humidity, temperature, and gas concentration inside of the clearance assay. Polydimethylsiloxane (PDMS) is one of the most popular materials for microfluidic applications: In addition to being easy to use, it features excellent optical properties, is gas permeable, and has been used in several cell applications (Sia & Whitesides, 2003) . There have been reports of PDMS monomer leaching out of microfluidics devices and being absorbed by cells(Regehr et al., 2009). Despite

potential leaching I've been successful in growing viable, differentiated cells inside of my device. It would still prove useful, however, to investigate potential interactions between PDMS and HBE cells in future studies.

As with most mammalian cells culture, the HBE cells in the mucus clearance assay will be housed in an incubator that will maintain a constant temperature, humidity, and gas concentration. Fortunately the choice of PDMS does little to interfere with the incubator's role in maintaining environment. In a 2000 review of PDMS microfluidics devices, McDonald et al. explicitly mention that PDMS's low thermal conductivity of $.2\text{Wm/K}$ makes it ideal for an incubator environment (McDonald, Duffy, Anderson, Chiu, & Wu, 2000). Additionally the high gas permeability of PDMS allows the incubator to regulate gas concentration and humidity in the chamber.

The last major environmental concern is that of toxicity: materials used in the clearance assay need to be biocompatible. PDMS, glass, and the PTFE scaffold will be the main materials that come in contact with the cells and growth media and are all generally biocompatible. Additionally I'll also need components that act as interfaces from the chamber to the outside world. This includes tubing, valves and ports that may come into contact with media. I chose to use PVC tubing, nylon ports, and polycarbonate valves. All of these materials demonstrate excellent biocompatibility and medical grade parts are available commercially.

3.1.2 Cell perfusion rate to determine basolateral volume

The goal of the clearance assay is not to optimize the cellular metabolism (although it's certainly an interesting problem). Instead the goal is to match the

metabolic conditions in current cell culture models as closely as possible. I based my cell perfusion amounts on the protocols of the UNC CF Center Tissue Procurement and Cell Culture Core (Fulcher et al., 2005); this involved exchanging 10ml of culture medium every 2-3 days. This works out to about 1.5 ml of media for every square centimeter of cells. As each chamber would have a growing area of about $.45\text{cm}^2$ for cells, I needed a media reservoir of at least .75 ml per device to remain consistent with changing media 3 times weekly.

3.1.3 Experimental Requirements

In this section I discuss how experimental requirements shaped the final design of the Mucus Clearance Assay system. In moving through this section it is useful to broadly discuss experiments in the system and break them down into their constituent parts. This approach allows us to spot commonalities in the different types of experiments and tailor the system and external equipment to that part of the experiment. This assay's purpose is to explore ASL-cilia interactions. In following that purpose experiments will consist of varying the properties of the ASL or cilia and then observing how that property affects the mucociliary clearance process. Ideally this requires

1. Control over the ASL
2. Control over Cilia
3. Observation of the ASL
4. Observation of the Cilia

The experiments in this dissertation will focus on controlling properties of the ASL.

Controlling the cilia is a harder problem to solve, however, the bilayer channel

makes it possible to access both the apical and basolateral compartments of the channel. This access opens up the possibility of future experiments controlling cilia behavior by administering agents such as *Pseudomonas aeruginosa* II lectin or halothane, which have both been shown to arrest cilia beating (Adam, Mitchell, Schumacher, Grant, & Schumacher, 1997; Manawadu, Mostow, & LaForce, 1979).

Additionally as optical microscopy will be the primary method of observing/measuring the system, I will condense observation of the ASL and cilia into one section that looks at optimizing the optical properties of the clearance assay and building the optical system to make those measurements.

3.1.3.1 Controlling the Airway Surface Liquid

Controlling the parameters and properties of the airway surface liquid is an essential part of the mucus clearance assay. Specifically in controlling the ASL I want to maintain the ability to remove the endogenous ASL, add exogenous material or simulants, and add tracer particles. The novelty comes with adding the ability to drive fluid over ciliated cultures and to tilt the system to study the effect of drainage. Using a microfluidic bilayer system facilitates most of these abilities: the bilayer system is designed to exchange the fluid in the top compartment and to drive the fluid with a syringe pump. The only real effect that these parameters had on design was in choosing the ports used to access the top compartment. Ports are a notorious issue in the microfluidics community, however, embedded screw insulators under a layer of PDMS function as robust access ports (Liu & Moiseeva, 2008). These ports were mechanically stable in the PDMS, allowed easy connections to

external “plumbing”, and as an added bonus they allowed pipette access for exchanging fluids.

One concern is that the interface between the ASL and chamber sidewalls would change the liquid height due to the influence of wetting. I minimized this issue by making the chambers significantly wider than the anticipated liquid depth (5-20um of ASL depth as mentioned in chapter 2). While wetting would still occur at the walls, this ensured that there was a large region in the middle of the channel to study the drainage phenomenon. I decided to stretch the width of the channel 3mm so that there would be more available space in the “middle” of the channel away from the sidewalls.

3.1.3.2 Optimizing optics: integrating the MCA with a microscope

In addition to designing the mucus clearance assay, I also designed a companion microscope. The primary goal of this scope was to enable tilting experiments: the microscope would make it possible to observe the ASL and cilia while the channel was in a tilted configuration. An added bonus, however, is that I had the opportunity to customize the channel design to the microscope and vice versa. Customizing the channel for optical microscopy was fairly straightforward. PDMS has excellent optical properties, the most important part is making sure that any PDMS in the optical path was level and relatively smooth. A minor issue with PDMS is that it has a tendency to get dirty, so to prevent this and for added mechanical stability I used glass for the bottom surface of the device.

The other factor in optimizing the optics was the working distance between the objectives and the cell layer. I had already chosen to use an inverted microscope, (in anticipation of the ports and tubing on top of the clearance assay potentially crashing against objectives.) This made the height of the basolateral compartment beneath the cells important in regards to the working distance. Minimizing this height would enable me to

1. Get higher NA objectives with shorter working distances closer to the cell layer to improve the resolution of cilia and tracked particles
2. Look higher in the liquid layer above the cells (an important feature for mapping out flow profiles)

I reduced the height of the basolateral compartment by adopting a “dog-bone” design: the basolateral compartment was relatively thin underneath the cell layer, but had two large reservoirs on both ends of the channel.

In addition to modifying the channel, I also modified the microscope so that it was capable of drainage experiments with the clearance assay. A key aspect of the drainage experiments was performing PIV to quantify the fluid behavior while having the ability to measure the cilia beat frequency. This required that the lower optics system (objectives and the fluorescent source), the device, and the upper optics (bright field source, condenser, and phase rings) all had to move to maintain the same relative light path through rotation. To accomplish this a custom built harness was designed so that the entire microscope could rotate in place (Fig. 3.6).

The harness consisted of an elevated board, which attached to external pillars via two axles. The microscope was secured to the board and configured so that the assembly's center of mass was slightly below the axis of rotation. A large disc on the left axle was included so that the microscope and board could be locked into place at 0, 30, 45, 60 and 90 degrees (Fig. 3.6).

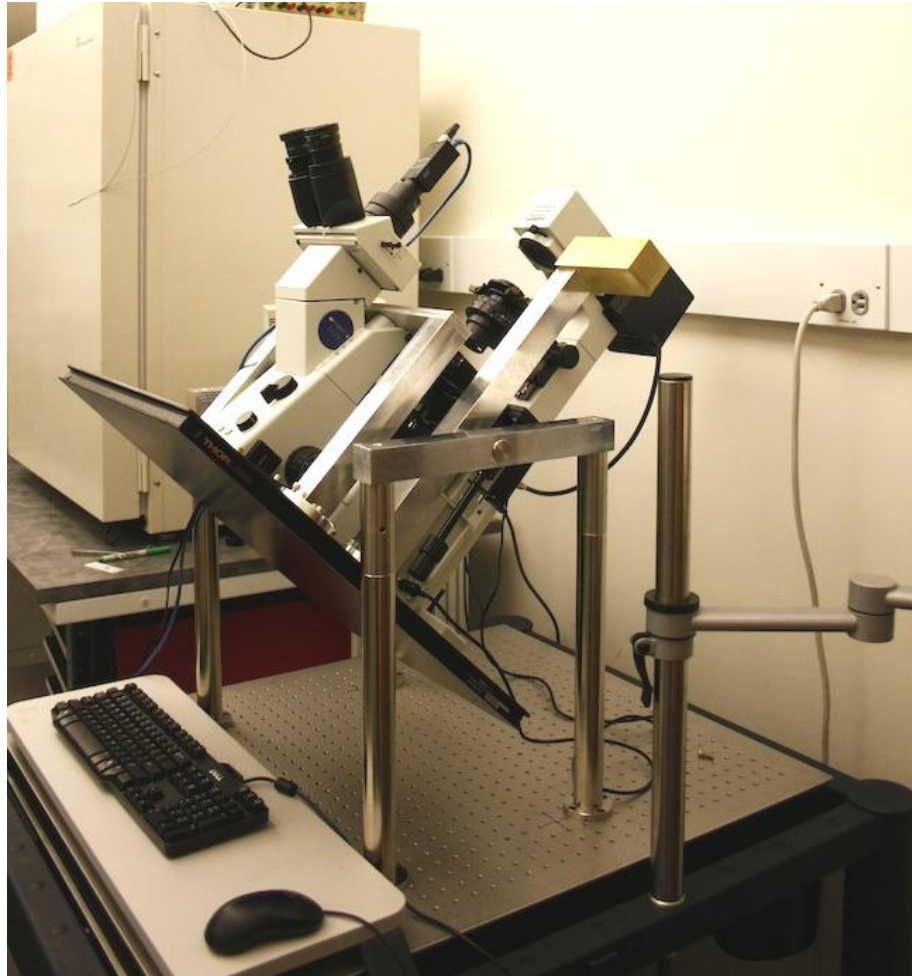


Figure 3.6 Tilting microscope "Ixion". Capable of performing both bright field and epifluorescent imaging while rotated at angles of 0,30,45,60, or 90 degrees.

One final adjustment was to secure the MCA device to the tilting microscope. I accomplished this by locking the normal stage in place and building a custom stage

with a positioner and MCA holder built via 3d printing (Stratasys, Dimension 1200es)
(Fig. 3.7).

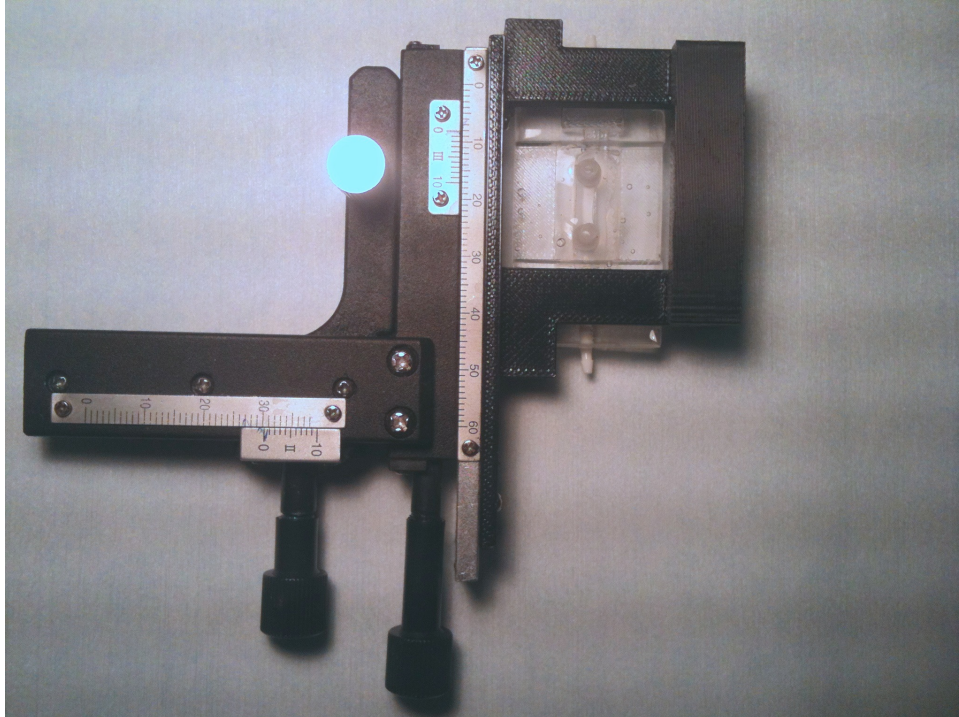


Figure 3.7 Custom built stage to secure the MCA device to the tilting microscope.

3.2 Channel Fabrication and Assembly

The following sections detail the fabrication process of the Mucus Clearance Assay. The device was composed of 2 parts that were individually molded and then assembled.

3.2.1 Mold Fabrication

Molds were designed using Google SketchUp (Fig 3.8) and then fabricated using a 3d printer (Stratasys, Dimension 1200es).

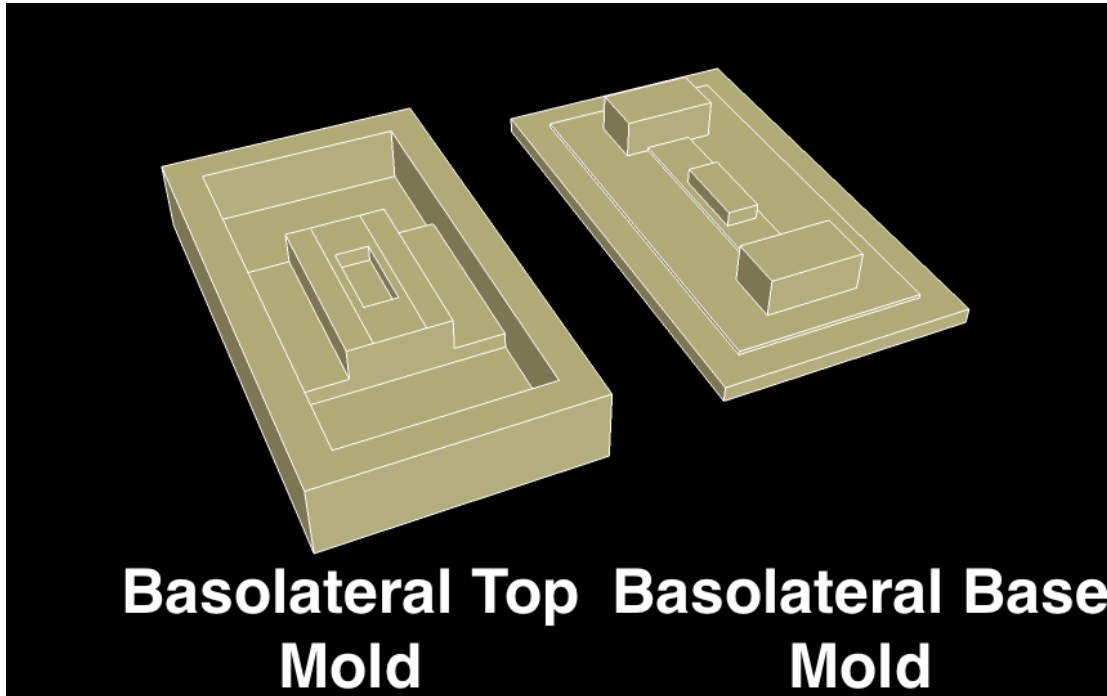


Figure 3.8 Early mold designs generated with Google SketchUp. Models were exported to .stl files and prototyped via 3D printer.

One of the most important features of the mold material was a smooth surface. Smooth surfaces were essential for plasma bonding surfaces together and for optical clarity in the final device. ABS plastic, the material used in the rapid prototyping system had a rough surface, however, it could be smoothed with a combination of acetone and sanding. This produced decent devices, but ultimately I discovered that acrylic was an excellent material: it produced smoother parts and it was easier to release PDMS from the acrylic surface. For any parts of the mold that needed to be smooth for optical clarity or bonding to another material, I used the

acrylic instead of the ABS plastic. Final molds were a combination of acrylic bases bound to ABS plastic parts with epoxy (Fig. 3.9).

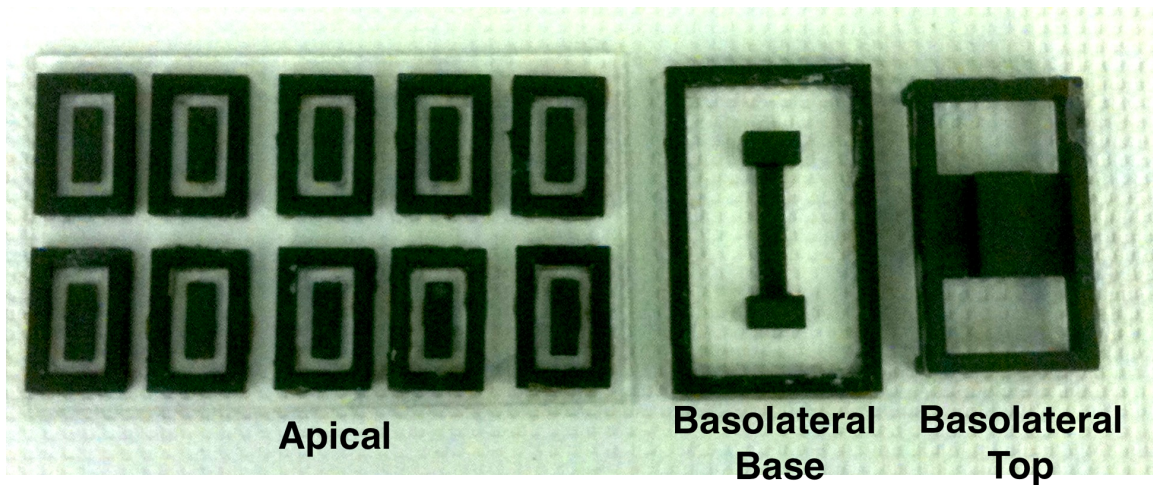


Figure 3.9 Various molds used in fabricating the Mucus Clearance Assay. Molds are a combination of rapid prototyped ABS plastic and sheets of acrylic. The left-most mold is designed to make the apical part of the bilayer channel, while the two parts on the right are for the basolateral chamber.

3.2.2 Channel Fabrication

The Mucus Clearance Assay consists of two separate units; a basolateral compartment to house media and an apical chamber for cell growth. Each unit was fabricated by casting PDMS into the previously described molds. The body of the apical compartment was created using a 2 step molding process as detailed in figure 3.10. This body was then attached to a millicell scaffold.

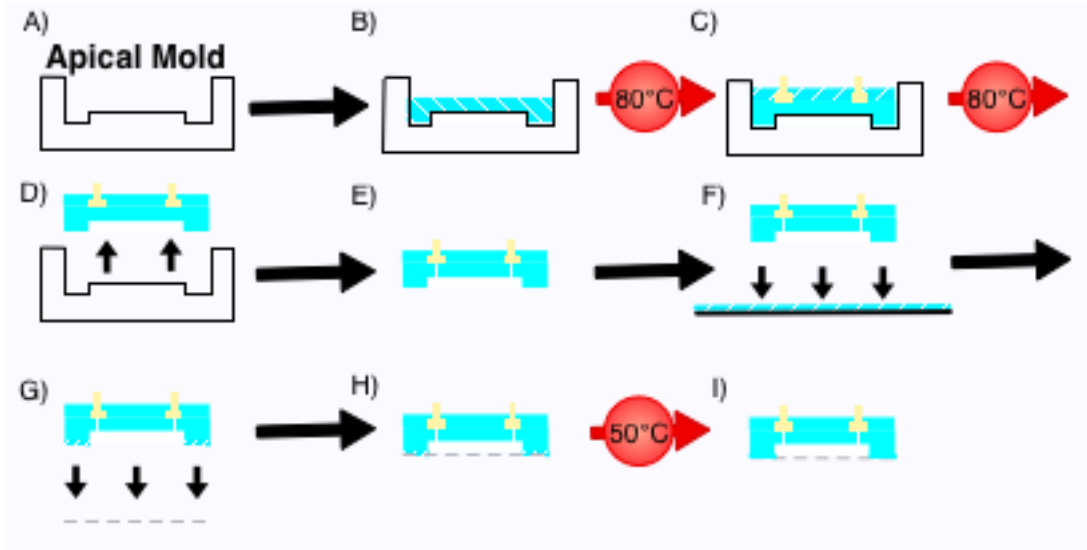


Figure 3.10 Processing steps to mold the apical compartment of the bilayer channel. A) The process starts with the apical mold. B) PDMS is poured into the mold and cured at 80°C for 1 hour. C) Screw insulators are placed on top of the cured PDMS and more PDMS is poured to embed the feet of the insulators. The PDMS is cured again at 80°C for 1 hour. D) The device is removed from the mold E) Holes are punched with a 2mm biopsy punch to make a path through the screw insulator into the channel region. F) A thin layer of PDMS is prepared via spin coating, Uncured PDMS was spin-coated on a glass slide at 1200 RPM for 60 seconds. The bottom of the channels was stamped into this thin PDMS layer. G) The stamped channel is pressed onto a millicell scaffold. H) The channel is cured in the oven at 50°C for 2 hours (the lower temperature is to prevent scaffold degradation) to produce I) The final apical compartment.

The basolateral chamber was produced by attaching a molded PDMS chamber to a glass slide as detailed in figure 3.11. The apical and basolateral ports were glued together with PDMS to produce the final device seen in figure 3.12.

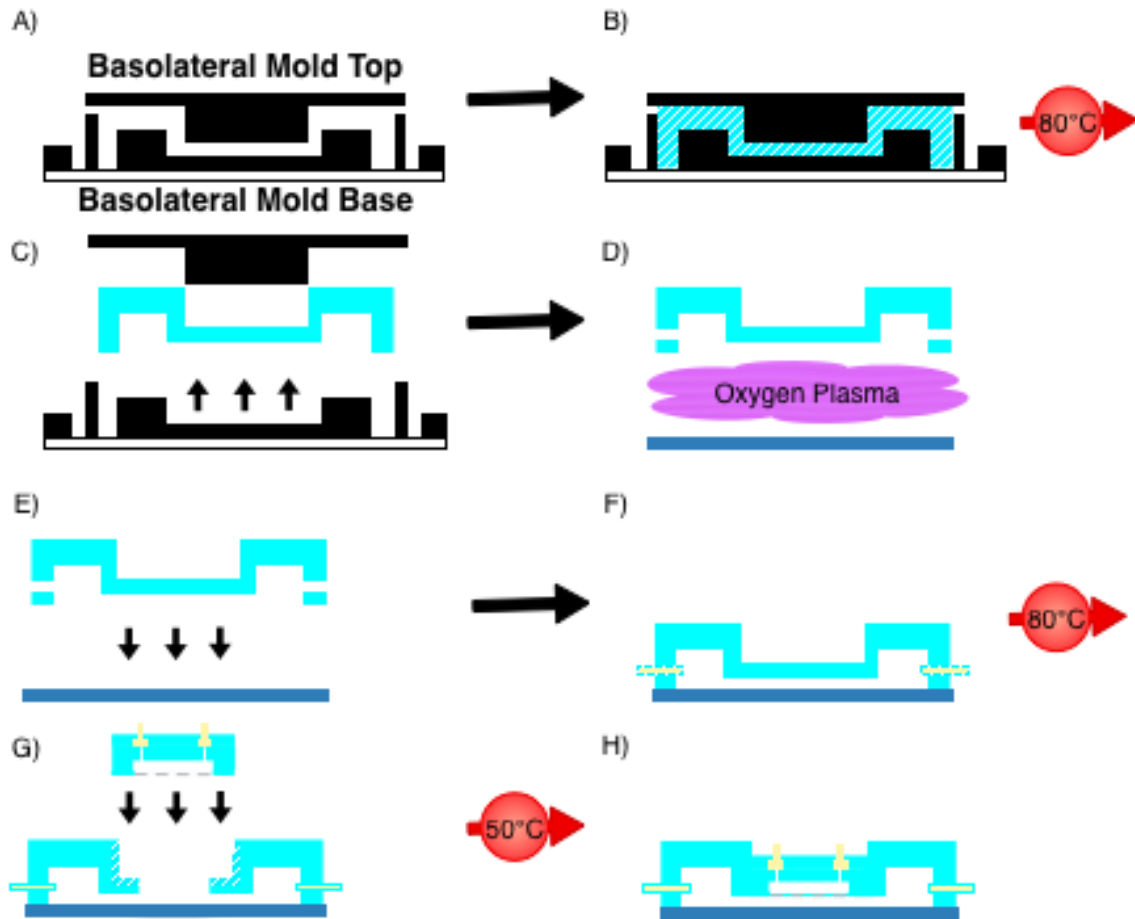


Figure 3.11 Processing diagram for the basolateral chamber and final chamber assembly. A) Starting with the combined Acrylic/ABS plastic hybrid mold B) PDMS was poured into the mold and cured at 80°C for 1 hour. C) The PDMS was removed from the mold assembly and a biopsy punch was used to make holes into the reservoir of the chamber D) The PDMS and a glass slide were both cleaned with isopropyl alcohol and methanol and exposed to a 10W oxygen plasma, which activated both surfaces. E) The activated PDMS was pressed against the activated glass slide to create a permanent irreversible bond. F) Uncured PDMS was placed around 1/16" hose barb adapter and placed into the reservoir holes. The system was then cured at 80°C for 1 hour. G) The basolateral chamber was "painted" with uncured PDMS, the apical compartment was lowered onto this uncured PDMS and the entire assembly was cured at 50°C for 2 hours to produce H) the completed Mucus Clearance Assay device

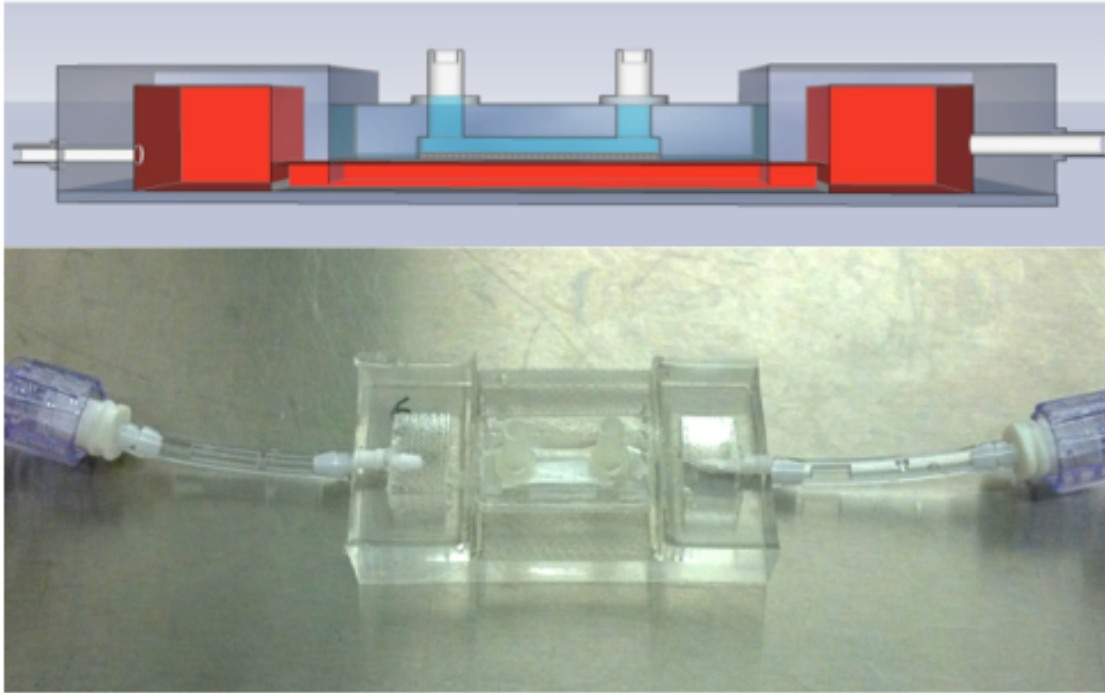


Figure 3. 12 Top: Cross section of the Mucus Clearance Assay. The basolateral chamber is colored in red, while the apical chamber is colored in light blue. Bottom: The completed Mucus Clearance Assay device. Tubing and valves have been connected to the basolateral ports.

3.3 Ciliated, transporting cultures in the Mucus Clearance Assay

After building MCAs, I sterilized them using the methods in section 3.5.1 and grew HBE cell cultures in the channels according to section 3.5.2. I then evaluated the confluency/viability of the cells, and then saw differentiation as well as long range transport in the cultures.

3.3.1 Cells span the MCA chamber and can be patterned

Approximately a week after seeding the cells into the MCA, I used the procedure in section 3.5.3 to look at the confluence and viability of the cell cultures. Figure 3.13 is a fluorescent image showing living cells (green) and dead cells (red).

While there are some areas showing cell death, in general the culture was largely viable. Most importantly the cells consistently spanned the scaffold and were “patterned” into the rectangular shape of the channel after growing for a week in the device.

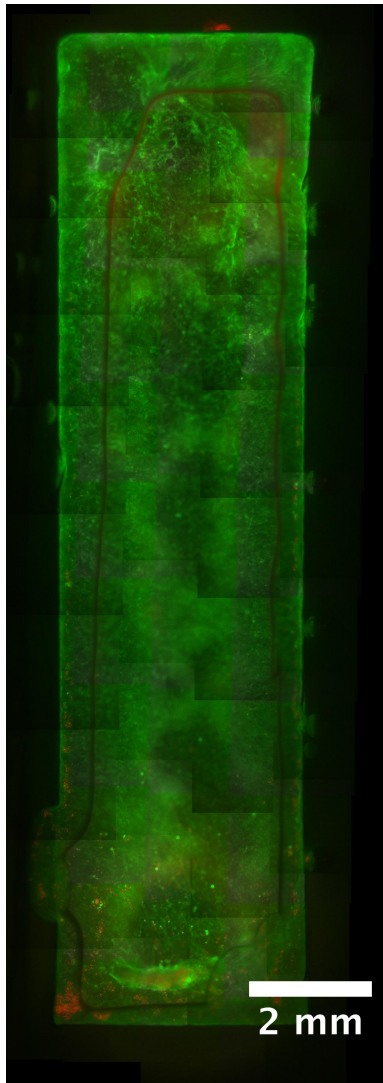


Figure 3.13 A composite image showing a live/dead assay of an entire channel. Live cells show up as green while dead cells are red. The majority of cells are alive and they have spanned the entire channel.

Additional experiments that I performed (although not appearing in this dissertation) demonstrate that I could pattern the cells into more complicated patterns such as the “Y” junction shown in figure 3.14.

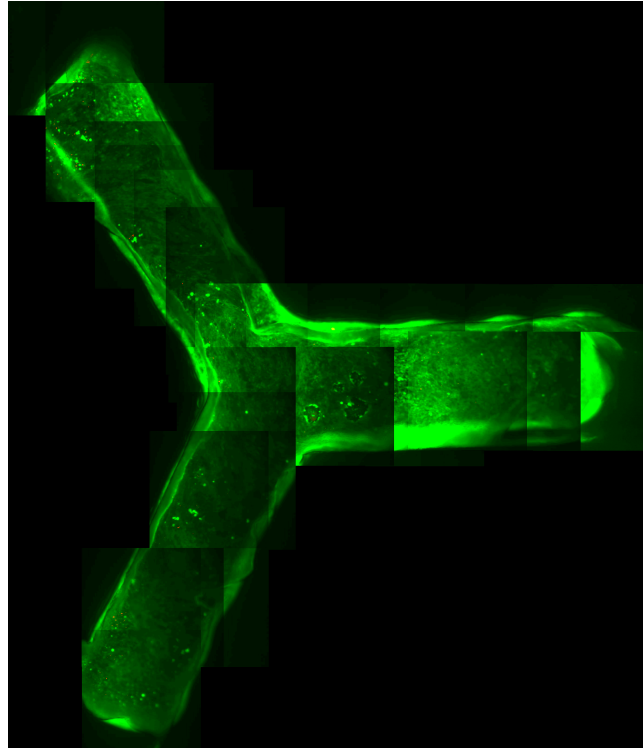


Figure 3.14 A composite image of a live/dead assay of HBE cells forming a Y junction. HBE cells can be patterned into arbitrary shapes simply by designing the appropriate mold for the apical channel.

3.3.2 MCAs differentiate and produce regions of long range transport

After the cells reached confluence in the channel, they were kept at an Air-Liquid interface. Soon after, the cultures in the Mucus Clearance Assay started producing mucus (first observed by the filance or forming of strands of the extracted ASL) and cilia. Sections 3.4.4 and 3.4.5 detail the procedures I used to measure ciliation as well as determine the flow in the channels. After regions of dense ciliation appeared in the MCAs I mapped channel flows. I often observed large coordinated

regions of cilia (spanning a few millimeters) pushing fluid down the axis of the channel (Fig. 3.15). While some coordination is known to happen in *in vitro* systems, e.g. mucus hurricanes (Matsui, Randell, Peretti, Davis, & Boucher, 1998b), the long linear coordination seems to be unique to this clearance assay. This didn't occur in every single channel, but such areas were typically found in the well-ciliated channels. Hurricanes also spontaneously formed in some MCA devices. During the course of the dissertation work, the availability of the regions of long-range transport was sufficient to proceed with further experiments. As a result I never explicitly determined the cause of the entrainment. My best guess is that the first cilia to sprout in the channel were randomly oriented, but due to wall effects of the rectangular channel, they generated a flow with a major component down the axis of the channel. Subsequent cilia would experience the shear-stress from this generated flow and entrain along the same direction. This is consistent with the entrainment mechanism discussed in 2.3.2. Another potential hypothesis is that draining fluid provided a background flow to entrain emerging cilia. The MCAs were kept on a 60° incline while in the incubator, the intention being that any generated Airway Surface Liquid would drain down the channel and apply an entraining shear-stress to cilia. Future studies should focus on improving control over cilia entrainment. In chapter 4 I discuss applying external fluid flows over the apical compartment, a capability that will prove useful in furthering entrainment studies.

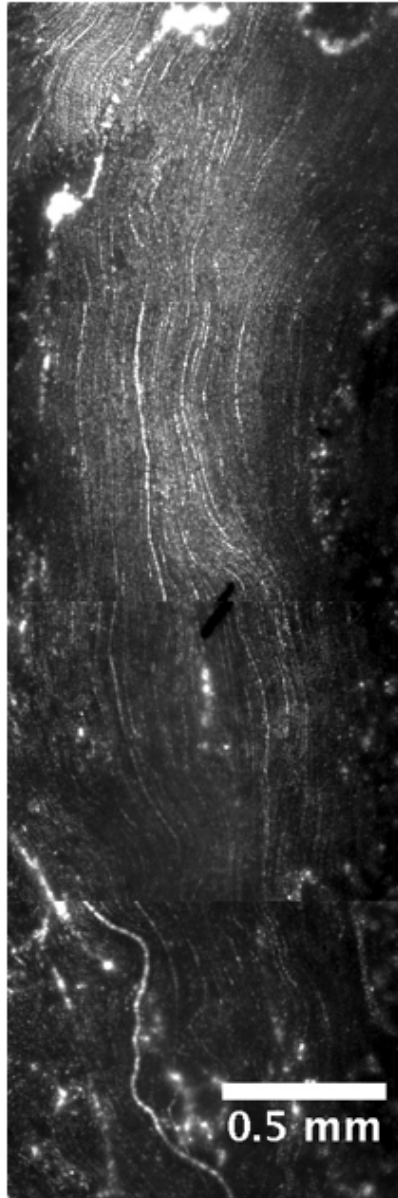


Figure 3.15 Maximum intensity projection (MIP) of fluorescent bead transport in a MCA device. The MIP of the fluorescent beads produces streaklines of the cilia driven flow. Frequently devices had regions spanning more than a few millimeters where cilia driven flow was aligned down the axis of the channel. Future studies will explore the effect of channel dimensions and aspect ratio on cilia entrainment.

3.4 Conclusion

In this chapter I was able to build upon existing *in vitro* models to create a mucus clearance assay. The primary advantage of the clearance assay is that it enables new experiments by incorporating external fluid flow, and drainage into a cell culture system. In designing the system I made it flexible enough to incorporate elements that would make the system more physiologically relevant, and enable further experiments using the system. I also demonstrated that the system was capable of growing well differentiated, well-ciliated cells and that I could measure properties of both the cilia and the ASL. Going forward I use this system in the following chapters to investigate the mucociliary apparatus. Chapter 4 examines the flow in the device in detail and uses external flow to learn about the cilia tips as a boundary. Additionally the system is adapted in such a way that the external flow can be used as a tool to identify and quantify biochemical interactions in the system. Chapter 5 uses the device as a true clearance assay: tilting proves to be an effective way to determine whether or not mucus and mucus simulants can be transported by the cilia against gravity.

3.5 Methods

3.5.1 Channel Sterilization

Initial channel sterilization was accomplished via Ethylene Oxide gas. Ethylene oxide is known to linger in PDMS/silicone rubber systems (Roberts & Rendell-Baker, 1972), so after treatment, the channels were aired out in a sterile environment. Following sterilization, a stock solution of Human Placenta Collagen

Type IV (Sigma C-7521) was used to treat the apical compartment. I pipetted 100ul of the collagen solution onto the millicell scaffold and allowed it to dry overnight. The next morning any excess fluid was removed and the channel was sterilized with a 30 watt UV light (Bulbtronics, G30T8) for 30 minutes. At the same time any external tubing and valves were sterilized with a 70% ethanol solution and then rinsed with Phosphate Buffer Saline (PBS). The tubing and valves were then attached to the mucus clearance assays.

3.5.2 Growing cells in the Clearance Assay

Human Bronchial Epithelial cells (HBE) were acquired from the UNC CF Center Tissue Procurement and Cell Culture Core after the cells' first passage. The cells were suspended in ALI so that there were approximately 250,000 cells per 100uL; this allowed me to maintain a seeding density above the density commonly used for the millicell inserts inside of the limited volume. I seeded 250,000 cells into each apical compartment, and then covered the access ports with PDMS caps to prevent contamination. The basolateral compartment was filled with 1mL of Air-Liquid Interface (ALI) media. The cells were allowed to settle and attach to the scaffold for a period of 24 hours, at which time the apical compartment was washed with PBS and filled with fresh ALI media. From this point on the media in the basolateral compartment was exchanged 3 days a week, typically on Monday, Wednesday, and Friday. The media in the apical compartment was exchanged every other day for the first week, but after the cells reached confluence, an air interface was maintained in the apical compartment. Any accumulated ASL fluid was pipetted out of the channels daily. The apical compartment was washed with PBS

once a week. The cell cultures were incubated at 37C, 96% humidity and 5.0% CO₂.

3.5.3 Cell viability and confluence

Cell viability was assessed using a live/dead cell assay kit (Invitrogen L3224). A buffer solution with 4uM Calcein-AM and 2uM Ethidium homodimer was pipetted into the apical compartment of each channel. After 15 minutes the solution was removed from the channel and replaced with buffer. Channels were examined under fluorescence and the images were processed using ImageJ(NIH). In order to map the channels e.g. Fig 3.14, the channels were manually translated so that there was an approximate 25% overlap between adjacent fields of view. At each field of view, an image was taken in both the red (617nm) and green (515nm) channels for Ethidium Homodimer and Calcein AM respectively. The images were stitched together using Adobe Photoshop and each image was imported as a layer and overlaid against its neighbors to confirm image registration.

3.5.4 Measuring Ciliation

In order to understand the role of cilia in propelling mucus forward, it is essential to have solid measurements of the Cilia Beat Frequency (CBF) and the ciliated cell density. During the course of this dissertation work, I employed several methods to assess CBF and ciliated cell density. The first approach that I used was simply taking high frame rate videos and counting cilia strokes. Using the 40X objective made it easy to resolve sparse individual cilia. Making certain assumptions about the beat pattern and beat frequency from literature, a 90 fps camera was more

than adequate for temporal resolution of individual cycles. In general this method worked well for sparse samples, but became increasingly difficult for denser cilia samples. Additionally getting a complete picture of all the cilia in a field of view would be prohibitively time intensive with this method.

The next step was to automate the counting process to easily capture the cilia dynamics of larger fields of view. In order to do this I used a method similar to the system/methodology developed by Sisson and Ammons (although their exact algorithm isn't available, the general methodology is the same)(Sisson, Stoner, & Ammons, 2003). In general the method is to take a video of cilia and look at the light flickering/modulation of the cilia. Using spectral analysis, it's possible to pull the frequency with the strongest signal, which should be the cilia beat frequency. Specifically I imported a video into MATLAB and essentially used the above process for each individual pixel of the video. For every pixel I had its intensity fluctuation as a function of time Fig 3.16. Next I smoothed the data and subtracted a line with endpoints that were the beginning and end point of the data (this step removes low frequencies that would be generated by this discontinuity). Next I applied a Gaussian window to the data and performed a Fourier transform on the processed data (also seen in Fig 3.16). In order to select peaks, I used MATLAB's built in peak detector, but I made sure that the largest peak was a certain number of standard deviations larger than neighboring peaks to discriminate against noise. Although this metric was somewhat arbitrary, its biggest effect is on calculations of density, not beat frequency. This technique produced a pixel-level map Fig 3.16 that showed beat frequency across the field of view. It made it possible to not only see the beats of

individual cilia, but also to see that neighboring patches of cilia were beating at different frequencies. I was also able to calculate % ciliation by comparing the number of pixels in the field of view with cilia activity against the non-active pixels. Although the CBF method is extremely useful, there are some flaws and artifacts with this approach. It's important to remember that I am indirectly measuring CBF and actually measuring fluctuating light intensity. An example of such an artifact is that if 2 cilia overlap and modulate the light over the same region of space, that pixel would actually show double the cilia beat frequency.

An additional concern is that as a cilium moves in and out of focus, there could be edge effects in the light intensity: in one stroke a cilium would approach the imaging plane out of focus, cross the imaging plane and return to the same out of focus intensity, then on the return stroke do the same. Overall the methodology gives a lot of insight and information into the system, but it should by no means be accepted as a perfect answer.

One last approach used to measure the beat frequency is a more refined (and serendipitous) version of the counting method. After adding beads to the system, an occasional bead would stick to a cilium. Tracking the stuck bead made it possible to finely watch the location of the cilia and to effectively count the beat strokes. Again this method isn't without flaws; it requires the assumption that the tethered bead isn't changing the beat frequency and that the bead is tethered to one cilium. Overall the best methodology was to use a combination of the above methods to determine CBF. The counting methods were useful for quick estimates, but also were valuable tools in verifying the results given by the image intensity spectral analysis.

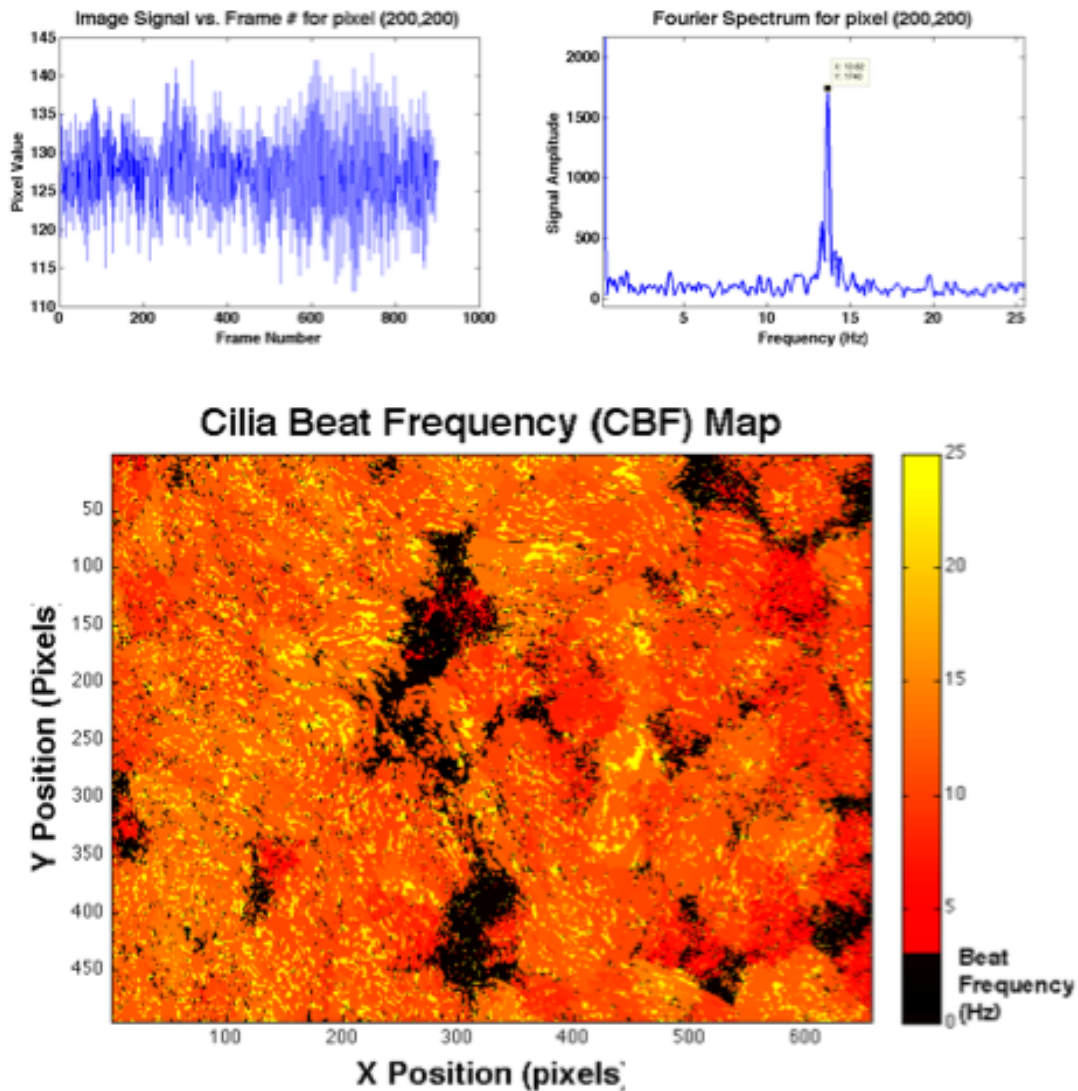


Figure 3.16 Processing used to measure Cilia beat frequency (CBF) in the MCA. Top left: The trace of light intensity for an individual pixel in a movie. Top Right: Fourier spectrum of the light intensity of a single pixel over the course of a video. Bottom: A CBF map constructed by choosing the highest discernable peak for each pixels light intensity Fourier spectrum.

3.5.5 Measuring ASL flow with PIV

I used particle image velocimetry (PIV) to ascertain the flow properties of the ASL inside of the MCA device. I added a 2 μm , fluorescent bead solution at a

concentration of 1:200 in PBS into the apical port. The beads were recorded and tracked via the Computer Integrated Systems for Microscopy and Manipulation's (CISMM) Video spot tracker program. The optical setup allowed me to successfully track 2 μ m beads at a 4x magnification. I developed several MATLAB scripts to further process the tracking data and determine the average velocity of beads in differing spatial bins in the video. Using this technique I was able to determine the properties of the cilia driven flow. I also typically mapped the cilia driven flow in channels to determine the best locations to perform experiments.

Chapter 4 Cilia and Fluid Flow: Building a model for the bilayer channel

In this chapter I discuss my work in attaching the mucus clearance assay system to an external flow system. This represents the first time that a well-ciliated, well-differentiated human bronchial epithelial cell culture has been integrated with a fluidics channel. I begin by characterizing fluid flows in the system and comparing them to well known canonical models. I then use these models to perform experiments to probe several aspects of the interaction between cilia and the airway surface liquid: specifically

- *How does heterogeneity in cilia spacing and frequency affect transport of the ASL? In what sense can the cilia tips be coarse grained into a single boundary?*
- *How does the cilia tip boundary condition respond under loading?*
- *What are the adhesive forces between constituents in the ASL and the epithelial surface?*

Performing these experiments I observed

1. Lateral heterogeneity in cilia distribution and beating influences heterogeneity in particle transport at the cilia tips. This heterogeneity diminishes as the distance above the cilia tips increases.
2. Coarse graining the cilia boundary layer produces flow profiles consistent with canonical models
3. External flow can be used as a tool to determine the adhesive forces between moieties functionalized on bead surfaces and moieties native to the epithelial surface.

These experiments allowed me to apply a simple model of the cilia boundary condition to the MCA and test the model with conditions not available in prior *in vitro* studies, namely external flow (this chapter) and gravity (chapter 5). Finally the development of the adhesion assay serves as a platform to study the cilia tip boundary further. The assay achieves this by identifying and quantifying adhesive interactions between the cilia and constituents of the ASL.

4.1 Fluid Mechanics Primer

The following serves as a quick background of fluid mechanics that introduces 3 canonical models derived from the Navier-Stokes equation that I will use to model the fluid flow in the mucus clearance assay.

4.1.1 Navier-Stokes

The Navier-Stokes equation (equation 4.1), the equation of motion for a fluid system, can be derived from conservation of mass, momentum and energy,

$$\rho \left(\frac{\partial v}{\partial t} + v \cdot \nabla v \right) = -\nabla p + \mu \nabla^2 v + f \quad (4.1)$$

A careful derivation can be found in Batchelor's *An Introduction to Fluid Dynamics* (Batchelor, 2000), but equation 4.1 is ultimately Newton's second law (for an incompressible fluid); the momentum change of a fluid element is equal to the net forces acting upon it. On the left hand side of the equation we see the fluid's density is multiplied by the linear acceleration and convective acceleration to account for changes in linear and angular momentum respectively. These terms can also be thought of as a measure of linear and nonlinear inertia. The terms on the right hand side are the forces experienced by that body element: the pressure gradient (normal stress) acting on the element, the shear-stresses acting on it and any external body forces (such as gravity) that might act upon it. Equation 4.1 can further be simplified by making the following three assumptions.

Steady flow: If we assume that we have steady flow, a condition where the velocity doesn't change with respect to time, then we can set the $\frac{\partial v}{\partial t}$ term to 0.

Uniform Flow: The uniform flow assumption allows us to set the convective acceleration term, $v \cdot \nabla v$ to 0, it assumes that the convective acceleration term is negligible compared to the viscous term on the right hand side of the equation. A scaling argument can be used to estimate the relative magnitudes of the terms. The convective acceleration has a magnitude of $\rho v^2/l$, where v is the velocity and l is a length scale. Using the same convention, the viscous term has a magnitude of $\mu v/l^2$.

We can setup a ratio of the inertial term over the viscous term to gauge their importance. This ratio called the Reynolds number (Re) is

$$Re = \frac{\rho v l}{\mu} \quad (4.2)$$

In a higher Reynolds number system $Re \gg 1$ inertia dominates and the flow is turbulent. In lower Reynolds number systems viscosity dominates over convective acceleration and the flow is laminar. Likewise in a low Reynolds number system, the convective acceleration term is negligible compared to the viscous terms and can be set to 0. To demonstrate that flow in the bilayer system will operate in the low Re number regime we can do a ballpark estimate of the system using PBS as a buffer ($\rho \approx 1000 \frac{kg}{m^3}, \mu \approx 1 \times 10^{-3} Pa \cdot s$) moving at a velocity of $100 \mu m/s$ from cilia driven flow in a channel of characteristic length (height) of 1mm. This calculation yields a Reynolds number of .1, meaning that we are in a laminar flow regime. It's also worthwhile to note that a fluid with a higher viscosity, e.g. on the order of mucus' viscosity, would have a smaller Reynolds number and still fall into the laminar regime.

No external body forces: For now I will only look at the system in a horizontal configuration, so we can ignore gravity for now and set $\rho X = 0$. I will, however, reintroduce gravity as a body force in chapter 5.

Applying these 3 assumptions

1. $\frac{\partial v}{\partial t} = 0$
2. $v \cdot \nabla v = 0$
3. $f = 0$

the Navier-Stokes equation simplifies to

$$\nabla p = \mu \nabla^2 v \quad (4.3)$$

which is also known as the Stokes equation. The vector form of the Stokes equation can also be expressed by the following equations in Cartesian space.

$$\frac{\partial p}{\partial x} = \mu \left(\frac{\partial^2 u}{\partial x^2} + \frac{\partial^2 u}{\partial y^2} + \frac{\partial^2 u}{\partial z^2} \right) \quad (4.4)$$

$$\frac{\partial p}{\partial y} = \mu \left(\frac{\partial^2 v}{\partial x^2} + \frac{\partial^2 v}{\partial y^2} + \frac{\partial^2 v}{\partial z^2} \right) \quad (4.5)$$

$$\frac{\partial p}{\partial z} = \mu \left(\frac{\partial^2 w}{\partial x^2} + \frac{\partial^2 w}{\partial y^2} + \frac{\partial^2 w}{\partial z^2} \right) \quad (4.6)$$

Where u , v , and w are the velocity components in the x , y , and z directions respectively. This simplified version of the Navier-Stokes equation with the non-linear terms removed makes it possible to derive exact solutions using boundary conditions. Additionally the linearity allows these solutions to be added together. The following sections discuss a few of the exact solutions of the Navier-Stokes equations that will be useful in evaluating fluid flow in the bilayer system.

4.1.2 Poiseuille flow

The first exact solution of the Navier-Stokes equations that I'll discuss is Poiseuille flow. In Poiseuille flow, the flow is generated via a pressure gradient along the direction of the flow, a situation often found in pipes. Similarly this can be used to model the flows created by pressure gradients along the axis of the MCA channel. Starting with our Cartesian Navier-Stokes equation, there are a couple of further assumptions that we can use to simplify the system. We'll only consider a 2d model for now, and there will only be flow in the u direction.

This allows us to simplify Equation 4.4-6 to

$$\frac{\partial p}{\partial x} = \mu \left(\frac{\partial^2 u}{\partial y^2} \right) \quad (4.7)$$

Integrating this equation twice with respect to y , we can solve for u and we get

$$u = \frac{1}{2\mu} \left(\frac{\partial p}{\partial x} y^2 + c_1 y + c_2 \right) \quad (4.8)$$

We can then invoke the no-slip boundary condition at both plates to solve for the constants and we are left with

$$u = \frac{1}{2\mu} \frac{\partial p}{\partial x} y(y - h) \quad (4.9)$$

Thus we see that Poiseuille flow results in a parabolic flow profile.

4.1.3 Couette Flow

The next exact solution, Couette flow occurs when we remove the pressure gradient from the system and change our boundary conditions. Instead of having both plates stationary, we now give one of the plates a velocity v . The no-slip boundary condition at this plate means that the fluid at the plate is now moving at velocity v in the lab frame. We can use this as a first approximation of cilia driven flow by abstracting the cilia tips at the bottom of the channel into a plate translating along the direction of the effective stroke. Starting with Equation 4.8 with the pressure term omitted, we have

$$u = \frac{1}{2\mu}(c_1 y + c_2) \quad (4.10)$$

Applying the boundary conditions $u(0) = 0$ and $u(h) = v$, we are left with

$$u = \frac{v}{h}y \quad (4.11)$$

Equation 4.11 shows us that Couette flow gives us a linear flow profile that is independent of the viscosity. It should be noted that the viscosity disappears because we have assigned one of the plates to move at a constant velocity; the amount of shear required to accelerate the plate to that velocity, however, is dependent on the viscosity.

4.1.4 Couette + Poiseuille Flow

If we combine the constraints of Couette flow and Poiseuille flow, we get a flow profile that takes on the characteristics of both. As stated before, the linearity of the individual solutions allows superposition of the solutions. If we return to equation 4.8 and keep the pressure term, while again changing the boundary conditions so that one of the plates moves at velocity v , we get

$$u = \frac{1}{2\mu} \left(\frac{\partial p}{\partial x} y^2 + c_1 y \right) \quad (4.12)$$

Where

$$c_1 = \frac{2\mu v}{h} - \frac{\partial p}{\partial x} h \quad (4.13)$$

Equation 4.12 can be expressed as to

$$u = \frac{v}{h} y + \frac{1}{2\mu} \frac{\partial p}{\partial x} y(y - h) \quad (4.14)$$

We can see that Couette + Poiseuille flow is the addition of Equations 4.9 and 4.11. So similarly the flow profile will look like the Poiseuille parabolic flow skewed by the linear Couette component. We will use this to model the combination of the cilia driven Couette-like flow along with any pressure drive Poiseuille flows.

4.2 Initial Channel Fluid Characterization (no external flow)

To begin characterizing the system I took initial measurements of the system without any external flow. Due to the uncertainty of the native ASL composition and rheology, this experiment and all following experiments were stripped of their native ASL and buffer was added apically (see methods in section 4.6.1).

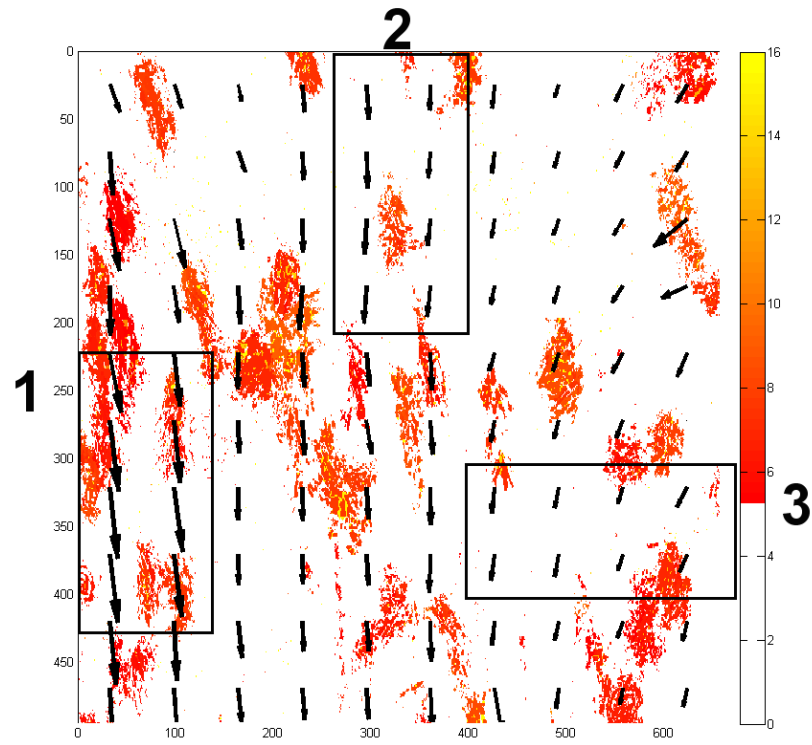
4.2.1 Lateral Heterogeneity of particle velocity due to variations in cilia diminish as a function of height

In the first experiment I examine the lateral heterogeneity in cilia activity and how that heterogeneity affects fluid flow. The ultimate goal of this exercise is to understand in what sense the cilia tips can be coarse-grained and modeled as a singular boundary condition.

I identified regions on the apical surface and used my cilia beat frequency script to generate a map of activity in the cilia mat. Next I performed the same flow profile analysis for each of those spatial regions thus getting a flow profile for the fluid column above each region.

Lateral heterogeneity diminishes as a function of height; near the surface I identified regions where the beads differed in speed by a factor of three. This speed difference, however, diminished away from the cell layer. In buffer the velocities converge well before the boundary condition at the ceiling of the channel, despite large differences 20 microns above the surface (Fig. 4.1). Although the highest data points converge at a height of 200um with a speed of "0", above this point I also saw a recirculation of fluid. This experiment shows that despite surface differences, fluid flow will converge to a uniform value at a distance above the surface. It follows that this distance should diminish as the uniformity of the surface increases. Furthermore

the accuracy of any course-graining model will improve as a function uniformity and distance away from the surface.



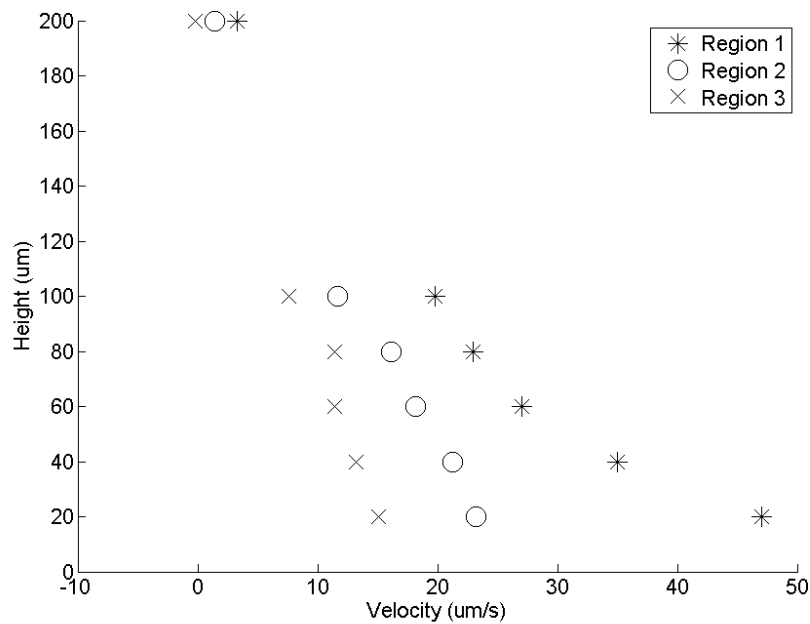


Figure 4.1 Correlative microscopy showing lateral heterogeneity at the cell surface Above) Cilia Beat Frequency (CBF) data overlaid with a velocity field of tracers near the cilia tips. Below) A flow profile for regions of different ciliation starts off heterogeneous near the cell surface, but becomes uniform farther away from the cilia tips.

4.2.3 Channels take on a Couette-Poiseuille flow profile in the absence of external flow

In this experiment I coarse-grain the cilia into a singular boundary condition and use this to model a Couette-Poiseuille flow profile for the entire channel. I used the methods in section 4.6.1 and generated the flow profile in figure 4.2. The first thing that jumps out is the bead velocity near the cilia floor: the average bead velocity increases as we move away from the cilia tips. As this is a closed system and the flow is cilia driven, I attribute this to lateral heterogeneity near the cilia tips. This explains the “hook” in the data set: near the cilia tips my region of interest has a lower average velocity than neighboring regions, however, this difference diminishes as we move away from the cilia tips. For now I’ll start at 40um above the cell layer

with the assumption that this height is sufficient to reduce the lateral heterogeneity in this particular area of the channel. Starting at this height, as we move further away from the cilia tips we see a reduction in velocity, until the velocity ultimately becomes 0 at around 250 μ m above the cilia tips. Moving further still, the velocity becomes negative (relative to the cilia driven flow). In explaining this profile, we start with the Couette solution. As discussed in section 4.1.3 Couette flow is the result of one of the boundaries moving at a constant velocity and the fluid's no-slip condition at that boundary. While there is a no-slip boundary at each individual cilium, the spacing of the cilia tips makes the use of a no-slip boundary a poor assumption (Blake, 1972). Instead we can borrow concepts from the traction layer mathematical models of clearance (Keller & Wu, 1975; D. J. Smith, Lubkin, Gaffney, & Blake, 2007). The traction layer models the ASL as 3 separate fluids, the PCL, a traction-layer, and a viscoelastic top layer. The traction layer is essentially an expanded interface between PCL and ASL; cilia penetrate into the bottom of the traction layer and apply a shear force along the direction of the effective stroke. The entire traction layer is then modeled as a coarse graining of the cilia applied force. Additionally because the fluid at the top of the traction layer is identical to the fluid at the bottom of the ASL, we expect the fluid velocities to be continuous at the ASL-traction layer interface (D. J. Smith et al., 2007). In borrowing this concept, we can model the interface between a traction layer and the upper ASL as a Couette boundary. Using this alone, we would expect the velocity to decrease until it reached 0 at the no-slip boundary at the top of the container. This solution, however, isn't enough as the velocity reaches 0 before the top of the channel and by virtue of the flow moving

opposite the cilia driven flow. The channel being a closed system necessitates that there is a flow counter to the cilia driven flow. In a 2010 paper, Shields et al. saw a similar phenomenon in a closed chamber with magnetically driven artificial cilia (Shields et al., 2010). They explained it as the cilia-driven fluid piling up against the container wall and creating a pressure that drives fluid in the opposite direction. They considered this recirculating, pressure-driven flow as a Poiseuille solution. Following that the flow profile has both Couette and Poiseuille components, I fit the data to the Couette + Poiseuille solution discussed in section 4.1.4. For the Couette component, used the velocity of 21um per second (40 um above the cilia tips) as the velocity of the lower boundary, and set the velocity of the upper boundary (1460um above this point) as 0. Using these parameters and leaving the pressure term as a free variable, I used a least squares algorithm to produce the fit line in figure 4.2, which has an r^2 value of .9736. The flow profile of cilia driven flow in the mucus clearance assay does show consistency with a Couette-Poiseuille model in which the fluid above the cilia tips is coarse grained into a traction layer, which provides a Couette boundary.

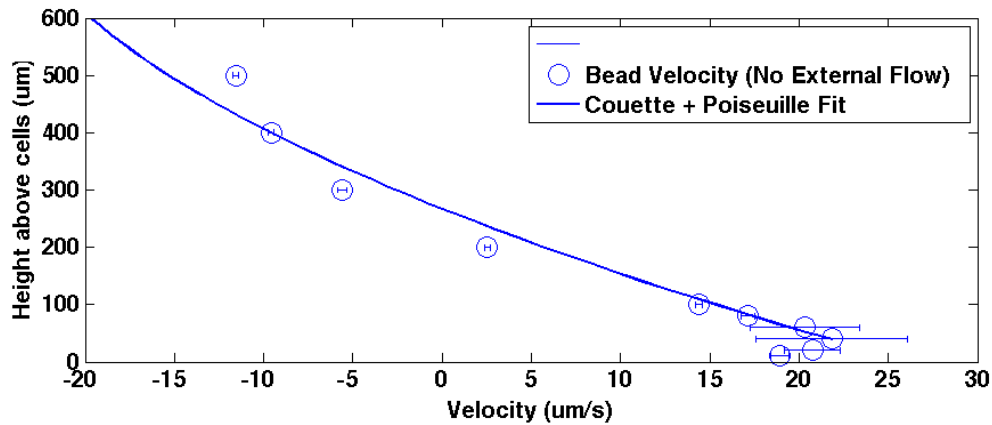


Figure 4.2 A flow profile of 2um beads in a ciliated fluidics channel with no external flow. The particle velocities are consistent with and fit to a Couette+Poiseuille model where the Couette term comes from coarse graining the fluid near the cilia tips into a traction layer and the Poiseuille term is the result of a pressure driven recirculation due to the closed nature of the system.

4.3 External Flow

In the previous section I was able to use diminution of lateral heterogeneity and coarse graining to model the cilia driven flow as a shear boundary. From there I observed that the closed channel had a flow profile consistent with a Couette-Poiseuille model. Using these simple models, it makes it possible to move on to more advanced experiments, namely challenging the cilia driven flow with an external flow. The primary goal of the experiments in this section is not to simulate physiological conditions; instead the goal is to use the force from an external fluid flow to better understand the nature of the boundary condition between the cilia and the ASL. Does the coarse-grained shear boundary work as a model in the presence of an external flow?

The first experiment characterizes the flow profile for the syringe pump driven flow. Next I determine if the CBF responds to an applied shear stress. Finally I

experimentally test the coarse-grained Couette boundary model with an external flow using a syringe pump as the source of the pressure gradient. These experiments pave the way for future experiments to further investigate the nature of the cilia tip boundary condition, the efficacy of cilia motion and the PCL at preventing infection in the absence of mucus, as well as airflow experiments. Additionally these experiments set the foundation for using the assay as an adhesion assay as described later in this chapter. Details regarding the experimental setup for these experiments can be found in the methods section 4.6.2.

4.3.1 Syringe pump driven Poiseuille profile.

First I needed to run a control experiment to characterize the external flow. In running this control I wanted the simplest externally driven flow profile available; I wanted to test a system without cells/cilia. To accomplish this, I simplified the system by replacing the millicell scaffold with a glass coverslip. I then followed the procedure for experiments under external flow as described in the methods sections. Using this procedure I created flow profiles (Fig 4.3) for volumetric flow rates of .9ml/hr, 1.8 ml/hr, and 3.6 ml/hr. Next I chose the maximum flow velocity for each flow profile, and used that number to construct a parabola consistent with the Poiseuille flow (equation 4.9). The rest of the data points in each flow profile are consistent with these Poiseuille flow model lines indicating that the fluid flow in the channel is a Poiseuille flow. I establish these flow profiles so that I can later compare the syringe pump volumetric flow rate to velocities in the channel,

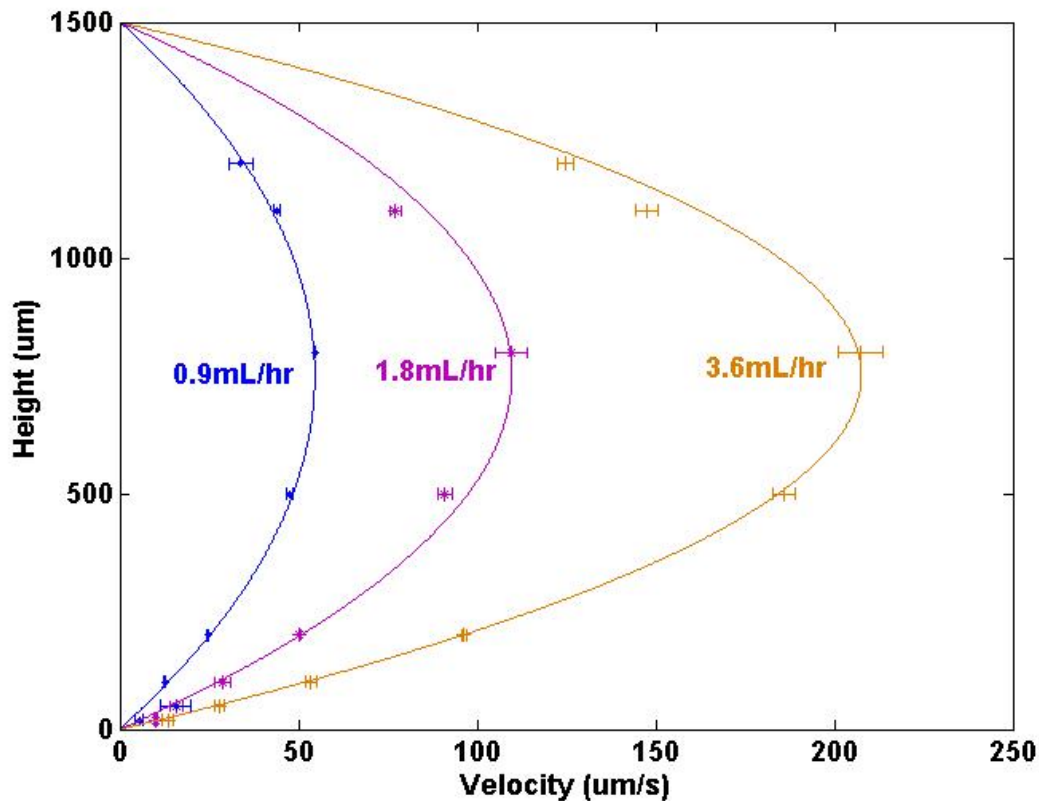


Figure 4.3 Flow profiles at several volumetric flow rates fit a Poiseuille model for syringe driven fluid flow in the apical chamber of the MCA.

4.3.2 Verifying negligible CBF change with applied shear stresses

In most of the transport experiments in this dissertation I am challenging the cilia with an external force: in this chapter I use a syringe pump to flow buffer opposite the cilia driven transport and in chapter 5 gravity is used to drain fluid over the cell cultures. In both instances, it is essential to know if the cilia, particularly the CBF, change as a result of these external forces. The relationship between applied shear-stress and CBF is investigated in a 2007 Winters paper (Winters et al., 2007). They found that

1. Shear stress on the order of 10^{-4} Pa had a negligible effect on CBF

2. Shear stress on the order of 10^{-3} and 10^{-2} increased CBF
3. This increased CBF may trail the applied shear stress by 15 minutes
4. Shear stress applied in the cephalad direction (with the effective stroke) and the caudal direction (against the effective stroke) both increased CBF, however, the increase was larger when applied in the caudal direction.

To test the relationship between CBF and applied shear stress, I applied a steady flow of buffer over my cultures and periodically measured the CBF (see methods).

Using the data from the Poiseuille flow in the empty channel, it's possible to solve for the pressure gradient. For Poiseuille flow, the maximum velocity, u (the velocity in the center of the channel,) is equal to

$$u_{max} = \frac{1}{8\mu} \frac{\partial p}{\partial x} h^2 \quad (4.15)$$

where h is the channel height. This makes it possible to solve for the pressure gradient in the channel given the maximum velocity in the channel center. Knowing all of the parameters in the Poiseuille flow equation makes it possible to solve for the wall shear stress, which is given by

$$\tau_w = \mu \left(\frac{\partial u}{\partial x} \right)_{y=0} \quad (4.16)$$

Using equation 4.16 I calculated that the applied shear-stress from the 2ml/hr flow rate is 1.4×10^{-4} Pa. In agreement with Winter's paper, applying this shear-stress

caudally and cephaladly does not stimulate CBF (Fig 4.4).

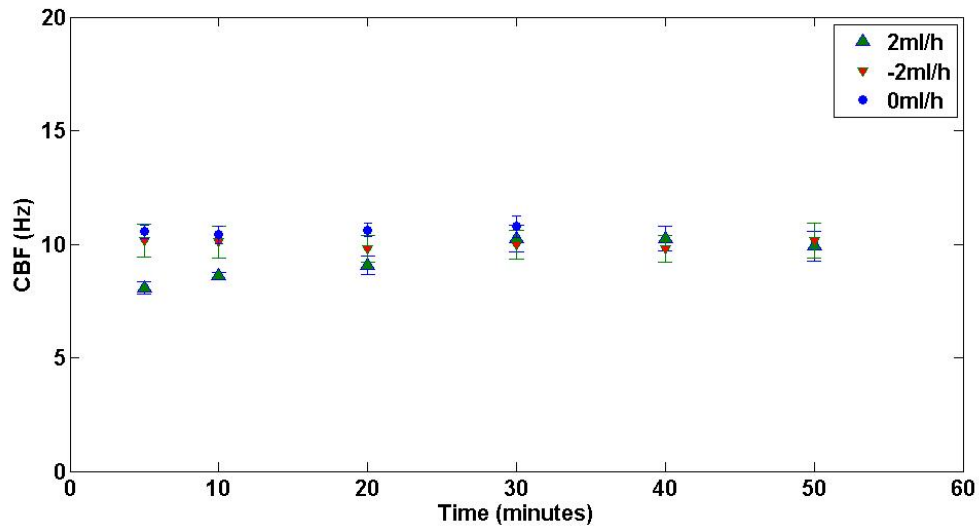


Figure 4.4 Cilia beat frequency isn't effected by a cephalad or caudal 2ml/hr flow (10-4 Pa shear stress) over the course of an hour.

This result allows me to do experiments in this stress range without worrying about a changing CBF.

4.3.3 Couette + Poiseuille revisited with an external fluid flow

After establishing the Poiseuille flow in the channel and the consistent cilia beat frequency, I could move on to challenging the cilia driven flow with an external flow. This serves to evaluate the coarse-grained boundary condition in the presence of an external fluid flow. Again I followed the procedure for using external flows as described in the methods section. For each experiment I took a z-profile with the syringe pump turned off, then took z-profiles at various volumetric flow rates, generally using the syringe pump to oppose the cilia driven flow in a region of

interest

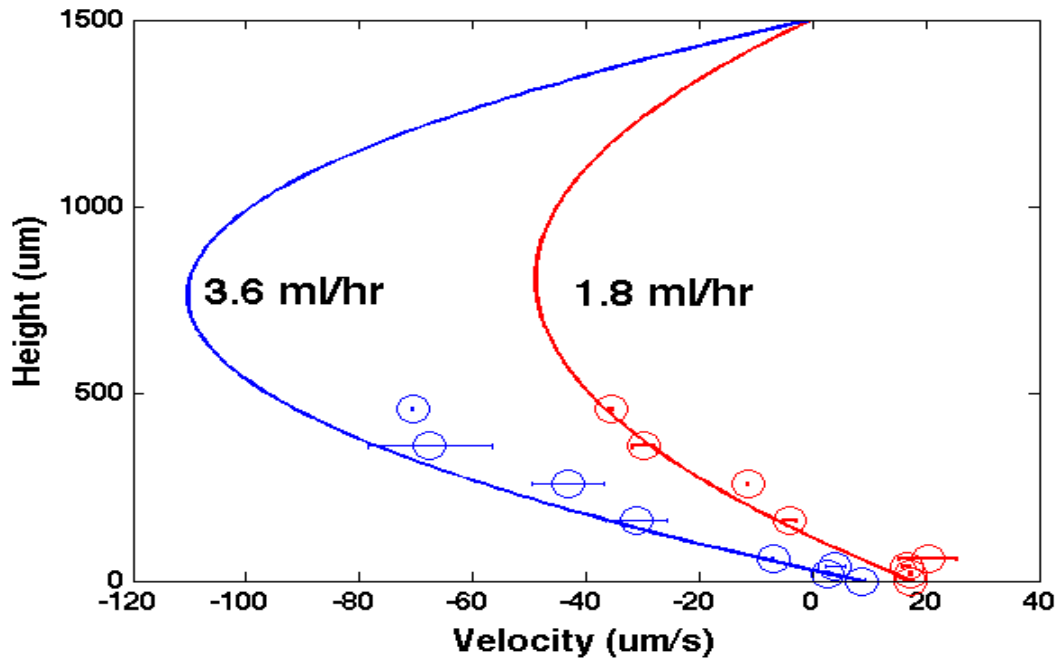


Figure 4.5 Flow profiles of cilia driven fluid flow being opposed by a syringe driven fluid flow are consistent with a Couette + Poiseuille model in the Mucus Clearance Assay. The bottom boundary condition (0) is set by fluid flow 40 above the cilia tips to reduce the effects of lateral heterogeneity.

The data do show a combination of Couette + Poiseuille flow profiles (Fig 4.5). The flow profile with the syringe pump turned off is the same as seen in section 4.2.2, with the addition of the flow the Couette + Poiseuille profile remains, however, the Poiseuille component is now the result of the syringe pump and resembles the control Poiseuille flows from 4.3.1. The Couette + Poiseuille curve model was fit based on the volumetric flow/Poiseuille calibration from the prior section and the average velocity of the beads just above the cilia tips.

4.3.4 Future flow experiments

The technique and data from the prior experiment lays the foundation for future experiments. One potential experiment lies in introducing airflow to the system. With success in running liquids through the channel and a programmable “breathing” machine already developed by collaborators in the Virtual Lung Group, attaching airflow to the system is mainly an issue of plumbing (another minor issue would be humidifying the air. The next experiment that this enables would be to use the syringe pump driven flow to entrain cilia. Currently I rely on a combination of the chamber geometry and drainage to entrain the cilia. I haven’t definitively shown that my increased cilia alignment is statistically significant as compared to millicell controls, however this will be the focus of future studies. Improvements in yield and in uniformity across the entire channel would be an enormous breakthrough. As you’ll recall from chapter 2, there are still several questions regarding the origins of cilia entrainment and this system is ideal for exploring entrainment in the airway.

The flow profile data suggests that a syringe pump could deliver shear-stresses comparable to those used in other entrainment papers, such as the experiments performed by Mitchell (Mitchell, Jacobs, Li, Chien, & Kintner, 2007) and Guirao (Guirao et al., 2010). While there are still some engineering challenges associated with this experiment (namely removing fluid to maintain the air-liquid interface after applying a shear-stress), it potentially can answer questions regarding patterning, the PCP pathway and cilia maturation in the airway.

Another use of external flow is using the shear-stress delivered by an external fluid to remove beads adhered to the epithelial surface. Using this technique makes

it possible to identify and characterize adhesion between the ASL and epithelium. Understanding adhesion is important in understanding how potential ASL-Cilia adhesion could alter the ASL-cilia boundary conditions; specifically how adhesion or lack of adhesion affects the transfer of force from cilia to ASL. In the next section I discuss my work on developing an adhesion assay, which will serve as a tool to answer these questions.

4.4 Adhesion Assay

Adhesion assays are useful for characterizing and quantifying adhesion forces, specifically they can be used to

1. Identifying potential interactions
2. Performing force spectroscopy to quantify bond strengths
3. Understanding how external agents and conditions can change those bond strengths

Microfluidics technology has presented itself as an excellent platform for adhesion assays. Lu et al. developed the first such system to study cell adhesion as a function of applied shear-force. Using the microfluidics platform enabled them to control shear force using a combination of different channel geometries and syringe pump flow rates. They used the device to investigate the shear rate at which fibroblasts would detach from a fibronectin coated substrate. (Lu et al., 2004) Since then, similar techniques have been developed to look at a variety of cell adhesion interactions. De La Fuente et al. did a comparison of bacterial cell adhesion as a function of pilli type(La Fuente et al., 2007). Several studies have examined adhesion of different types of human cells including activated neutrophils(Gutierrez & Groisman, 2007),

fibroblasts(Christophis, Grunze, & Rosenhahn, 2010), and endothelial cells (Rossi, Lindken, Hierck, & Westerweel, 2009) (Hwang et al., 2010). All of these studies, however, focused on the cell-substrate adhesion. Javanmard et al. generalized the technique to look at receptors (bound to the channel substrate) and ligands (bound to microbeads) and were able to achieve piconewton resolution in their adhesion measurements (Javanmard, Babrzadeh, & Davis, 2010). This measurement, however, requires that the ligands/receptors are known and can be attached to the substrate/bead. In the case of trying to identify a biochemical interaction between ASL constituents and cilia, we need a mechanism of identifying potential receptors on the cilia. By incorporating an active cell culture as the substrate and using beads functionalized with individual ASL constituents, it greatly reduces the complexity of the problem. Furthermore it makes it possible to determine whether an ASL constituent plays a role in adhesion and quantification of the adhesive force.

All of these experiments are useful in trying to understand the potential role that biochemistry plays in transport and the ASL-cilia boundary. In addition to identifying and quantifying bonds between the cilia/epithelial surface and constituents of the ASL, this technique could also be used to investigate adhesive forces between mucus and the epithelial surface. In the next section I'll briefly discuss the relevant forces in the system followed by experiments using the mucus clearance assay as an adhesion assay.

4.4.1 Forces on the bead

To determine how the bead releases, we need to consider the forces acting on the stuck bead (Fig 4.6). The following is a brief overview, but Burdick et al. give

a much more thorough treatment and examine particle removal as a function of Reynolds number (Burdick & Berman, 2001). I'll quickly compare several forces that act on a bead in our system and also explore the conditions under which these forces will allow the bead to release from the substrate. The relevant forces are gravity/buoyancy, drag, lift, and adhesion. I will also perform example calculations to put these forces into perspective in the context of the mucus clearance assay chamber; I will use a 10 μ m polystyrene bead attached to a glass substrate with a 1ml/h volumetric flow of PBS going through the channel.

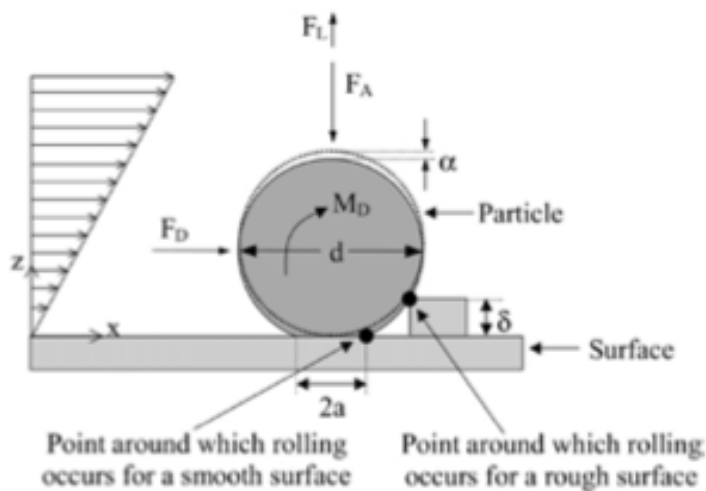


Figure 4.6 Free body diagram of an adhered bead undergoing fluid flow. The bead will experience drag force, lift force, and adhesion force. The surface roughness, contact area, and bead/substrate materials determine the adhesion force (Burdick & Berman, 2001).

4.4.1.1 Gravity/Buoyancy

The extremely small mass of the beads makes the gravitational force of little consequence compared to other forces, but a quick calculation is included as a

reference. A 10 μ m polystyrene bead has a density of 1050kg/m³ and a mass of approximately 5.5x10⁻¹³ kg. Using

$$F_g = \frac{4\pi}{3} \rho_{bead} r^3 g \quad (4.17)$$

where ρ is the bead density, r is the bead radius and g is the Earth's gravitational constant, we calculate that the bead will experience a gravitational force of 5.4 pN. Since the bead is completely submerged in the fluid, the buoyancy will closely follow the gravitational force; the only difference being that the density of the fluid is used instead.

$$F_b = \frac{4\pi}{3} \rho_{buffer} r^3 g \quad (4.18)$$

The buoyancy force on the bead is 5.2pN and thus the net downward force is .2pN.

4.4.1.2 Drag

As fluid flows past the spherical bead, the bead will experience a drag force. This drag force can be determined by Stokes' law:

$$F_D = 6\pi\mu r v \quad (4.19)$$

Where μ is the fluid viscosity, r is the bead radius, and v is the fluid velocity. This equation needs to be modified slightly, however, because of surface effects(Burdick & Berman, 2001). We add a constant of 1.7009 to account for surface effects on the drag(O'Neill, 1968) and get

$$F_D = 10\pi\mu r v \quad (4.20)$$

Using our example 10 μ m bead in a buffer solution with a velocity of 1 μ m/s at the bead center, we get a drag force of .14pN. (The 1 μ m/sec flow rate at the bead center was calculated using the 1ml/hour flow rate, the linear channel velocity, and the parabola equation for Poiseuille flow.)

4.4.1.3 Lift

A stuck bead will also experience lift as a result of the pressure differential along the height of the bead. The fluid moving near the bottom of the bead (and thus the no-slip boundary) is moving slower than the fluid closer to the center of the channel. The lift equation is given as (Burdick & Berman, 2001)

$$F_L = 1.615\mu d^2 \left(\frac{\rho}{\mu} \frac{du}{dz} \Big|_{z=\frac{d}{2}} \right)^{1/2} V_p \quad (4.21)$$

Where μ is the fluid viscosity, d is the bead diameter, ρ is the fluid density, $\frac{du}{dz}$ is the change in fluid velocity in the direction normal to the substrate and V_p is the fluid velocity at the center of the bead. This gives us a lift force of 42aN.

4.4.1.4 Adhesion

Adhesion will be the unknown in our adhesion assay; it'll be by controlling the other forces via the applied shear-stress and noting the method of bead release that we will be able to determine the adhesion. To put the magnitude of the adhesion force in perspective with the other forces, I've included a quick calculation to show the binding van der Waals force between a bead and a glass substrate. Adhesion

forces include the van der Waals interaction, hydrogen bonding, ionic bonds, and covalent bonds amongst others. An approximate van der Waals interaction can be calculated from (Burdick & Berman, 2001)

$$F_v = \frac{Ad}{12h^2} \left(1 + \frac{2a^2}{hd}\right) \quad (4.22)$$

where A is a quantity called the Hamaker constant, d is the particle diameter, h is the particle-surface separation, and a is the contact radius between the particle and surface. Again I'll do a rough calculation with a $10\mu\text{m}$ polystyrene bead to get a sense of the magnitude of the van der Waals force. We'll use a Hamaker's constant of $1.14 \times 10^{-20}\text{J}$, an h spacing of $.4\text{nm}$, a contact radius a of 30nm (adapted from Burdick's value using DMT theory (Takadom, 2010) and a $10\mu\text{m}$ diameter. This results in an adhesion force of $\sim 86\text{nN}$.

These forces are summarized in the table below

Force	Value from our example	Dependence on bead radius	Dependence on viscosity	Dependence on velocity
Gravity-Buoyancy	.2pN	r^3	n/a	n/a
Drag	.14pN	r^+	μ	v
Lift	43aN	r^2	$\mu^{1/2}$	v
Adhesion	86nN	$\sim r$	n/a	n/a

The key points from this table are as follows

- 1) For our example system, adhesion dwarfs the other forces.
- 2) Changing the bead radius is going to have the greatest effect on gravity and then lift. It should be noted that drag will increase more depending on how the flow profile changes as a function of height. If the bead radius increases enough so that the bead center experiences a much faster velocity, this will also increase the drag force, but at this scale it will still follow a linear relationship.
- 3) Gravity and adhesion don't have a dependence on viscosity and velocity: tuning viscosity and velocity can greatly help in generating enough force to remove the bead without increasing adhesion or gravity.

4.4.2 Releasing the bead

Now that we have an understanding of the forces involved, we can determine when and how the bead is detached from the substrate. Once again a more thorough treatment of these methods can be found in the Burdick paper. There are three primary mechanisms by which the bead can move away from the substrate. The first of which is lift. This mechanism is straightforward; the lift and adhesion vectors oppose each other, so if the magnitude of the lift vector is larger than adhesion, the bead will lift off of the surface. Lift occurs when

$$F_L > F_a \tag{4.23}$$

The next release mechanism is sliding. Similar to the macroscale, the force required to initiate sliding will be the coefficient of static friction times the downward force.

Sliding occurs when

$$F_D \geq \mu_f (F_a + F_L) \quad (4.24)$$

The final release mechanism to discuss is rolling. In rolling we need to consider both the lift and drag forces applying a torque about the bead. Adding these along with the moment of surface stresses, M_D which is defined as (O'Neill, 1968)

$$M_D = .943993 \times 2\pi\mu d^2 V_p \quad (O'Neill, 1968) \quad (4.25)$$

gives us the forces that will contribute to rolling. Rolling occurs when

$$M_D + F_D l_1 + F_L l_2 \geq F_A l_2 \quad (4.26)$$

where l_1 represents the distance offset between the drag vector, F_D and the point of rotation, and l_2 represents the distance offset between the lift/adhesion vectors and the point of rotation (Fig 4.7.)

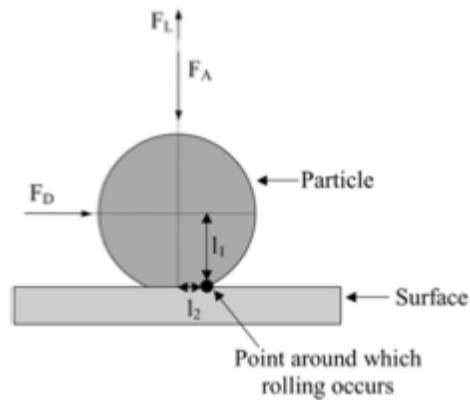


Figure 4.7: Diagram showing the mechanism of bead rolling. The drag vector and lift vector apply a torque about the rolling point. If this torque along with the moment of surface stresses is greater than an opposing torque from the adhesion vector, the bead will release via rolling.¹

4.4.3 WGA beads demonstrate stronger adhesion than PEG beads on an untreated epithelial surface

An important first step in constructing the adhesion assay was demonstrating that a bead functionalized with a moiety behaved differently than a control bead. Specifically the goal is to show that the beads release from the epithelial surface at different forces. For these experiments I chose to use polyethylene glycol (PEG) beads as a control; PEG beads demonstrate a near zero zeta potential and have been used to minimize adhesion to mucus (Suk, Pace, Cone, & Hanes, 2008). I also switched to using an HBE cell line (HBE 16) to evaluate the adhesion assay. For the specific moiety I functionalized beads with the lectin wheat germ agglutinin (WGA), WGA has been shown to bind to the airway epithelium (Yi, Harson, Zabner, & Welsh, 2001). WGA binds primarily to the sugar N-acetylglucosamine, which is found in the glycocalyx as well as on mucins (Martins & Bairos, 2002). Beads were prepared according to the procedure in 4.6.5 and the experiment was performed following the methodology in section 4.6.6. All bead experiments were performed pairwise: both

types of beads were introduced into the same channel and released during the same experiment. This eliminated potential channel-to-channel or culture-to-culture variability.

Performing this experiment I found that on average the WGA beads released at a higher flow rate than the PEG beads (fig 4.8). Figure 4.8 also shows the corresponding average drag force for which the different beads released, and the average force is statistically different for PEG beads and WGA beads. The force was calculated by taking the flow rate, matching it the Poiseuille fit for the channel at a height of the bead radius above the cells and then using the modified Stokes drag equation (4.20). I used drag as the release mechanism for force calculations because I couldn't calculate rolling without knowing the contact points.

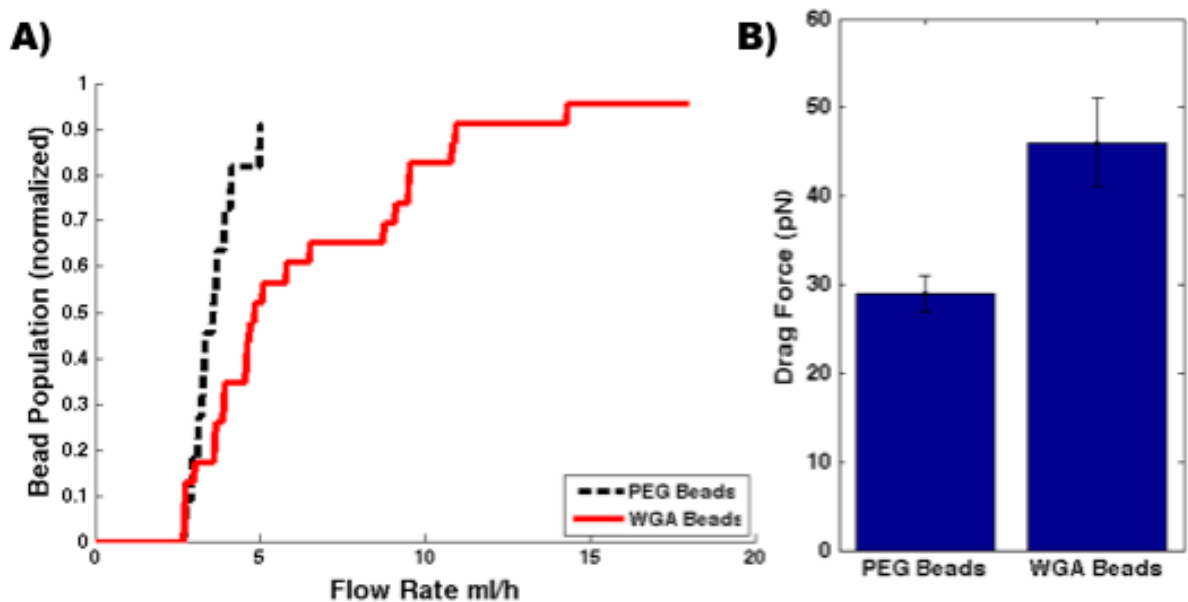


Figure 4.8 Plots comparing the adhesion of PEG beads and WGA beads on a normal **HBE16** epithelial surface. A) Characteristic plot of the released fraction of the bead populations as a function of flow rate. WGA beads released from the cells at a higher flow rate. B) An average across 4 experiments (2 different channels) of the corresponding average drag force at which beads released. Error bars are standard error where n is 52 and 67 for PEG beads and WGA beads respectively. PEG beads released at an

average drag force of 29 ± 2 piconewtons while WGA beads released at an average of 46 ± 5 piconewtons.

4.4.4 WGA beads demonstrate similar adhesion as PEG beads on an epithelium incubated with free WGA

After demonstrating that WGA beads had a stronger adhesion to the epithelial surface than the PEG beads, my next step was to demonstrate that I was specifically measuring the WGA-epithelium attachment. In this experiment I pretreat the epithelial culture with the same lectin so that I can essentially “block” the beads from adhering to the N-acetylglucosamine on the epithelial surface. I used a fluorescein isothiocyanate (FITC) conjugated Wheat Germ Agglutinin solution and allowed it to sit on the culture for two hours. Afterwards I washed the solution out of the channel and imaged the epithelial surface in a FITC channel. Figure 4.9 shows fluorescence wherever the WGA is present, which is distributed across the entire surface. Next I performed the same types of experiments as I did in the prior section.

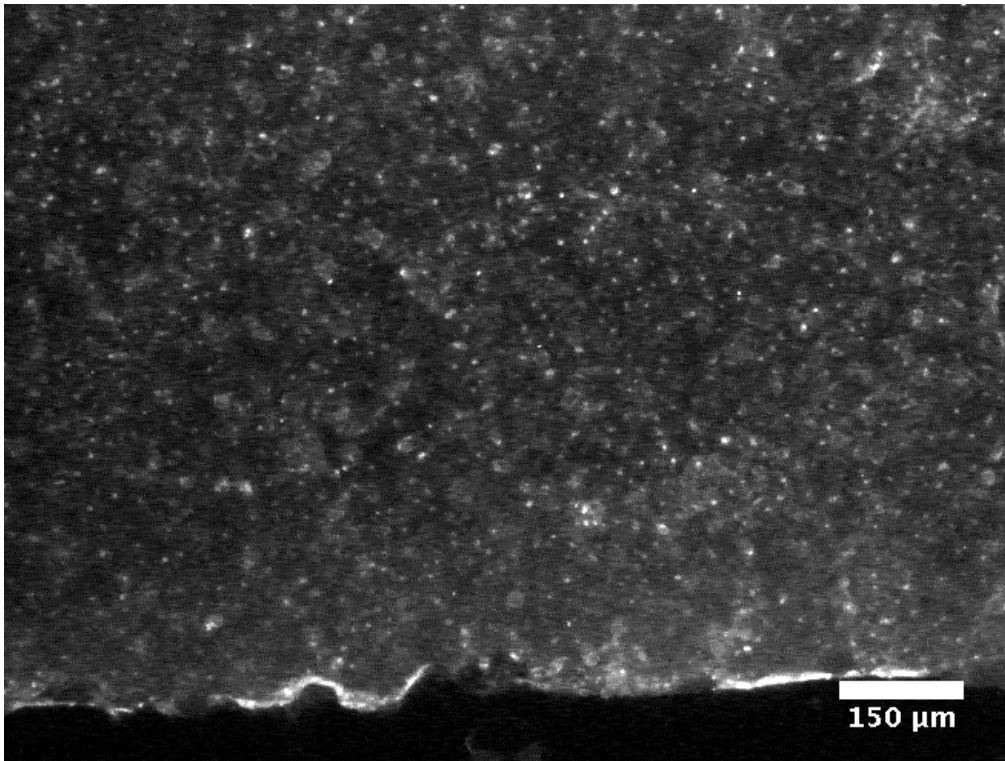


Figure 4.9 **HBE 16** cell surface decorated with FITC-conjugated Wheat Germ Agglutinin

Figure 4.10 shows that the bead release curves of the different bead types look similar as compared to the untreated surface. Additionally, when averaging across 3 experiments performed in two different channels, the average release force is statistically the same for both types of beads. The data shows that I was able to reduce the adhesion between the WGA bead and the epithelium by using the free

WGA as a blocking agent.

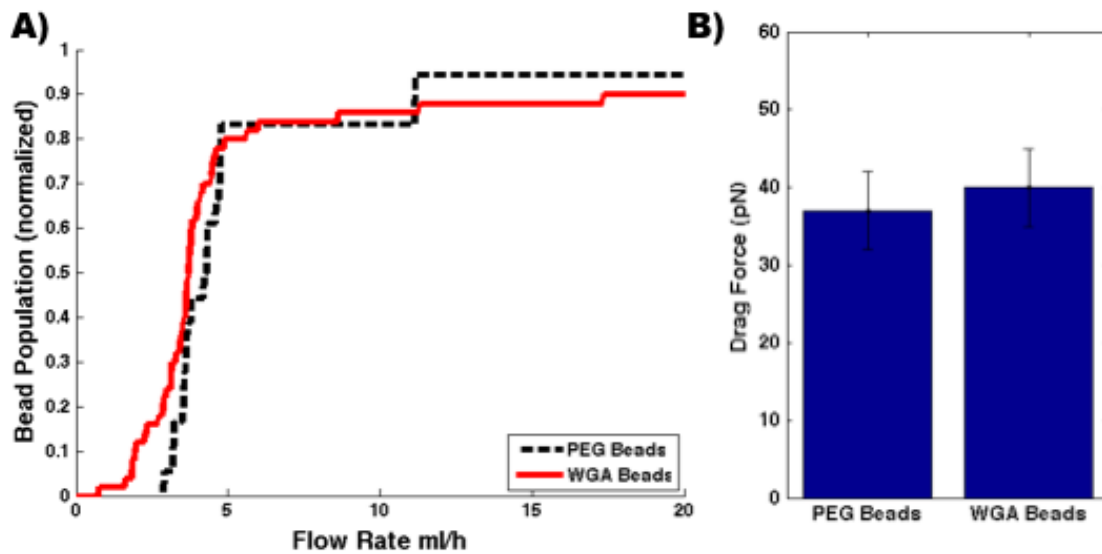


Figure 4.10 Plots comparing the adhesion of PEG beads and WGA beads on a WGA treated HBE16 epithelial surface. A) Characteristic plot of the released fraction of the bead populations as a function of flow rate. Both bead types released from the cells at a similar flow rate. B) An average across 3 experiments (2 different channels) of the corresponding average drag force at which beads released. Error bars are standard error where n is 72 and 113 for PEG beads and WGA beads respectively. PEG beads released at an average drag force of 37 ± 5 piconewtons while WGA beads released at an average of 40 ± 5 piconewtons.

Plotting both of the average forces for the untreated channels and WGA treated channels on the same plot shows that there is a difference between removing

WGA beads from untreated and WGA treated cells (fig 4.11). Figure 4.11 also

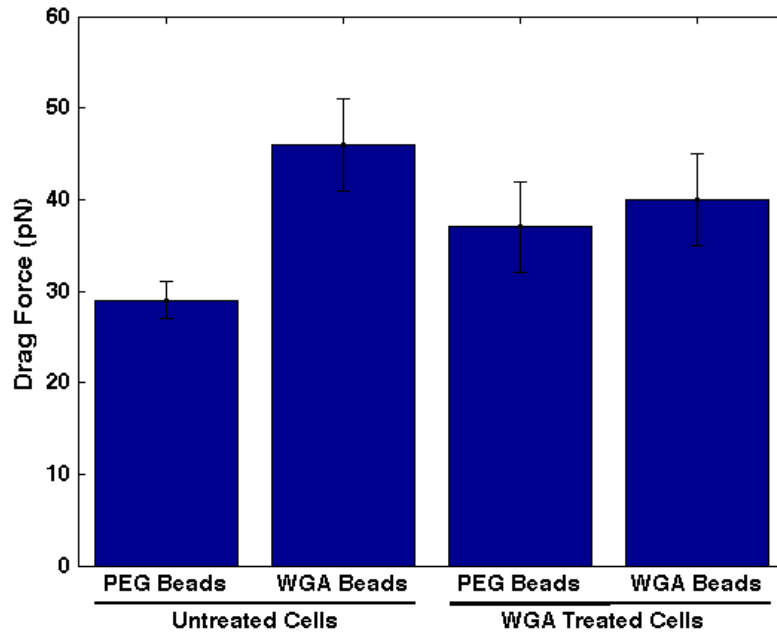


Figure 4.11 Average release force of PEGylated and WGA functionalized beads on both normal and WGA treated cell cultures. While PEG and WGA beads demonstrate similar adhesion on the WGA treated cultures, they are statistically different than their untreated counterparts. This suggests that the WGA adheres less and that the PEG is stickier on the WGA treated cultures.

shows that the PEG beads appear to be stickier on the WGA treated culture. Despite the PEGs inertness, the presence of the free lectin molecules on the cell surface could serve to increase the adhesion with the “neutral” PEG bead.

4.4.5 Future Direction for the Adhesion Assay

I've demonstrated functionalizing a bead with a specific ligand (WGA) known to bind to the epithelial surface and shown that it had a stronger adhesion than a control PEG bead. I then demonstrated that I could block this interaction by treating

the epithelial surface with WGA, which reduced the adhesion between the WGA beads and the surface. The next step in the adhesion assay is demonstrating the specificity of the blocking. This would be achieved by functionalizing a bead with another lectin, such as Concanavalin A (Con A), which is also present on the airway epithelium, but binds to a different saccharide (mannose) (Yi et al., 2001). Ideally the Con A beads would not show a difference in adhesion between the normal epithelium and the WGA-treated epithelium, because the mannose would remain unblocked by the free WGA treatment. Demonstrating specificity in blocking interactions makes it possible to test for specific adhesive interactions by blocking a specific interaction and checking for a reduction in adhesion force.

The true power of the adhesion assay lies in its ability to determine what moieties play a role in unspecified adhesion. The ultimate goal for this system is to have beads functionalized with components of the ASL (primarily mucins) and to have those beads adhere to the epithelial/ciliated surface. The assay would be run as above to determine an adhesive force between the beads and the epithelial surface. Then the epithelium would be treated with a specific blocking agent to see if that agent diminishes adhesion. Performing the experiment with a battery of blocking agents would make it possible to determine which moieties were important in mucin-epithelium adhesive interactions and each moiety's relative contribution to adhesion. Once these interactions are discovered, the adhesion assay would further serve as a platform to determine how pharmaceutical agents affect adhesion.

4.5 Conclusions

In this chapter I used the mucus clearance assay to characterize the cilia mat as a boundary condition. The first step in this process was fitting the flow profile of the system to canonical exact solutions of the Navier-Stokes equations. Doing this required that I modeled the cilia-driven flow as a coarse-grained Couette flow. I found that the cilia driven flow was consistent with this model, which will allow me to make prediction for the system when I add additional forces such as gravity in the next chapter. Next I tested the boundary's response to external flow. I determined a shear regime in which the CBF should stay relatively constant. Data suggests that despite the constant CBF, the boundary lost the ability to transfer force to the ASL in the presence of an external flow; the data suggests that there may be some slippage at the cilia/ASL interface. Finally I used the flow characterization of the system as a powerful technique to explore and discover adhesion interaction between the ASL and the epithelial surface.

4.6 Experimental Methods

4.6.1 Preparing channels for flow experiments

Briefly the procedure for removing the native ASL consisted of washing the cells in PBS to remove as much endogenous material as possible. Next the culture was washed/incubated in a 50 μ M ATP solution, which helped to stimulate goblet cells to release stored mucus. The culture was rinsed again with PBS and then washed with a 5mM Dithiothreitol (DTT) solution. The DTT helped to breakup/remove remaining endogenous mucus by breaking the disulfide bonds

between mucin subunits (I'll go into more detail about this process later in Chapter 5). Finally the culture was washed again and the simulant was added to the culture. For this particular set of experiments I used a 1:200 solution of fluorescent 2 μ m carboxy coated beads in a PBS solution.

Prior to starting the experiment, I identified a region of interest by observing the transport of endogenous material prior to washing. In general this region of interest was well-ciliated and towards the center of the channel. Using the combination of the micrometer x-y stage, and "fiducials" in the culture I had success in revisiting fields of view, even when taking the stage off of the microscope. After identifying a perspective region I focused on the cell layer and took a high magnification (20-40x) video of the cilia layer. Most experiments were performed at 4x magnification in epifluorescence mode to maximize the field of view as well as the contrast of the microbeads. With each data set I started imaging at the cell layer and then raised my focal plane in steps of 20 microns, stopping to take a few videos at each focal plane. In general very few beads were in the focal plane at the cell layer. I attribute this to cilia, which occupy 6-7 microns of the depth of field, excluding particles. I also had an upper limit in taking videos "far" above the cell layer. Above a certain point, usually 600-1000 μ m above the cell layer, the imaging quality and signal to noise ratio of the fluorescent beads would drop enough as to make subsequent tracking extremely difficult if not impossible. For these reasons my flow measurements were typically constrained to 20-1000 μ m above the cell layer. I should also note that the depth of field was large enough that I was still able to capture particles that were in the vicinity of the cilia tips. This was verified by

occasionally seeing beads at the 20um level that were attached to cilia. Videos were processed in ImageJ, tracked in VideoSpot tracker and then the tracked data was fed into custom written MATLAB scripts to produce flow profiles.

4.6.2 Performing experiments with an external fluid flow

Performing these experiments required that the MCA's apical ports were connected to a syringe pump. Connecting the syringe pump was simply a matter of plumbing: a 1/16" hose barb elbow fit snugly into the apical port without adding unnecessary obstructions to the optical path. From the hose barb, tubing was connected to attach the channel to a syringe pump as well as a waste container for spent fluid. Once the syringe was connected to the system, all of the tubing was completely filled with a bead buffer solution and the system was allowed to recover from any shear stresses before the start of the experiment. In the first attempts to perform the experiment I quickly learned the necessity of submerging the "waste" tubing in liquid. Otherwise the formation of a drop and its subsequent fall would dominate the channel flow at low volumetric flow rate speeds.

4.6.3 Experiment to test CBF response to shear-stress

To test this I followed the experimental setup used in the above external flow section. I found a ciliated field of view, and took 20 second videos at 5 minute increments. After the first 15 minutes, I turned on the syringe pump and let it run with a volumetric flow rate of 2ml/hr for the next 45 minutes while continuing to take videos every 5 minutes. I then reversed the flow direction so that the 2ml/h

volumetric flow rate opposed the cilia's effective stroke and took video every 5 minutes. I then analyzed the CBF with the algorithm set out in section 3.4.2.

4.6.4 Modifying the chamber for adhesion assay experiments

I modified the mucus clearance assay channel to perform the adhesion assay experiments. My chief concern was that the increased pressure in the channel required for adhesion assay experiments would cause the membrane to bow. This bowing would distort the optics during experiments and make it difficult to perform measurements. While this bowing could be avoided in the unmodified mucus clearance device (by making sure that the basolateral chamber and reservoirs were completely filled with fluid), I opted to modify the chamber to perform initial experiments. The first modification was to use only the apical portion of the channel and using a glass slide as the cell substrate instead of the membrane. I attached the apical compartment to the glass slide using the same oxygen plasma technique that I used in the previous chapter. After bonding the system, I immediately pipetted in collagen, which was adsorbed onto the activated glass surface. After an hour I removed any excess collagen from the channel. While this modified channel wasn't capable of growing cells at an air-liquid interface or for the weeks required for well-ciliated, well-differentiated cells, it serves as an essential proving ground for adhesion experiments. I would like to reiterate that the bilayer channel can be used to perform these experiments as well, but is more expensive in terms of time and cell type.

My second modification was the addition of a bubble trap. Bubbles are often troublesome in fluidics applications and in passing over surfaces they can apply a huge shear stress to cells. Huh et al. used bubbles in a fluidics system as a model system for rupturing mucus plugs found in several airway diseases and found massive cellular injury as a result of these bubbles (Huh, Fujioka, Tung, Futai, & Paine, 2007). To avoid bubbles I implemented a bubble trap to reroute the bubbles away from the cells. By adding another port to the channel, I could route any bubbles to the bubble trap before starting the experiment and in this way remove bubbles from the system (Fig 4.10).

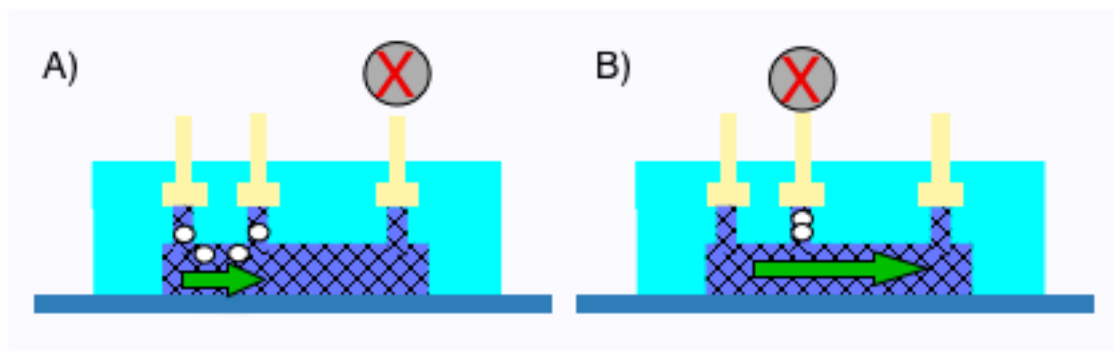


Figure 4.12 Diagram of the bubble trap. A) Closing a valve over the exit port will force flow out of the middle port. Bubbles are vented from this system via the middle port. B) Closing the middle port allows flow to proceed through the entire length of the channel.

4.6.5 Functionalizing beads with Wheat Germ Agglutinin and PEG

The following procedure was used to functionalize beads with Wheat Germ Agglutinin (WGA). Carboxy-functionalized polystyrene microbeads

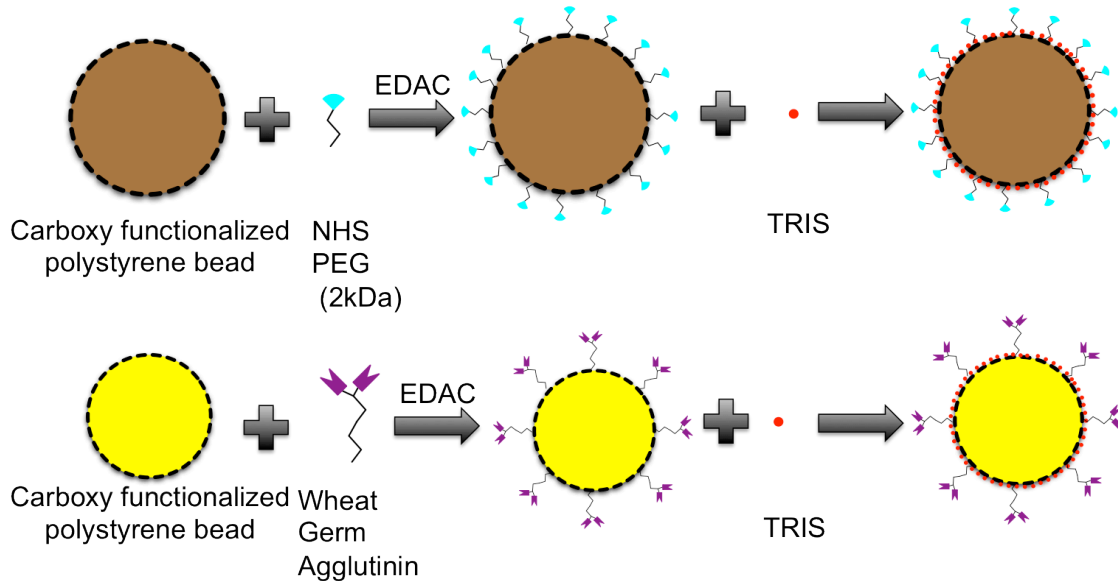


Figure 4.13 Bead functionalization protocol. Top: 2kDa Amino PEG was attached to the surface of a carboxy functionalized bead with an EDAC reaction, the remaining carboxy sites were quenched with TRIS. Bottom: Wheat Germ Agglutinin was attached to the surface of a carboxy-functionalized bead and remaining carboxy sites were quenched with TRIS.

(20 μ m) were linked to wheat germ agglutinin using the 1-ethyl-3-(3-dimethylaminopropyl)carbodiimide (EDAC) reaction. The beads were then quenched in a tris(hydroxymethyl)aminomethane (TRIS) buffer. The beads were then spun down and resuspended in DMEM/F12 media.

PEG beads were prepared using the same EDAC reaction, quenched with TRIS, and also resuspended in DMEM/F12.

4.6.6 Performing the Adhesion Assay experiments

To perform the adhesion assay experiments, HBE16 cells were seeded into the modified chambers at similar densities as the regular MCA chambers. The

reduced cell media capacity in the modified chambers made it necessary to change the media every 12 hours. Once the cells reached 100% confluence, they were ready for experiments.

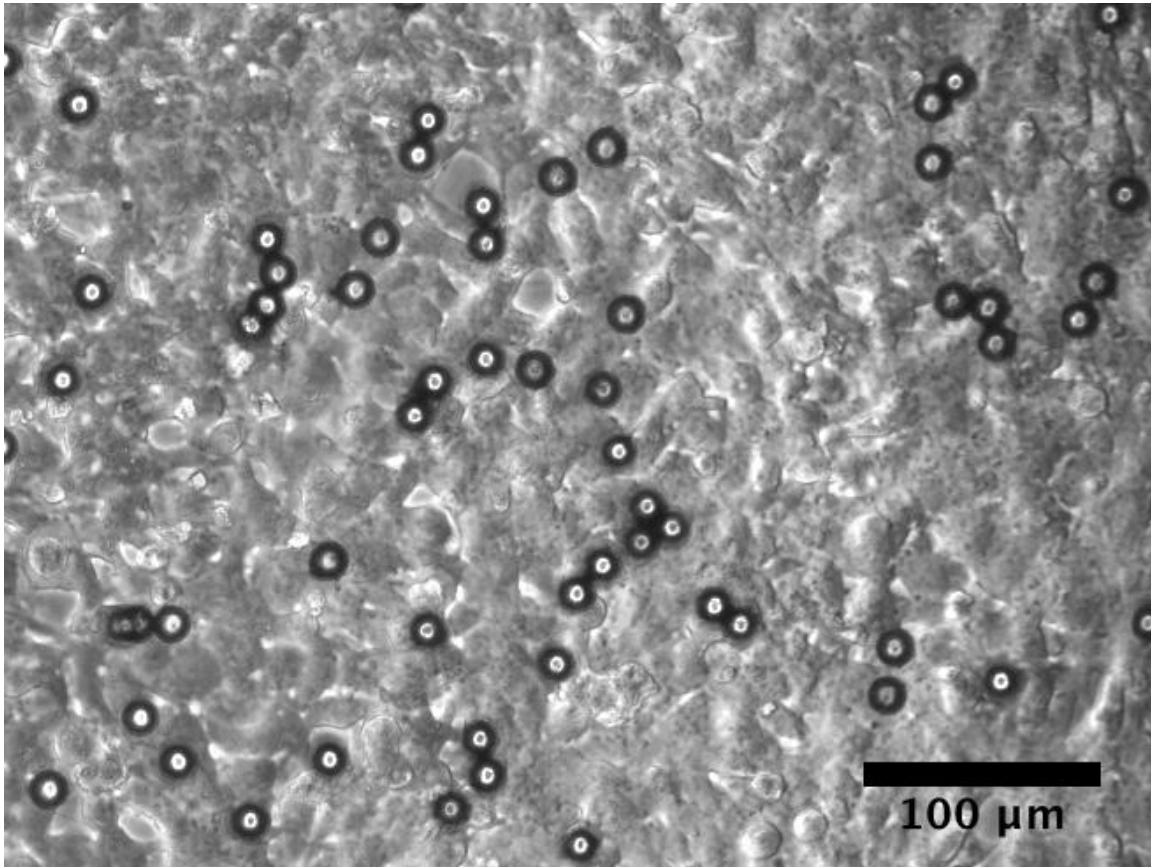


Figure 4.14 WGA functionalized microbeads (16µm) attached to the top of a confluent HBE 16 cell layer.

In my first several attempts at running the adhesion assay experiment, I noticed a huge variation (orders of magnitude) in the adhesion between beads and the epithelium. My main concern was that there was variability between different channels and also potential variability from the history of each channel; time since the culture had been removed from the incubator, prior exposure to shear-stress, etc. To nullify these differences I performed experiments pairwise: I tested control beads and experimental beads simultaneously. I did this by using volume labeled

fluorescent beads as my experimental bead and non-fluorescent beads as my control PEG beads. Using a mix between fluorescent and bright field microscopy I could image both bead populations simultaneously and also differentiate them so that each population could be tracked individually. I should note that I did notice improved consistency across channels when I started using TRIS to quench the beads, but the consistency across channels will require further study.

To perform the experiment functionalized beads as described in the prior section were added to the cultures and allowed to settle and adhere over the course of 10 minutes. The channel was attached to the syringe pump as described in the external flow experiments, and the syringe pump was set to linearly increase the volumetric flow rate over a time interval. The syringe pump was loaded with DMEM/F12 media. In using this method, each time point represented a different volumetric flow rate and by extension a different shear stress. I used CISMM's Video Spot Tracker software to track all of the beads present in the first frame until they either became "untrackable", left the field of view, or the flow program ended.

Chapter 5 Clearing against gravity

In this chapter I discuss my work to incorporate Vertical Air-Liquid Interface (VALI) transport measurements into the Mucus Clearance Assay system. Using this new technique, I demonstrate differences in vertical transport between buffer and mucus. Using the same field of cilia, I show that buffer transport decreases and ultimately ceases as the system switches from a horizontal to vertical conformation. Reconstituted HBE mucus, however, continues to successfully transport when the system is in a vertical conformation. This marks the first time that this phenomena has been demonstrated in an *in vitro* system. Demonstrating that buffer transports in a horizontal system, but not at VALI makes two important points:

1. False positives exist in horizontal PIV measurements: fluids that demonstrate horizontal transport don't necessarily transport vertically.
2. Tilt angle is a necessary requirement to accurately measure the ability of cilia driven transport to "clear" a fluid.

Building on this experiment I then demonstrate that the system is a "true" mucus clearance assay. It is the first *in vitro* cell culture system that can discriminate between fluids that successfully transport. I then use this clearance assay to demonstrate that fluid viscosity alone is not sufficient in enabling successful transport. I do this by showing successful transport of dilute mucus and also

unsuccessful transport of a Polyethylene Glycol (PEG) solution with an effective viscosity comparable to that of healthy mucus.

5.1 Gravity and Clearance

In the model that I've built up to this point, I've ignored body forces. All of my experiments have been performed in a horizontal conformation, so gravity could be ignored. The lung, however, isn't horizontal and mucociliary clearance has to work with gravity, against gravity and every angle in between. This raises the question of whether or not gravity plays a significant role in mucus clearance; how much does clearance change when we add drainage into the system? The medical community has already started answering that question. A therapeutic technique called postural drainage has been used since the 1950s to assist with clearing excessive mucus associated with several diseases (MCSP, DMS, & FRCP, 2012), in particular Cystic Fibrosis. Patients are oriented in several different postures to facilitate drainage from different regions of the lung. It's clear from the efficacy of this technique that gravity does play a role in clearance. In this chapter I will use the mucus clearance assay to look at transport against gravity and update my model to include gravitational drainage. During the course of this work I discover that incorporating gravitational drainage provides a new transport/clearance test with different results from the horizontal models. I then use this new platform to evaluate my drainage model and discover that there is another mechanism in play besides the fluid rheological properties that optimal MCC has been attributed to for the past 35 years.

5.2 Tilting the clearance assays

As previously discussed in chapter 3, I designed and built a tilting microscope system (figure 5.1) so that channels could be tilted while maintaining an imaging plane parallel to the epithelial surface. Using this system allowed me to perform PIV experiments in which cilia driven transport competed against gravitational drainage.

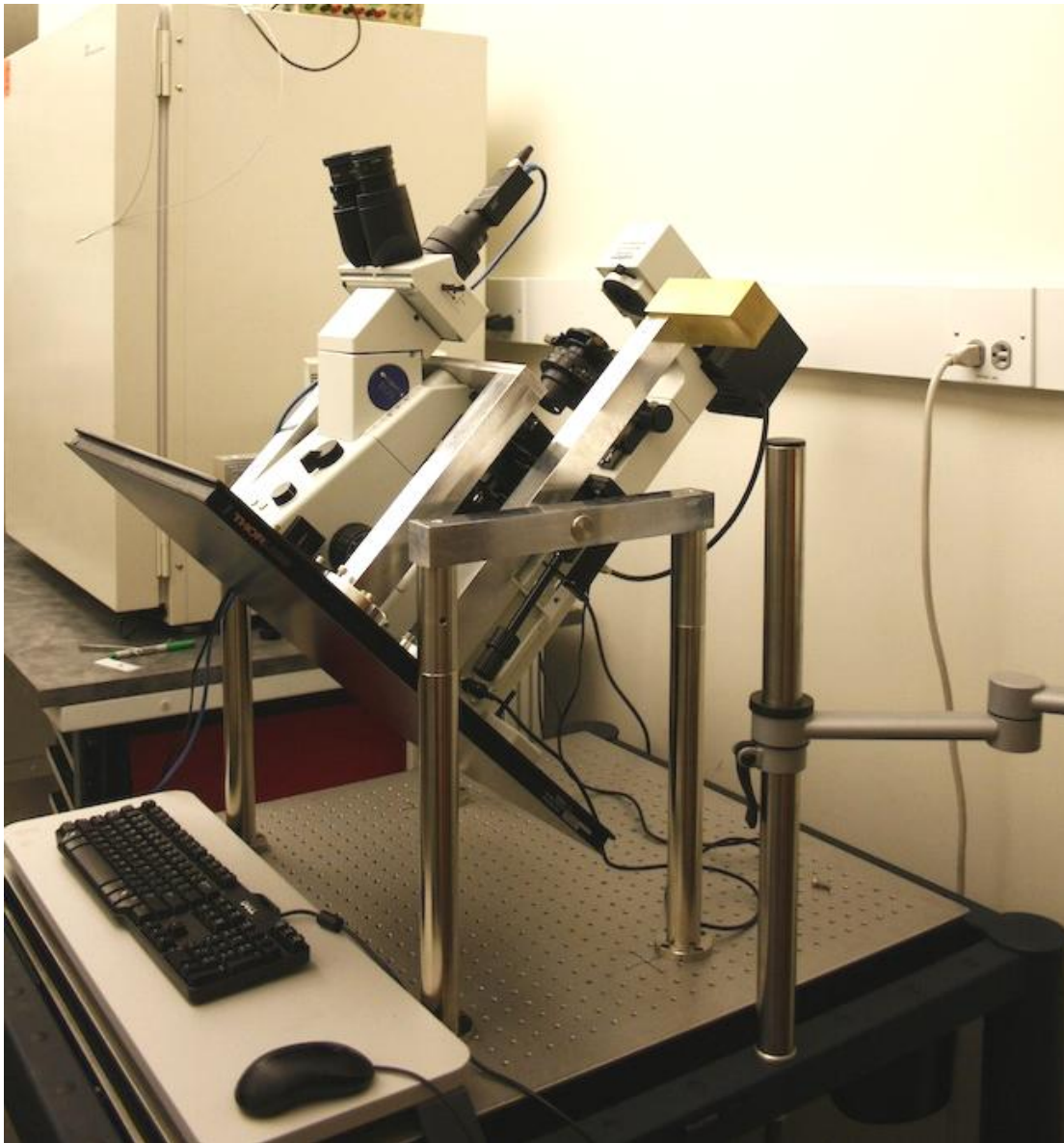


Figure 5. 1 The custom built microscope IXION. The microscope is capable of bright field, phase, and epifluorescence microscopy and can be tilted so that the optical path is 30, 45, 60, or 90 degrees from vertical.

When tilting a partially filled channel, it's useful to think about the channel as three distinct regions (Fig. 5.2). Region 1, the Air-Liquid Interface (ALI) Zone, represents an area where the majority of the airway surface liquid (ASL) has drained away.

Region 2, the Meniscal Zone, is dominated by the surface tension of the (ASL) and

the wetting of the channel's floor, ceiling, and walls. Region 3, the Submerged Zone, is entirely filled liquid.

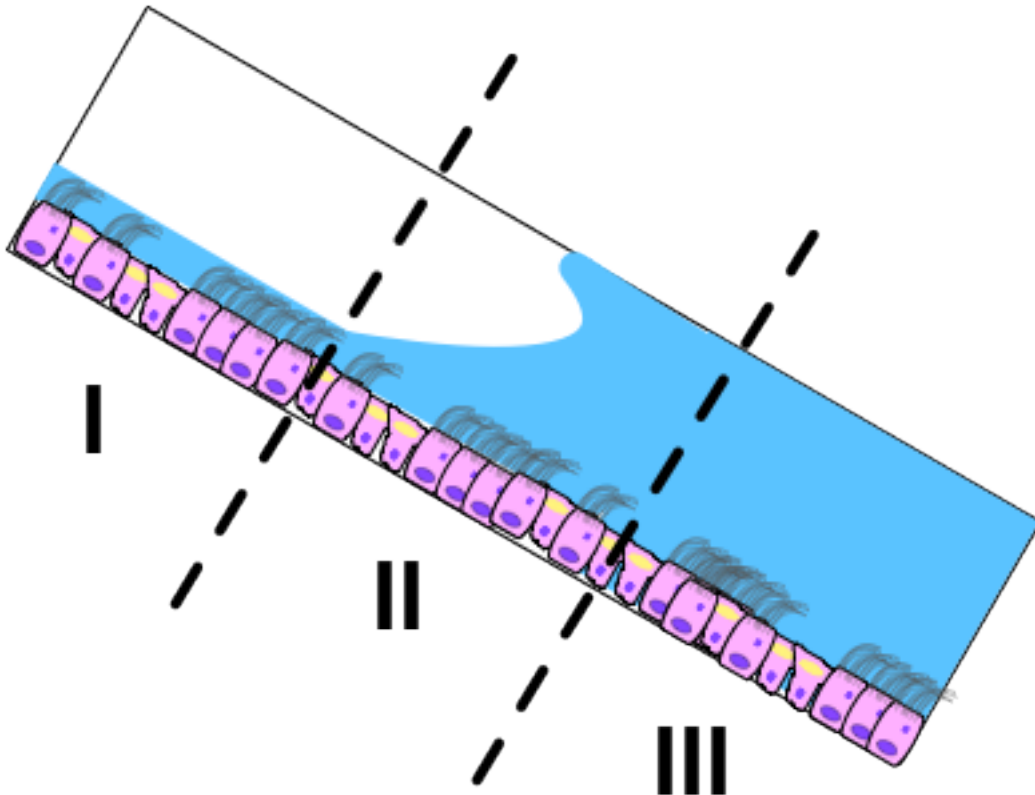


Figure 5. 2 Different fluid regimes in a partially filled channel. They are the I) Air-Liquid interface zone II) Meniscal zone III) Submerged zone

5.2.1 Submerged Zone

The submerged zone is the region of the channel in which the liquid spans the entire height of the channel. A defining feature of this zone is the lack of drainage. Drainage is a function of a denser fluid being located above a less dense fluid. As there is no air in this region and the simulant will generally have a constant

density, there will be no drainage in this region. This lack of drainage is something shared by *in vitro* cell culture studies performed on horizontal cultures. As discussed in chapter 2, the epithelium is capable of regulating fluid (Matsui et al., 2000), however, this is a slow process compared to the timescale of clearance. Button et al. showed that ASL volume regulation requires about 12 hours to absorb an added fluid with a depth of 30 μ m (Button, Picher, & Boucher, 2007b). This means that in both the submerged zone and in traditional cell culture models, the depth of any apically added isotonic fluid is dependent on the amount of fluid initially added. The large reservoir of fluid above the cells in the submerged zone will dominate the fluid regulation of the epithelium. Due to the similar conditions between this region and the flat channel used in chapter 4, we expect similar flow profiles. We would expect a cilia-driven Couette component along with a recirculation driven Poiseuille flow as we go away from the cell layer.

5.2.2 Meniscal Zone

The Meniscal Zone represents a transition between the submerged zone and the Air-Liquid Interface zone. The height of the liquid here is governed by the surface energy of the liquid-solid boundaries: the ability of the liquid to wet the epithelial layer and the ceiling/walls of the channel. As a hybrid of the other two zones this region takes on the properties of both: drainage is possible near the ALI interface, but not near the submerged zone interface. Strictly speaking the contact line is the interface between the solid surface, the liquid and air. The rough cell surface and the wetting of the cells' external structures make it difficult to strictly define such an interface. In general when I refer to the contact line, I will define it as though the tips

of the cilia form a solid surface. This plane and a couple of bead diameters above it, will constitute the “contact” line.

5.2.3 Air-Liquid Interface

The Air-Liquid Interface is of great interest because of its physiological relevance. Essentially the height of the liquid is determined by properties of the epithelium and gravity. Specifically the amount of liquid is controlled by the following parameters

1. The wetting of the epithelial apical surface
2. Cellular secretion and absorption
3. Cilia driven transport of liquid
4. Draining of excess liquid

Coupled with these factors are the properties of the ASL. The ASL composition, which will in part be controlled by cellular secretion and absorption, affects all of the parameters. The ASL's composition determines the ASL's interfacial energy and thus is important in the wetting of the epithelial surface. Finally, ASL viscoelasticity is going to affect cilia driven transport as well as how quickly the liquid layer drains.

The ASL liquid height affects mucociliary transport (Randell, 2006). If the epithelial surface is sufficiently hydrated there will be a maximum velocity at the cilia tips that will fall off as a function of distance from the cilia. In a tilted system, there is a point sufficiently far enough away from the cilia tips that the downward force of drainage dominates the upward cilia driven flow. These opposing forces determine the maximum height of fluid that the system can support, above which any additional

liquid would drain. This total height determines the volumetric flow rate of the ASL and ultimately shows how much the system is capable of clearing.

5.3 Adding Drainage to the model

As the system is tilted gravity begins to play a role in fluid flow. In the horizontal conformation the fluid self-leveled; the denser buffer/ASL occupied the bottom of the apical chamber with the less dense air above. As the system is tilted, the denser ASL drains into the lower regions formerly occupied by the air. This drainage is what gives us the different fluid zones in the channel. In a 1973 paper, Blake modeled the effect of gravity on mucus flow using an expression equivalent to equation 5.7 (Blake, 1973). The following is a derivation of that expression starting with Navier-Stokes.

$$\rho \left(\frac{\partial u}{\partial t} + u \frac{\partial u}{\partial x} + v \frac{\partial u}{\partial y} \right) = \rho X - \frac{\partial p}{\partial x} + \mu \left(\frac{\partial^2 u}{\partial x^2} + \frac{\partial^2 u}{\partial y^2} \right) \quad (5.1)$$

Similar to our derivation of Poiseuille flow, we can use the following constraints to simplify the equation.

1. Steady flow
2. Uniform Flow
3. Velocity in the y' direction is 0 (direction perpendicular to the plane of the channel bottom)

4. No external pressure gradient in the x' direction

In this case, however, we do have an external body force, which is gravity.

This leaves us with

$$0 = \rho g + \mu \left(\frac{\partial^2 u}{\partial y^2} \right) \quad (5.2)$$

We can generalize this for several tilt angles by using the projection of gravity along x' , which will be the sine of our tilt angle α .

So equation 5.2 becomes

$$\mu \left(\frac{\partial^2 u}{\partial y^2} \right) = -\rho g \sin \alpha \quad (5.3)$$

Integrating this equation gives us

$$\rho g \sin \alpha y + \mu \frac{du}{dy} + c = 0 \quad (5.4)$$

We can solve for the constant c if we assume there is no shear at the gas-liquid surface. This means that τ_{yz} which equals $\mu \frac{du}{dy}$ is equal to 0 at $y = h$. We get a value of $-\rho g \sin \alpha h$ for c . Plugging this value back into 5.4 and integrating again gives us

$$\mu u + \frac{\rho g \sin \alpha y^2}{2} - \rho g \sin \alpha h y + c = 0 \quad (5.5)$$

Solving for u gives us

$$u = \frac{\rho g h^2 \sin \alpha}{2\mu} \left(\frac{2y}{h} - \left(\frac{y}{h} \right)^2 \right) - c/\mu \quad (5.6)$$

We can solve for this constant c by assigning a boundary condition to the liquid/channel surface. As a first attempt let's just consider this boundary as a stationary vertical wall and apply a no-slip boundary condition at $y=0$. This assumption gives c a value of 0.

$$u = \frac{\rho g \sin \alpha}{2\mu} (2yh - (y)^2) \quad (5.7)$$

In Blake's 1973 and 1975 papers he used this to model the effect of gravity on mucus transport and came up with the following conclusions (Blake, 1973; 1975).

1. Gravity is an important factor in the transport of mucus when the mucus layer is thickened or reduced in viscosity.
2. Gravity is also important when the periciliary liquid increases in depth.

The first conclusion can be seen in the context of postural drainage. Blake notes that in a pathological state that gravity can be used to aid in draining mucus out of the airway. This conclusion also has interesting consequences in terms of hydration. Excessively hydrated mucus transports faster than normal mucus (Randell, 2006), but the decreased viscosity and increased mucus depth make a hydrated mucus more susceptible to gravitational drainage. To better understand the relationship between viscosity, film thickness, and drainage I've constructed several plots in

figures 5.3-5.5. Figure 5.3 represents the flow profile of a vertical 10 μ m film for buffer, normal mucus and pathological mucus. In this profile the velocity at the wall is 0 μ m/s. I use a viscosity of 8.9×10^{-4} Pa s for buffer .16 Pa s for 2.5% reconstituted mucus, and 10 Pa s as a low end estimate for COPD sputum (Puchelle & Zahm, 1984).

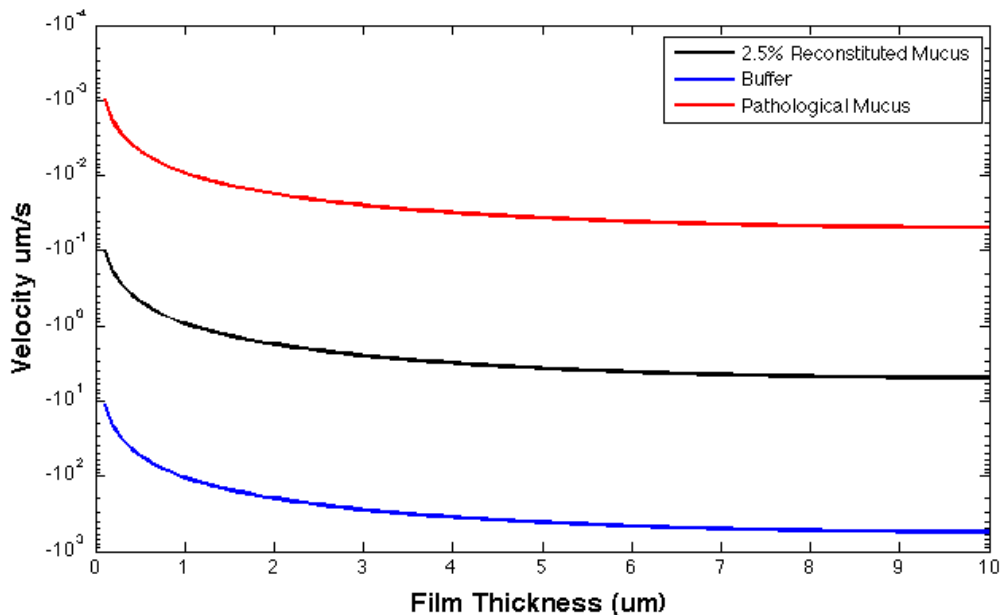


Figure 5. 3 The velocity profile for liquid films of various viscosities on a vertical wall. The drainage speed of the liquid spans several orders of magnitude, the pathological sputum drains on the order of 10 nanometers per second while the buffer will drain at hundreds of microns per second.

Using figure 5.3, we can start getting a sense of the relationship between viscosity and drainage. All of the fluids will experience some drainage, however, the timescale is the most important part. A buffer film draining at a velocity of half a millimeter per second will thin much faster than the pathological mucus film draining at 10 nanometers per second. This becomes more interesting if we compare the drainage rate to the mucociliary clearance transport rate.

We do this by changing the boundary condition at the wall to account for cilia driven transport. Fig 5.4 is a model of upward cilia driven fluid transport subject to gravitational drainage. For the sake of simplicity we will use the same coarse-grained traction layer from chapter 4, but assume that the ciliation is highly uniform so that we can start the traction layer at the cilia tips. Using this boundary condition, the velocity at the cilia tips, with equation 5.6 will give us the flow profile for our cilia model propelling fluid up a wall against gravitational drainage.

$$u = \frac{\rho g h^2 \sin \alpha}{2\mu} \left(\frac{2y}{h} - \left(\frac{y}{h} \right)^2 \right) - U \quad (5.8)$$

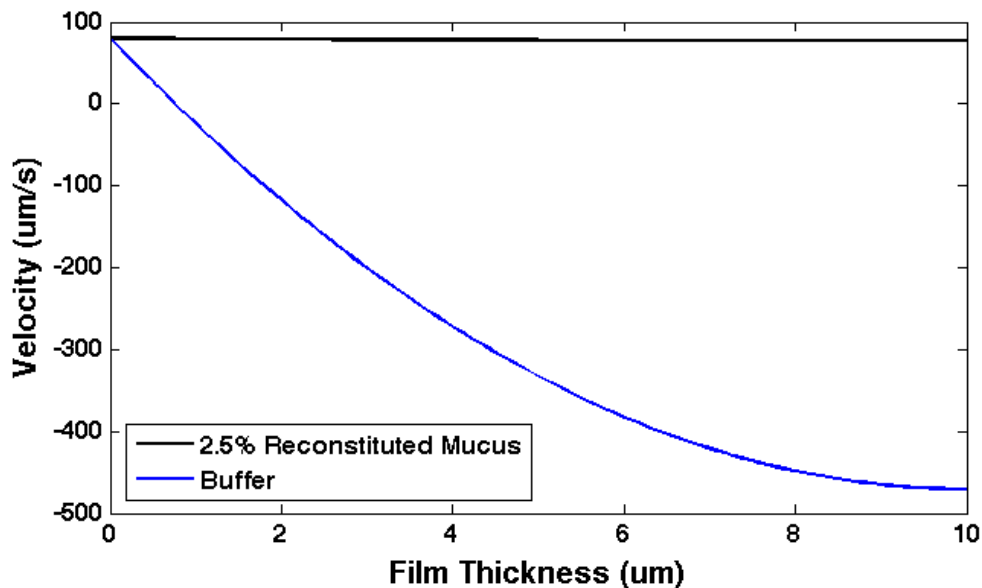


Figure 5. 4 The velocity profile for 10um films of buffer and 2.5% reconstituted mucus on a vertical surface. A boundary condition has been applied so that the velocity of the fluid at the wall is 80um/s up the wall. The mucus film will continue up the wall with a positive velocity while the majority of the buffer will drain down the wall.

This profile shows that for a 10um film of 2.5% mucus vertical, cilia-driven transport is practically unaffected by gravity. A similar film of buffer, however, predominately drains. If instead we use a thinner buffer film size of 1um, we see that cilia driven transport prevails over gravitational drainage (figure 5.5).

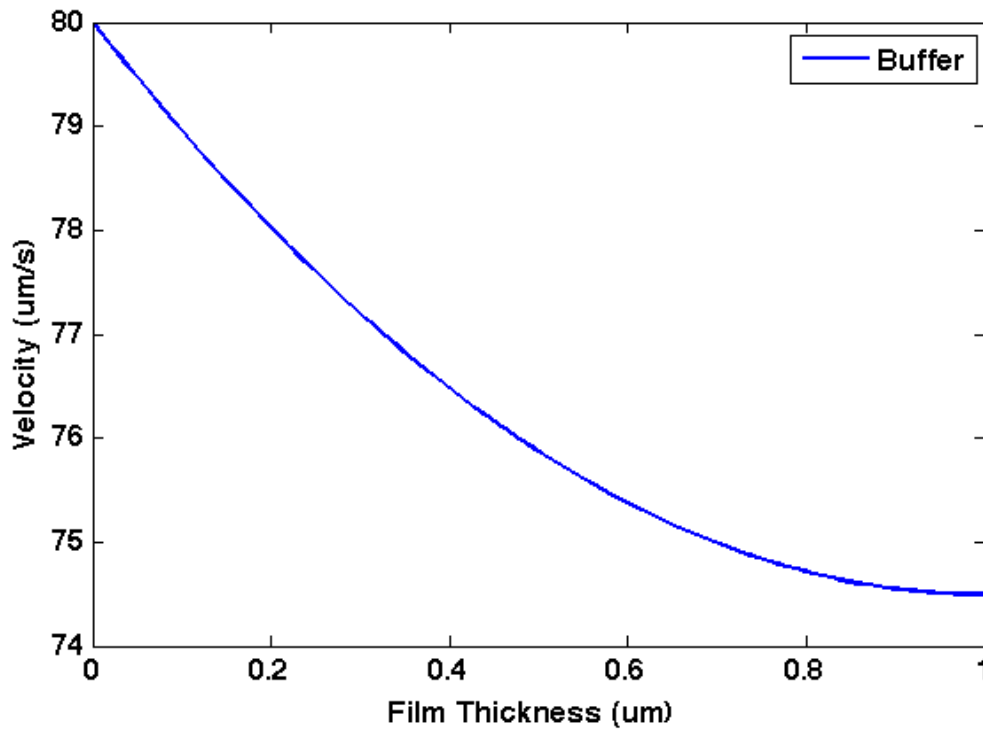


Figure 5. 5 The velocity profile for a 1um film of buffer on a vertical surface. A boundary condition has been applied so that the velocity of the fluid at the wall is 80um/s up the wall. In this scenario the thin 1um film of buffer will continue up the wall.

If we set $u(h) = 0$, we can solve equation 5.8 for h to get an equation for the steady state thickness of the film.

$$h = \sqrt{\frac{2\mu U}{\rho g}} \quad (5.9)$$

Plugging in viscosities and approximate densities of liquids in figure 5.3, and using a boundary velocity of 80um/s I generated a table of film thicknesses (table 5.1)

Liquid	Supported film thickness
Buffer	2.7 um
2.5% HBE Mucus	21 um
COPD Mucus	160 um

Table 1 Cilia boundary supported film thickness of several fluids on a vertical wall.

Overall this drainage model predicts that upward cilia driven transport dominates the effects of gravitational drainage for thin films of mucus and fluids of similar viscosity. It also predicts that fluids with viscosities similar to buffer are affected by drainage, but that even buffer can still maintain a thin film (on the order of a micron) when propelled upward by cilia. In the next sections, I use the tilting microscope and mucus clearance assay to test this model.

5.4 Vertical Air-Liquid Interface (VALI) transport

In the following section I use the mucus clearance assay and tilting microscope to test the predictions of the drainage model. Experimental methods for this section can be found in section 5.8.1. Broadly these experiments are looking at the transport of buffer and reconstituted 2.5% HBE mucus as a function of tilt angle.

5.4.1 Mucus Transports at VALI while Buffer does not

My first experiment, which used the methods in section 5.8.1, compared the VALI transport of PBS and 2.5% reconstituted mucus over a region of linearly entrained cilia. For both PBS and mucus my initial field of view was located in the meniscal zone, which can be identified by the change in brightness seen in transmission microscopy (fig. 5.6).

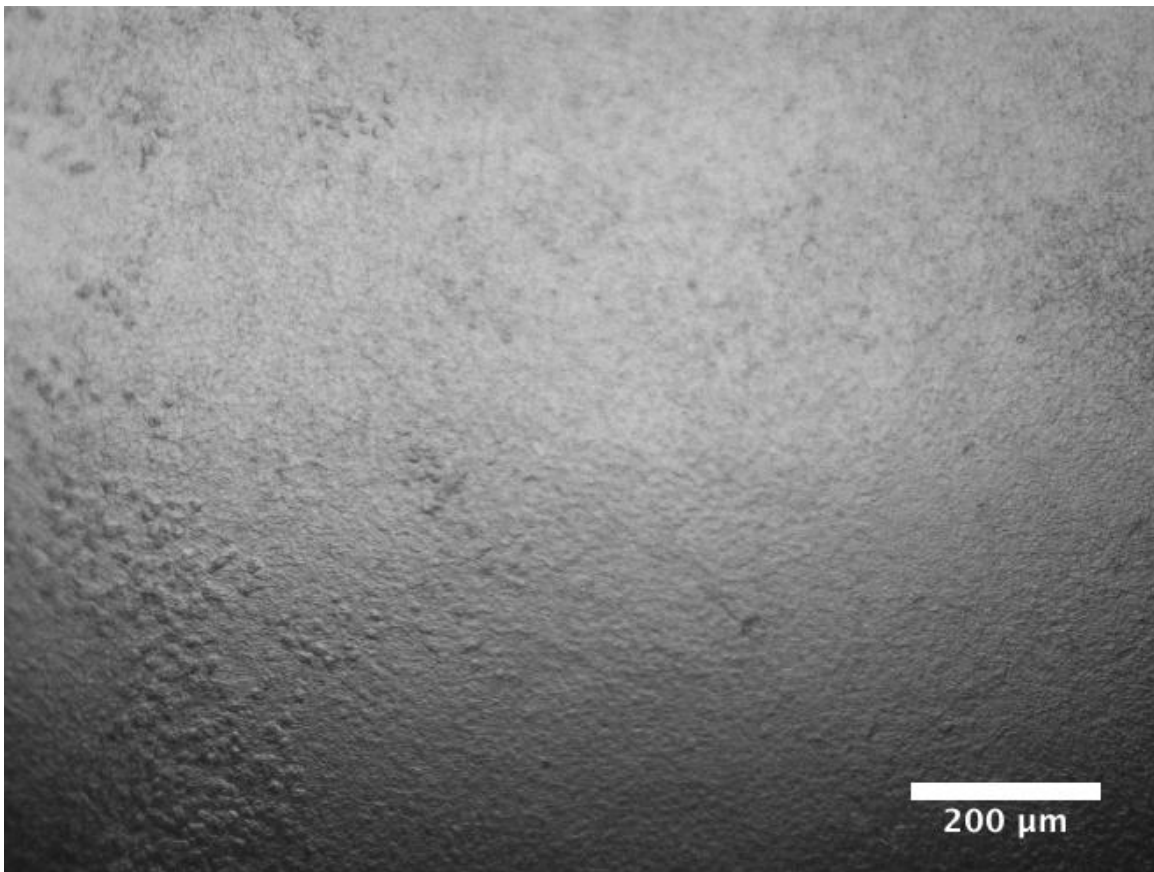


Figure 5.6 Field of view showing the meniscal and ALI zones of a tilted channel. The reduced brightness in the bottom of the image is from light refracting off of the curved water surface of the meniscus. I refer to the region above this dark band as the ALI zone

My first observation was that the microbeads did not transport from the meniscal zone to the ALI zone. As I tilted the channel the extent to which the beads

transported up the channel diminished: beads were confined to the regions downhill of the meniscus (fig. 5.7). The exact line of the meniscus isn't well determined, but there is a boundary that the beads do not cross: instead they approach the boundary and then move along it. More importantly this behavior happened over regions of cilia that had transported beads uphill at lower tilt angles. It's from this that I infer that not only is the buffer draining as a function of tilt angle, but also that the beads can't cross the meniscal interface in this system. As the channel is tilted, the meniscal interface moves down the channel and bead transport is confined to the region below the interface. In going back to equation 5.9 and accounting for the tilt angle, a boundary moving 80um/s would support a film of ~4um. Considering the maximum heterogeneity at the cilia surface, and a boundary moving less than 80um/s is sufficient in accounting for the lack of transport as a function of tilt angle. Likewise I should note that there could be an interfacial penalty as well as the bead would potentially have to break through the surface of the buffer to transport uphill in a thin fluid.

Following the PBS experiment, I removed the PBS and added mucus to the channel. During the mucus experiment I observed that beads in mucus were able to transport from the meniscal zone into the ALI zone, although there still appeared to be an interface region. Figure 5.7 shows a clear region where beads still continue to turn laterally as they reach the meniscus. The key difference, however, is that there is a population of beads which transports through this interface and further uphill. In fact beads travel at least another 1000um uphill from the interface (Fig. 5.8). In

looking at table 5.1, a boundary of 80 μ m/s is capable of supporting a mucus film up to 21 μ m in depth. These experiments establish two important principles.

1. Mucus will transport at a Vertical Air-Liquid Interface, but buffer will not.
2. Tilt angle is an important parameter that has an influence on transport measurements.

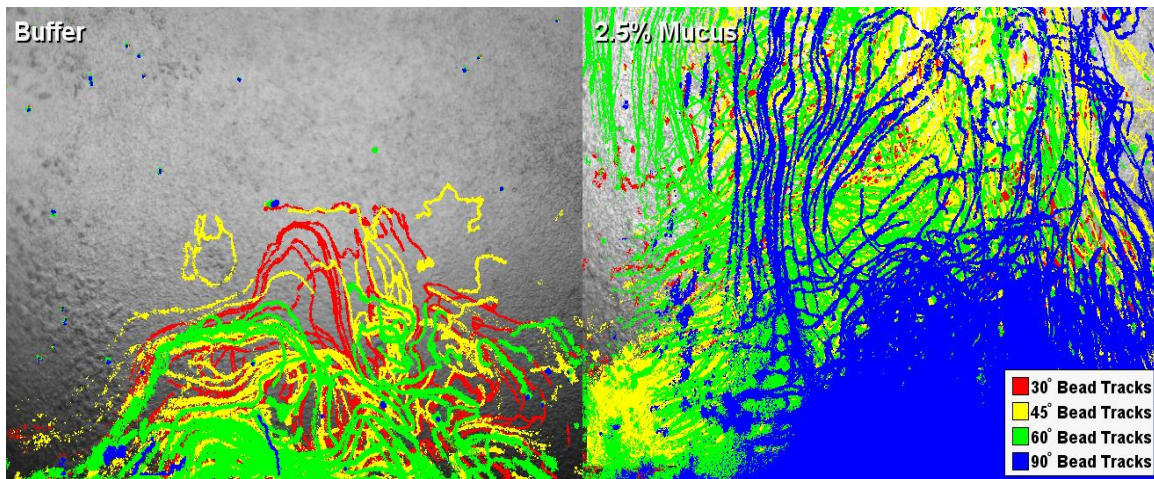


Figure 5.7 A composite image showing tracer paths of beads in both buffer and mucus over a ciliated cell culture at varying tilt angles. Left) The extent to which particles travel uphill in the buffer over the ciliated cells is reduced with increasing tilt angle. Presumably the particles are confined behind the meniscus. Right) Particles in mucus continue to travel uphill beyond the meniscus at all tilt angles including 90 degrees.

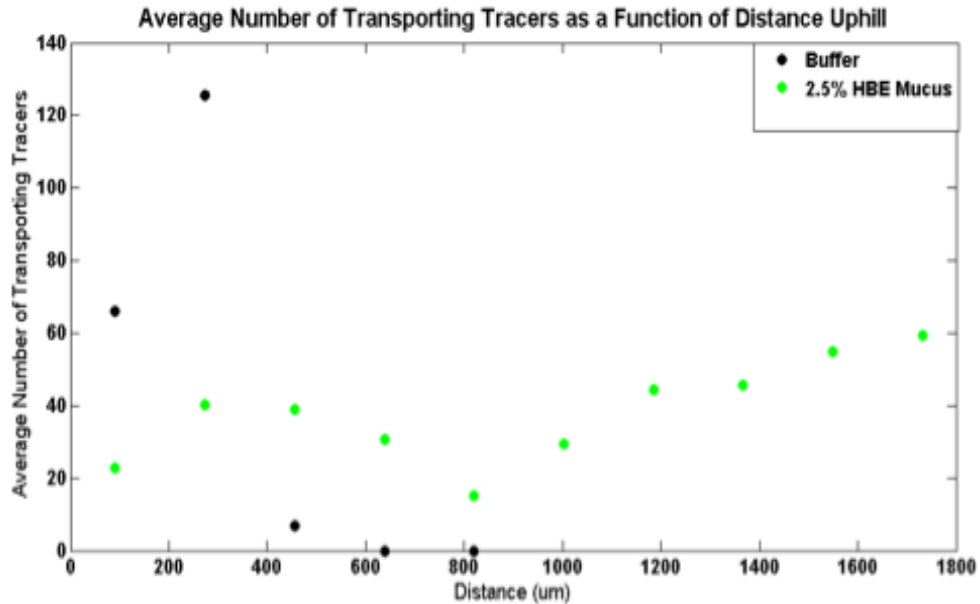


Figure 5. 8 The average number of particles transporting as a function of distance uphill in the channel at a 60-degree tilt angle. Buffer reaches a maximum extent, while mucus continues to travel over the same region of cilia.

5.4.2 Vertical Hurricanes

After identifying that mucus was capable of VALI transport and that buffer wasn't I tried a slightly modified experiment. Instead of using a linear region, I found a "mucus hurricane", a circular organization of cilia driven transport described in Matsui et al. (Matsui, Randell, Peretti, & William Davis, 1998c). I followed the same procedure detailed in the prior section with one key change to address my concern that inhomogeneity in cilia density could skew results. If a minimum cilia density is required for VALI then the contact line of that liquid must be present over this region of minimum density. Although I became fairly adept at adding fluid into the channel to control the position of the contact line, errors of a couple of hundred microns in either direction could give misleading results. I intentionally placed much less mucus into the channel to allay any fears that the mucus' transport uphill in the prior

experiment may have been a function of a contact line located further uphill than buffer. The end result is that the mucus contact line was at least a millimeter downhill of the buffer contact line.

The resulting bead paths in buffer were not nearly as smooth and uniform as the original endogenous hurricane, a phenomenon also observed in Matsui's 1998 paper (Matsui, Randell, Peretti, & William Davis, 1998c). As I tilted the system, I saw activity consistent with the linear experiment. The buffer hurricane transport only occurred in regions below the buffer contact line. In the experiment with 2.5% HBE mucus, the mucus was transported up to the hurricane over the course of several minutes and hurricane activity started. The tilted mucus hurricane appeared similar to the endogenous hurricane; the tracers had smooth, concentric paths (Fig. 5.9). The mucus continued transporting circularly as I tilted the system to 90° (Fig. 5.9).

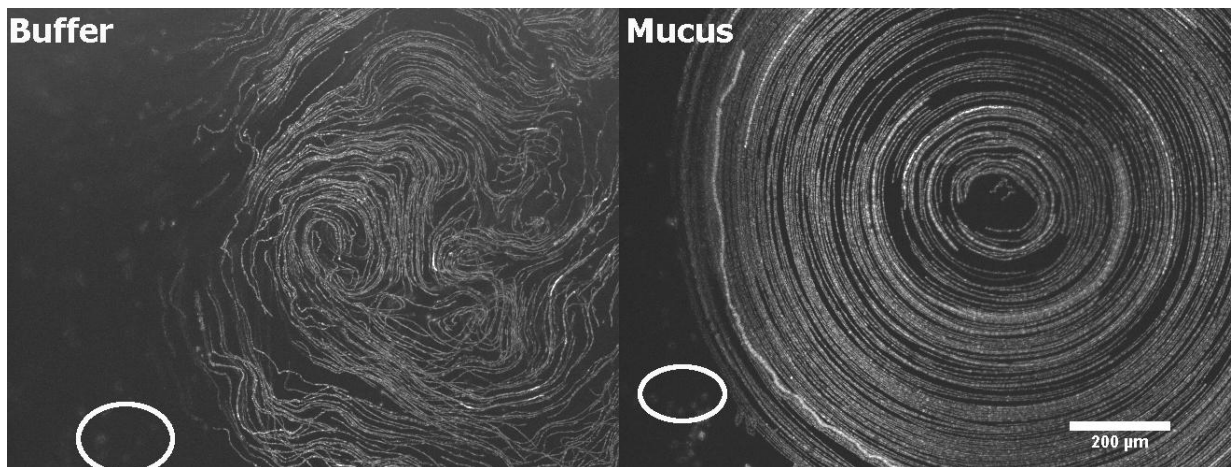


Figure 5.9 Maximum intensity projections (MIPs) show pathlines of fluorescent microbeads being driven by the same field of cilia in both buffer and reconstituted mucus. Pathlines of the beads in buffer solution are unordered while pathlines of beads in the mucus are circular and form a “mucus hurricane”. The white ellipse marks the same spot in both projections.

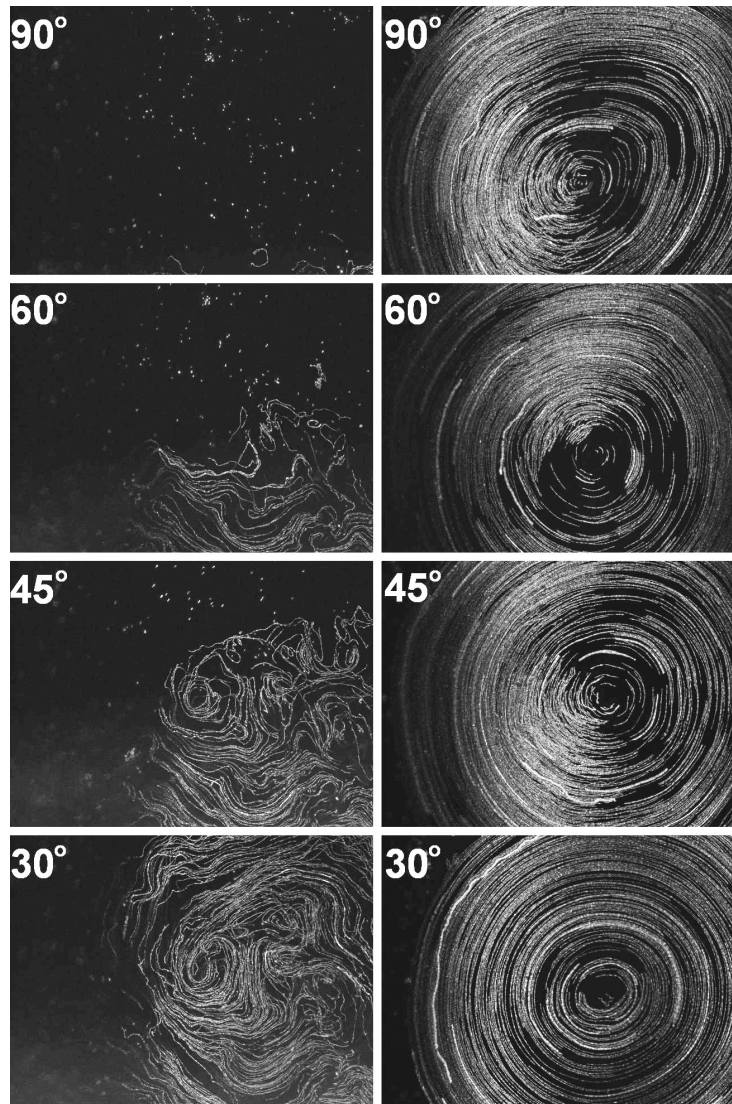


Figure 5.10 MIPs showing the pathlines of fluorescent tracer particles. Left) Pathlines of buffer tracers as a function of tilt angle. In buffer transport is confined to the region behind the liquid contact line. As tilt angle increases and this line retreats due to drainage, the region capable of supporting bead transport diminishes. Right) Pathlines show that the “mucus hurricane” is maintained regardless of tilt angle. Transport doesn’t diminish as a function of tilt angle and persists at 90 degrees.

The behavior of the two fluids reemphasizes that drainage affects cilia driven transport of low viscosity fluids. Another interesting observation can be drawn from the organization of the hurricane: the hurricane has a region of cilia that are pushing

the mucus “downhill” in the vertical conformation. The fact that the tracers “turn the corner” supports the notion that the mucus gel is behaving as a monolithic block.

5.5.1 A True Clearance Assay

VALI transport represents an additional step towards improving the physiological relevance of mucociliary clearance experiments: non-horizontal conformations and by extension the ability to drain are both commonplace, if not dominant characteristics of the lung. The two prior sections demonstrate that not all fluids are capable of VALI transport, which implies that parameters exist that allow for a liquid to successfully perform VALI transport. The goal of the mucus clearance assay is to develop a system and methodology that can identify the parameters and their required ranges to support VALI transport. The experimental methods for these experiments can be found in section 5.8.2.

5.5.2 Developing a Methodology

In discussing the buffer and mucus experiments in the prior sections, I glossed over the countless failures that preceded the successes. It wasn't until my third or fourth batch of devices that I found cultures capable of consistent VALI transport. In my first couple of batches I didn't get VALI at all and started having serious doubts about the lungs' ability to clear mucus against gravity. I think that ultimately the key to a successful device is cilia density. I made a small design change in the device (I increased the size of the gap between the media reservoir

and the basal channel) and became more aggressive with clearing any collected liquid on the apical surface.

After these changes I was able to perform the experiments in the prior section. Even with the changes I still only had ~50% yield amongst devices and typically only 1 successful region in a successful device. While I could intuitively identify potential regions via microscopy (through high cilia density and fast endogenous transport “rivers”,) I never developed a quantitative method for determining if a region supported VALI without performing a test. So for any potential test I needed a positive control (at this point reconstituted HBE mucus) to establish the device as a working mucus clearance assay. Additionally I was concerned about temporal variation, both long-term changes and short-term changes. Long term there is no guarantee that the morphology of a culture would stay the same over the course of days, in fact it is a guarantee that the culture morphology will change. This necessitated that the positive control had to take place the same day as the experiment. Short term I had to worry about the health of the cells. Performing the experiments required a lot of time, time that required the cells to be out of the incubator in a non-ideal environment. Over the course of a 5-hour experiment I could stress the system enough that I could “break” a successfully clearing region. While there are definitely improvements that I could make to the system, I decided that the best way to proceed was to always end the experiment using the positive control. I wouldn't declare that anything wasn't capable of VALI transport unless I could demonstrate that the system itself was still capable of VALI transport. There are of course some flaws to this methodology. It is important to be aware that any potential

test fluid could also “break” the system in such a way that the following positive control becomes impossible. This could include the blocking of a potential biochemical interaction or something that would change the local rheology.

5.5.3 Choosing Simulants

After developing a methodology to test for VALI, it was equally important to develop a methodology to choose a fluid/mucus simulant to use in the test. From discussing the literature in chapter 2, there is no consensus on which rheological property of the mucus has the most influence on transport. In considering and looking for a biochemical interaction between mucus and cilia, it quickly becomes apparent that this parameter space is just as large and daunting as the rheological space. Between the various combinations of oligosaccharides, potentially exposed proteins on the apomucin, and receptors on the cilia/epithelial surface, there are a plethora of possibilities. The parameter space is way too large to try everything, so it's essential to have a focused hypothesis to effectively choose a simulant that's test returns meaningful results. I'll go into more detail with hypotheses and potential simulant choices after I present the data that I've taken thus far, but I'll also strive to make clear my choice of simulants and their ramifications in the following sections.

5.5.4 DTT treated mucus: A direct assault on rheology

My central hypothesis in this dissertation is that rheology is not the only fluid property that governs mucus clearance. I also posit that there is something biochemically special about mucus that enables it to transport. Ideally the perfect

test for this would be a material that is vastly different from mucus rheologically, but similar to mucus biochemically. I've already mentioned the reducing agent dithiothreitol (DTT) as part of the protocol for removing endogenous mucus from cell cultures. DTT works by reducing the disulfide bonds between mucin subunits (Fig 5.11)

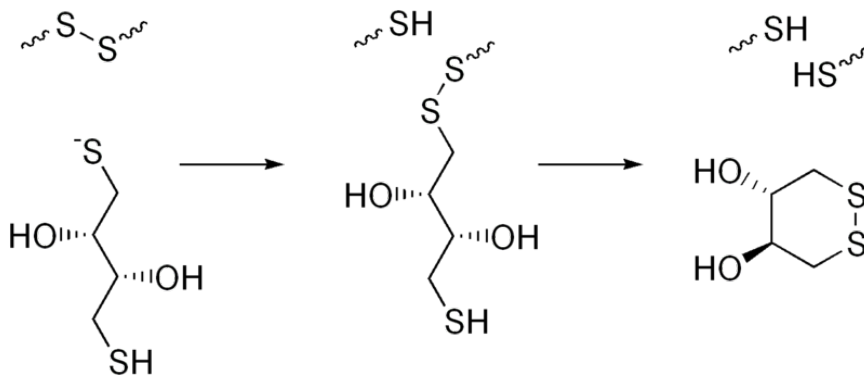


Figure 5.11 Process by which DTT reduces a disulfide bond via thiol-disulfide exchange. The thiolate end of the DTT replaces one of the sulfurs in the disulfide bond. Next the thiolate on the other end of the molecule replaces the original sulfur in the new disulfide bond.

During the process the DTT molecule is essentially consumed; breaking all of the crosslinks requires that there are at least as many DTT molecules as disulfide bonds. Also the DTT can only break bonds that it can access, “hidden” bonds will remain intact. The power of this is that it enables me to change the rheology of mucus, while keeping the biochemistry largely intact. To test this I made a 200mM solution of DTT and added it to the 2.5% reconstituted mucus to tumble overnight for a final DTT concentration of 20mM. Admittedly the concentration choice was just an educated guess; the end goal of this experiment was to radically change the

rheology. Performing passive bead rheology on the final solution made it possible to ascertain the rheological differences between the DTT treated mucus and the regular reconstituted 2.5% HBE mucus. Addition of the DTT dropped the effective viscosity of the mucus from .16 Pa s down to .02 Pa s (figure 5.12). Even more dramatic was the change in elasticity; breaking the crosslinks almost completely removed any elasticity.

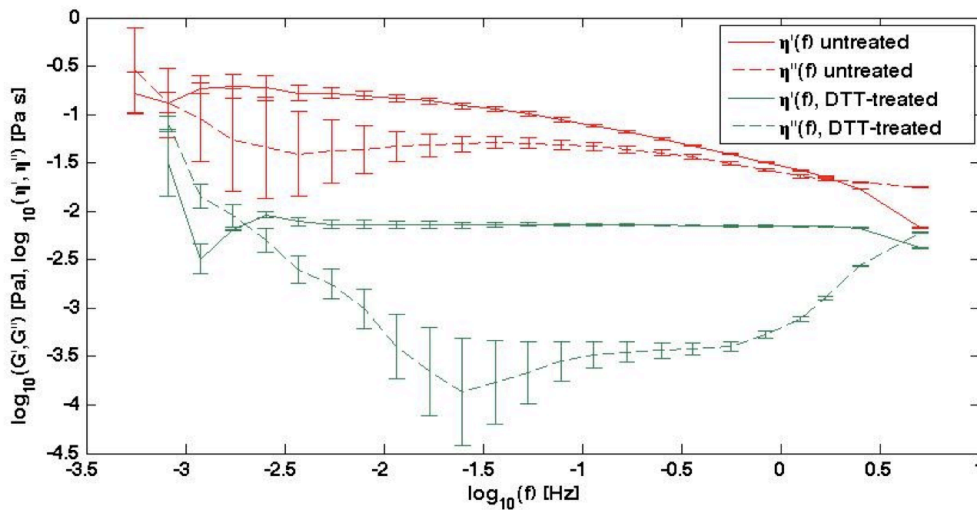


Figure 5.12 Frequency plot of effective viscosity of normal and DTT treated mucus. The DTT treated mucus exhibits both lower viscosity and elasticity than the HBE mucus control.

After determining that the rheology of the DTT mucus had been substantially changed (Fig. 5.12), I proceeded to use it to test for VALI transport at a 60° incline. While I was performing an initial negative control with beads and buffer, I observed VALI transport. Interestingly enough, however, the transport stopped after about 15 minutes. Presumably the system had left over endogenous material, which transported until it was depleted from the system. To test this, I pulled the remaining fluid from the top apical port and administered a fresh bead/buffer solution to the

bottom port. Over the course of 15 minutes I observed that there was no VALI transport. I removed the bead/buffer solution from the top port and added the bead/DTT mucus solution to the bottom. VALI transport quickly resumed. Figure 5.13 shows a maximum intensity projection image of tracer particles moving up the channel in the 3 different fluids. I took all of the movies for each experiment and each field of view and tracked the particles using CISMM's video spot tracker. From there I binned each field of view into smaller units of spaces and found the average velocity of each bead while it was in that bin. I averaged the average velocity of each bead in that region and used that information to produce a velocity map of the channel (Fig 5.14). The magnitude of the velocity vector has been scaled to make the direction easier to see, but the map shows a "river" of transport roughly centered

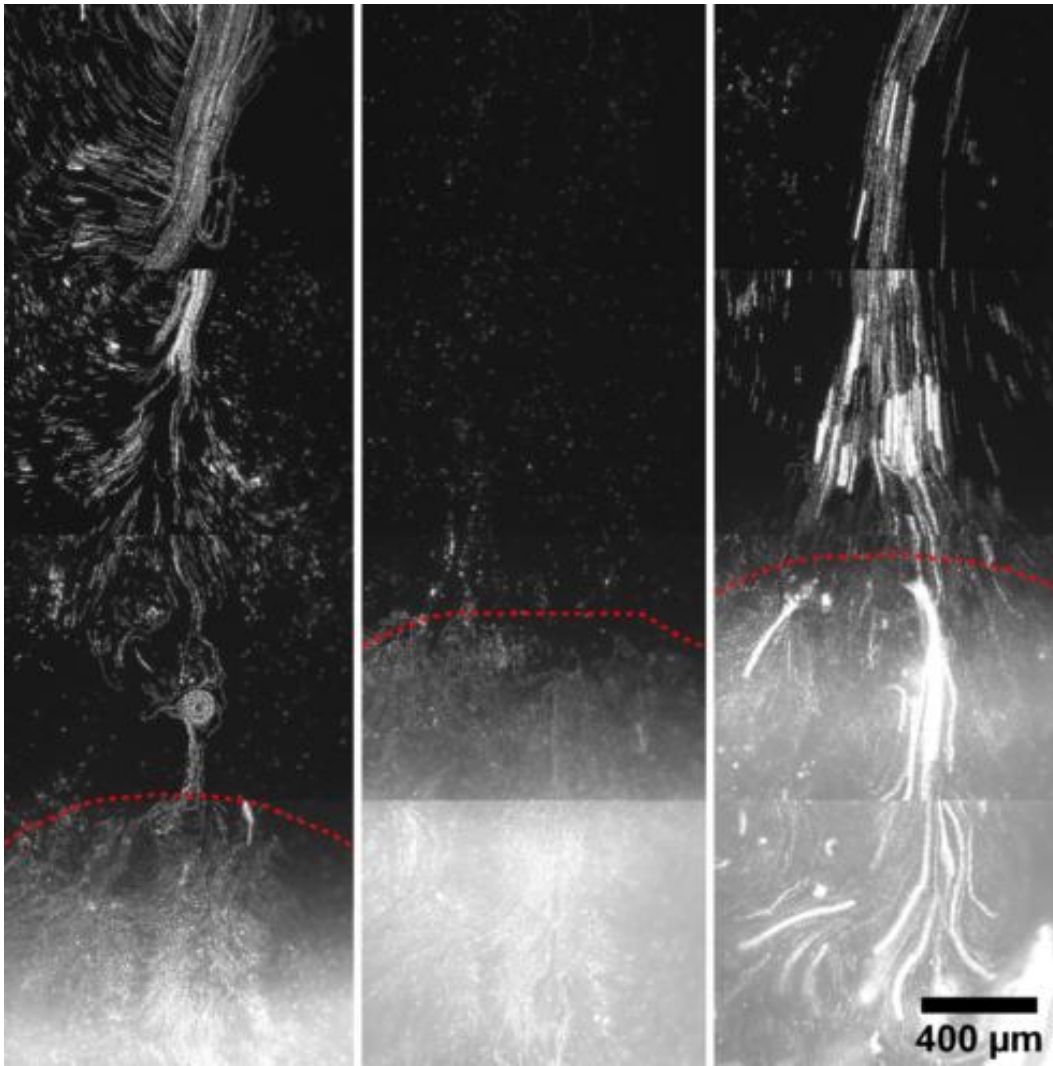


Figure 5.13 Maximum intensity projections (MIPS) of bead transport over the same region of cilia inclined at 60°. To the far left is the initial bead/buffer solution, presumably with remaining endogenous material. The middle panel is of a freshly administered bead/buffer solution. The final panel is with the addition of DTT treated mucus. These panels show that despite being over the same patch of cilia, buffer doesn't undergo VALI transport, while endogenous mucus and reconstituted mucus demonstrate VALI transport.

in the channel (fig 5.14). There appears to be a downward component at the very top of the channel, but in looking at the video, this can all be attributed to 1 bead during a minute of observation. This is somewhat of an anomaly as the other bins were typically averages of anywhere between 20-300 beads. This appears to be a

“falling” bead that just managed to go by a region of low transport and bead density. Next I plotted the velocity vectors for the bins in the “river” region of the field of view (fig 5.15). Similar to section 5.4.1, the buffer transports up to, but not beyond the meniscus. The DTT mucus, however, consistently transports beyond the meniscus albeit at a slower rate.

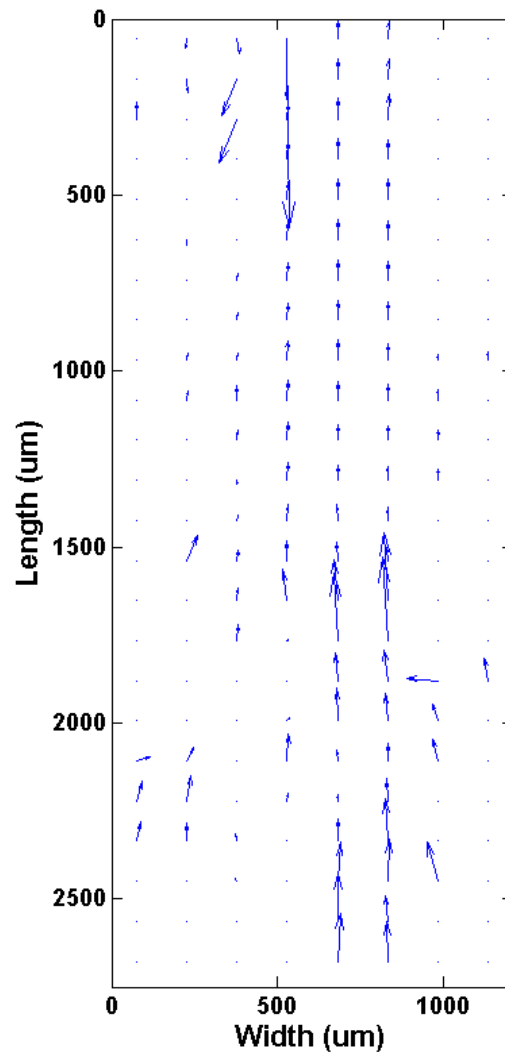


Figure 5.14 A velocity field showing transport of DTT treated mucus as it leaves the meniscal region and continues transport in the ALI region of the channel. The length in microns of each vector correlates to the speed in $\mu\text{m/s}$, but I've multiplied by a scaling factor of 5 to make the direction apparent visible in this figure.

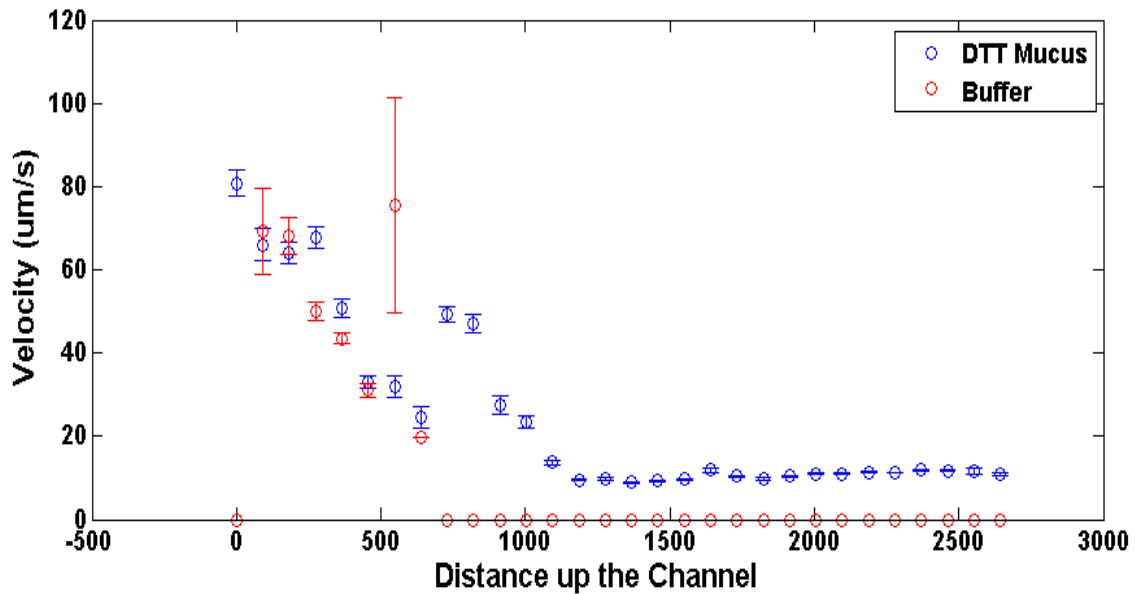


Figure 5.15 Velocity plot as a function of uphill distance in the channel. The edge of the meniscus is at approximately 600-700um, which corresponds with the large bright areas on the MIPS. The pure buffer/bead solution completely halts beyond this point while the DTT treated mucus continues to transport.

Transport of DTT reduced mucin would definitively demonstrate that the rheology was not the only fluid parameter that enabled fluids to transport vertically. The passive bead rheology studies indicate that rheologically the DTT mucus was much closer to buffer than it was to the original 2.5% reconstituted mucus. There are, however, a few caveats that prevent me from making the claim that the DTT mucus was completely uncrosslinked. In looking at the video, the DTT solution seemed to be an aggregation: it seemed as though the beads were linked together. All other signs pointed to the DTT treated mucus being significantly different than the original mucus. In handling the material it was clearly less viscous and had no significant filance (formation of elastic strands) as compared to normal 2.5% reconstituted HBE mucus. From these observations I've come up with an

explanation that attempts to reconcile the contrasting behavior: aggregation vs. low viscosity/low filance. I suspect that in adding DTT to the mucus, I created a two-phase system: a “watery” mucin phase and the remaining polymer phase. In performing passive bead rheology, I sampled 2ul out of a total volume of ~200ul. In addition to sampling a small percentage of the total volume, there could also be a pipetting bias to drawing the more watery/less viscous phase. If I extracted only the watery phase, then that is consistent with the passive bead rheology results. In pipetting a larger volume for the clearance experiment it’d be possible and more likely to draw both phases. Having enough of the watery phase would explain the perceived lower viscosity and filance, but the remaining gel phase may preferentially transport once on the cell culture. So minimally this experiment demonstrates the system as a clearance assay and as a confirmation of the positive control/simulant/negative control protocol, where endogenous mucus represented the positive control, beads and buffer the test fluid, and the mucus phase of the DTT treated mucus as the positive control. It is essential to repeat this experiment in the future and verify the molecular weight of the DTT solution via Dynamic Light Scattering or another technique.

Another interesting result comes in the form of the transporting endogenous material. During this point in the experiment, the channel had already been washed several times with PBS; any remaining mucus would have been extremely hydrated. The transporting beads also looked as if they were “beads on a string”: possibly beads joined together by the remaining endogenous material. While I wasn’t able to measure the rheology of this transporting material, the combination of the dilute

mucus transporting and the “beads” on a string suggest that lower viscosity mucus may have been transporting, which brings into question the importance of viscosity for transport.

5.5.5 Matching mucus' apparent viscosity with PEG

The next simulant tested was a polyethylene glycol (PEG) polymer solution. PEG was chosen for a few reasons; it was possible to choose a PEG molecule with a high molecular weight that was similar to mucus (1MDalton). Furthermore at the appropriate concentration (4.5%), it was possible to tune the PEG so that it had a nearly identical loss modulus to healthy mucus at a timescale of the CBF (Fig. 5.16). While the elasticity remained lower than that of the 2.5% mucus, the matched loss modulus meant that the cilia saw a viscously similar material to mucus. Presumably this would prevent the PEG solution rheology from having a deleterious effect on the cilia beat shape. At the same time, the PEG also had an apparent viscosity of 14 Pa s (Fig. 5.17). This viscosity falls in the range of viscosities (10-15Pa s) in which Puchelle saw optimal transport of the simulant Xanthan Gum over frog palate (Puchelle et al., 1987). Additionally, the apparent viscosity (the viscosity as angular frequency goes to 0) is the quantity that we need to use to determine the rate at which the PEG would drain. Using this apparent viscosity and plotting the flow profile, drainage would have a negligible effect on a 10um film of PEG. At the surface of a 10um film, 4.5% PEG would drain at .035um/s (Fig 5.18). Plugging the apparent viscosity of PEG into equation 5.9 shows that the cilia should support a PEG film on the order of 100um.

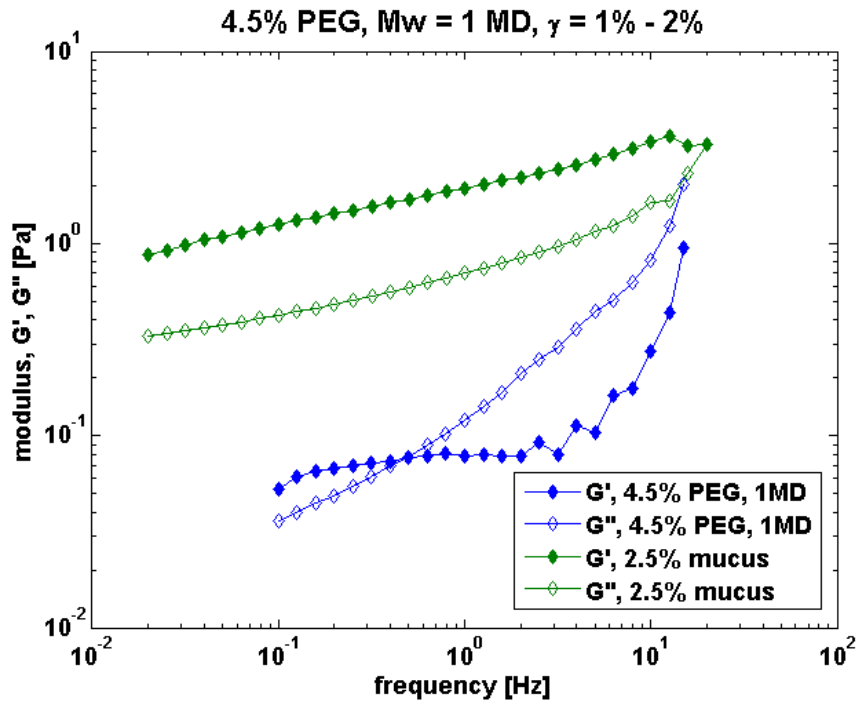


Figure 5.16 4.5% 1MD PEG has an identical loss modulus to 2.5% HBE mucus near the CBF (10Hz).

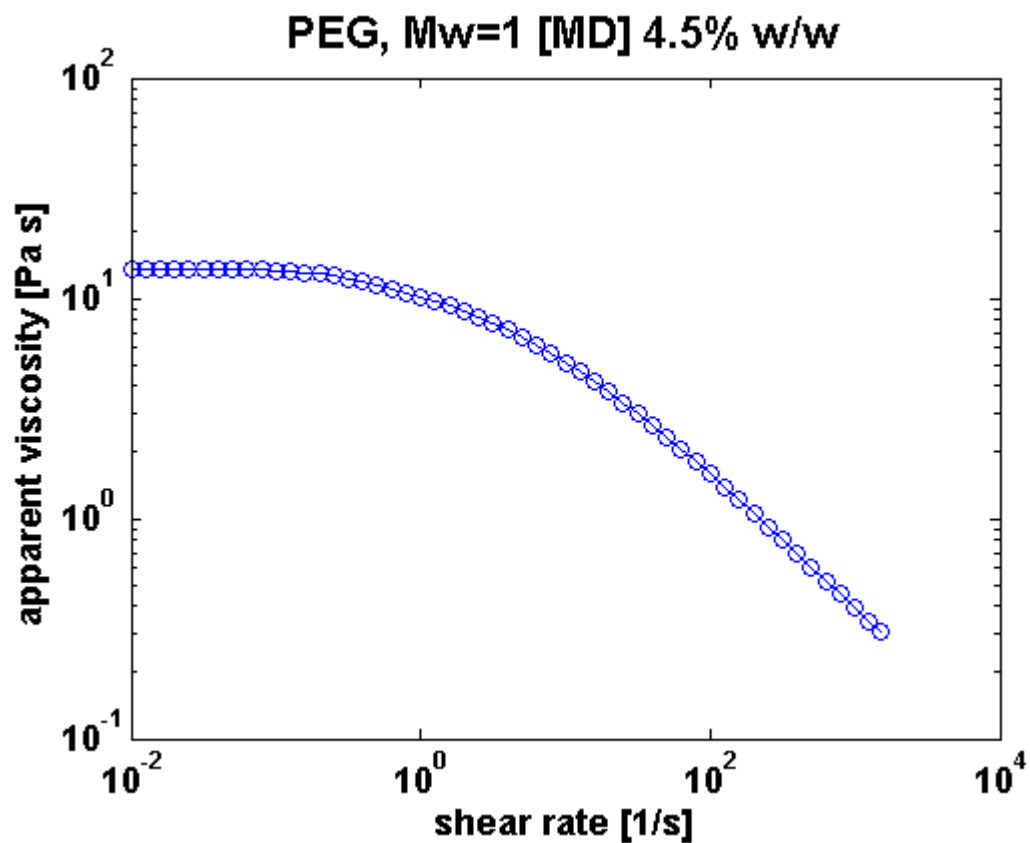


Figure 5.17 Cone and plate measurement of the apparent viscosity of 4.5% 1MDalton PEG as a function of shear rate. As shear rate goes to 0, the apparent viscosity goes to ~14 Pa s.

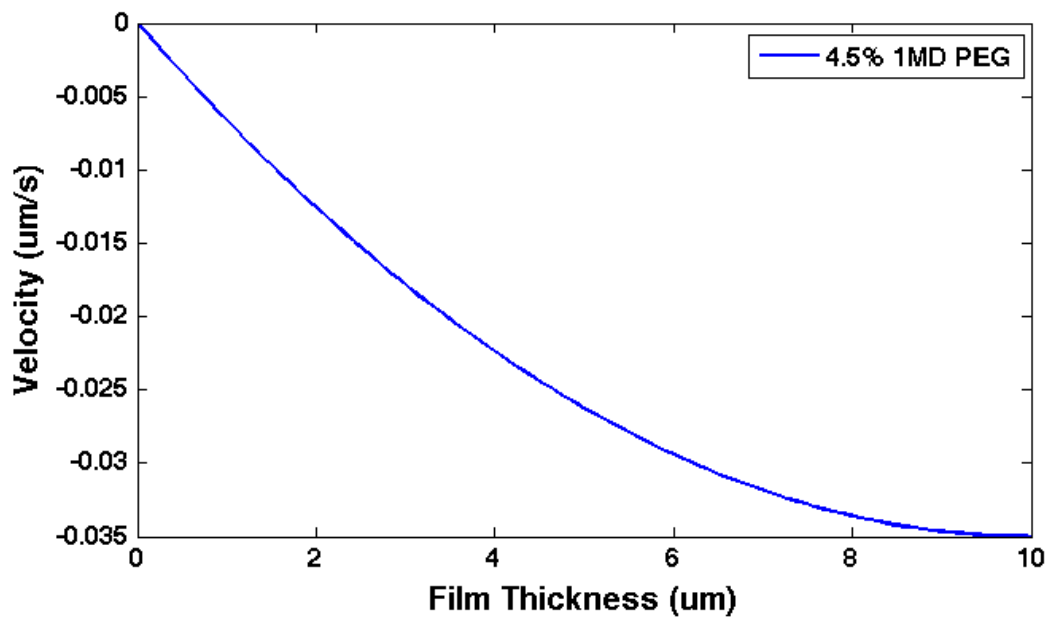


Figure 5.18 Flow profile of a 10µm film of 4.5% 1MDalton PEG. The surface of the Peg film would drain at less than .04µm/s, a drainage rate that is negligible compared to the typical transport rate of mucociliary clearance.

Additional benefits of PEG include its charge neutrality and general inertness: PEG is often used exactly for its resistance to interacting with biological systems. Essentially the PEG allowed me to test the loss modulus/viscosity as a VALI enabling parameter.

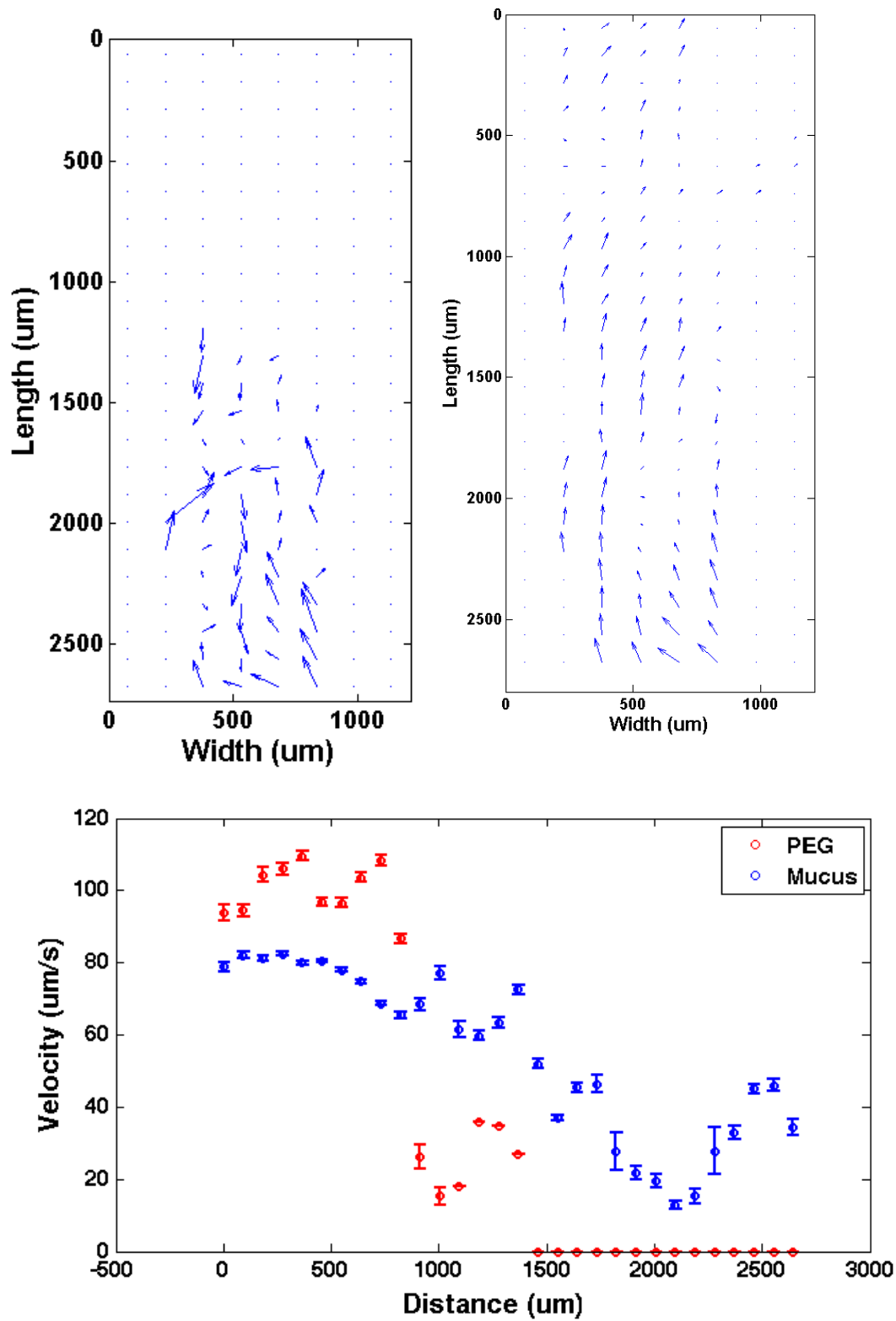


Figure 5.19 A) Velocity vector map of bead transport in a 4.5% 1 MD PEG solution at a 60 degree incline. Bead transport is confined to the region below the liquid contact line. B) Velocity vector map of bead

transport in 2.5% reconstituted HBE mucus at a 60 degree incline over the same field of view as panel A. Bead transport is present both below and above the liquid contact line. C) Comparison of bead velocity rates uphill as a function of distance up the channel. The beads in the PEG solution cease transporting uphill while the beads in the mucus solution continue to transport uphill.

In performing the experiment, the selected channel demonstrated remarkable horizontal transport, tracers were observed moving in excess of 100 $\mu\text{m/s}$. When tilting the system I again saw initial endogenous VALI, but no VALI was present in the PEG. The final mucus positive control was also successful at VALI. Figure 5.19 shows the velocity map for the PEG solution as well as the positive mucus control. As with the buffer, the PEG also seems to be confined by the contact line. Figure 5.19 shows the average speed of beads moving uphill. It's worth noting that again the mucus transport is slower in the ALI zone than it is in the submerged/meniscal zones.

The inability of the PEG to transport beyond the contact line, coupled with the subsequent transport of the mucus over the same field of view allows us to conclude that 4.5% PEG doesn't transport at VALI. The key lies in deciphering why the PEG solution doesn't transport. According to the drainage model presented at the beginning of the chapter, the PEG solution should transport. Comparing the flow profile (fig 5.18), to the average particle velocity beneath the contact line shows that cilia driven transport would dominate any gravitational drainage seen in a PEG film on the order of 10 μm . Tracers beneath the contact line average 100 $\mu\text{m/s}$ uphill while drainage is 4 orders of magnitude lower at .03 $\mu\text{m/s}$. From this I conclude that PEG's inability to undergo VALI transport is not an issue of drainage overwhelming cilia driven transport, but instead a reduction of the cilia driven transport.

Understanding the underlying cause of the reduction in cilia driven transport is key in determining the mechanisms of mucociliary clearance. The first step is to go back and examine the assumptions made in the simple model and try to determine if any faulty assumptions or conditions can explain the lack of PEG VALI transport. At the simplest level cilia transport depends on

1. Cilia activity
2. Cilia-simulant interaction
3. Simulant Properties

In coarse graining the cilia into a traction layer or cilia sublayer, I'm making the assumption that if the cilia activity and the cilia-simulant interaction are conserved then the shear provided at the boundary condition will be the same.

The next assumption lies in treating the simulants as Newtonian fluids. Both the 4.5% PEG and 2.5% mucus are viscoelastic fluids. While I matched the viscosity of both fluids at the CBF, there could be another rheological property (such as elasticity) that makes the mucus transport better than the PEG for the same shear boundary condition. This clearly is not the case, however, as figure 5.19 shows that PEG transports faster than mucus in the region beneath the contact line. I'd like to emphasize that in an experiment in a horizontal conformation this would reflect that PEG demonstrates better transport than mucus. PEG's relatively faster transport beneath the contact line, but complete lack of transport above illustrates the importance of the contact line. This suggests that our conditions are changing at the contact line.

In explaining the difference above and below the contact line, the first item discussed has to be the amount of solvent. The uniqueness of the tilting clearance assay is that above the contact line, any excess liquid drains away. In looking at just buffer alone, the drainage model suggests that a shear boundary based on coarse-graining cilia would be sufficient to support a small film of buffer 1-2 μ m thick. This boundary layer, however, was assumed to be at or above the cilia tips. The buffer below the tips is also exposed to the gravitational body force and susceptible to drainage. While wetting to the epithelial surface will support some buffer, the rest will be a competition between PCL transport and gravitational drainage. Without the overlying mucus, PCL transport is greatly reduced (Matsui, Randell, Peretti, Davis, & Boucher, 1998b), so it follows that the system above the contact line is in a dehydrated state. The PCL dehydration above the contact line explains the reduced transport of the mucus beyond the contact line (Randell, 2006).

This still leaves an important issue: why is mucus better suited to transport with a depleted PCL than PEG? One possibility is that the mucus is able to carry more water with it than PEG. The extra water can be donated to the PCL to increase hydration (Randell, 2006), but also would help maintain the rheology. Another consideration goes back to the cilia-simulant interaction. If a simulant is “pulling” the fluid along with it, the cilia have to be able to move the simulant. Above the contact line, the cilia are able to transfer more force to mucus than to PEG. This interaction could be the result of either rheological properties of the fluids or adhesion between the solute and the cilia. We know from chapter 2 that adhesion occurs between the gel forming mucins MUC5B and MUC5AC and membrane bound mucins MUC1 and

MUC4 (Knowles & Boucher, 2002). Furthermore we now know that MUC1 and MUC4 aren't only on the cell plasma membrane, but are also on each cilia stalk (Button et al., 2012) in the form of a periciliary brush. So a mechanism for cilia adhering to the mucus gel is already in place and established. I'm suggesting that this adhesion is what enables to mucus to travel at VALI. Rheology could also play a factor. While I discounted rheology earlier because of PEG's rheology being closer to "optimal", the possibility exists that the rheology changes at the contact line. If the solvent does drain away, the solute's concentration increases and the rheological properties could change locally. In looking at the two possibilities, several sources of anecdotal evidence suggest the adhesion mechanism.

1. Transport of dilute mucus solutions (after heavy washing)
2. Unattached cells (presumably covered with mucins) transporting at VALI in a buffer solution

These observations aren't definitive, but they suggest a route for future experiments that I discuss in section 5.7.

5.6 Conclusions

Over the course of this dissertation I developed and engineered a system to grow well-ciliated cells in a bilayer fluidics channel. This system represents the first to grow well-ciliated cells inside of a fluidics channel. I observed cilia driven transport in the channel and then compared the cilia-ASL interaction into a simple model of a coarse-grained shear boundary, the essence of which is broadly used in several models of mucociliary clearance. I then tested and confirmed aspects of this model

using external flow. Next I took advantage of the fluid flow to develop the first system to use flow to quantify adhesion between functionalized microbeads and a cell surface. I demonstrated the ability to functionalize the beads with moieties known to adhere to epithelial surfaces, and demonstrated that these beads required more force to remove than “inert” beads.

My next major contribution was the use of the bilayer channel and a tilting microscope to create a mucus clearance assay. Tilting the system I was able to perform the first *in vitro* PIV measurements against gravity. I used this feature to show that gravitational drainage plays a role in mucociliary clearance. I added gravity into my simple model and then verified it by testing clearance of buffer and mucus against gravity. Buffer’s ability to clear in a horizontal conformation, but not at a tilt angle shows that gravity is a necessary element of any system measuring mucociliary clearance. Finally I tested clearance for 4.5% 1 MDa PEG, using it as an ASL simulant, for which drainage shouldn’t have been a contributing factor to transport due to the viscosity. In observing that the PEG could transport horizontally, but not vertically I was able to identify problems with my model and suggested PCL depletion as a major element in preventing VALI transport for PEG. I then outline how adhesion could play a role in enabling the vertical transport of mucus.

5.7 Future Directions

5.7.1 Clearance isn't the same as transport

An important detail is the distinction between clearance and transport. The words are often used synonymously, however, I'd like to refine the definition that I use

Transport: Directed cilia-driven movement of mucus or a mucus simulant

Clearance: Directed cilia-driven movement of particles (e.g. bacteria or microbeads)

The experiments performed so far are all clearance experiments: I am relying on the movement of tracer particles to evaluate movement of both mucus and simulants.

While clearance is the process in which I'm interested, transport is the more fundamental of the two processes. Clearance requires that the simulant transports and furthermore that the tracer particles move with the simulant. The experiments described thus far by the MCA would be blind to a simulant transporting, but not clearing the tracer particles. This is important for two reasons. The first is that in trying to determine the interaction between mucus and cilia, a transporting, but non-clearing simulant could yield a false negative when trying to narrow down the parameter space. The second reason is that at the end of the day, I am testing the clearance of microbeads. Clearance of microbeads doesn't guarantee the clearance of other pathogens nor does lack of clearance of microbeads guarantee that other pathogens won't transport. This isn't stated to trivialize the results presented; it is of vital importance that the lungs clear microbead sized debris and in fact I showed that mucus is capable of clearing microbeads. Instead it is stated to show awareness and serve as a reminder that it is important to differentiate the two phenomena: Lack of

clearance could just as easily be an issue of tracer/simulant interaction as it is simulant/cilia interaction. The solution to testing for this is simple enough; the simulant should also act as the tracer.

Ultimately this becomes an issue of chemistry; aside from the buffer, most of the simulants have a fluorescent analog. In following with the mission of this dissertation, two particular experiments come to mind, which would be invaluable in exploring the mucus-cilia interaction. The first is revisiting and modifying the DTT mucus experiment and the second is looking for clearance of mucus-coated particles.

5.7.2 DTT Revisited

In performing and repeating the DTT experiment I showed that monomeric mucins don't clear microbeads. In accordance with the point that I belabored in the previous section, this says nothing about transport of the monomeric mucins themselves. Even without the clearance aspect, transporting monomeric mucins would unequivocally implicate adhesion as a part of mucus-cilia interactions. Even longer strings of "chained" mucins, such as the "beads-on-a-string" would demonstrate the role of adhesion. Fortunately the methodology already exists; the Sears paper details a protocol for labeling MUC5B (Sears, Davis, Chua, & Sheehan, 2011). The main challenges in performing this experiment are in producing sufficient amounts of MUC5B, performing the protocol, and tuning the optics of the system to pick up the MUC5B. While the preparation may be a lot to chew on, this experiment would produce rather conclusive results.

5.7.3 Mucin covered particles

Another mechanism to directly test the interaction between mucus and cilia is to forego the use of a simulant. Coating particles with potential adhesive moieties makes it possible to test for clearance as a function of adhesion and not rheology. An ideal experiment confirming adhesion would demonstrate that particles coated with the adhesive moieties cleared. The mechanism would presumably be an adhesive interaction between cilia and the particle coating acting long enough to sweep the bead along the cilium stroke and transfer to the next cilium. While several functionalizations of beads are possible (including mucins) are possible, there are still issues to solve with this experiment. Most difficult is the Goldilocks' principle for adhesion; too little adhesion and there is no transport and likewise with too much adhesion. This would be directly related to the density and spacing of moieties attached to the particle as well as the particle size. While this experiment is further away from being realized than the DTT experiment, the adhesion assay can serve as a platform to start addressing some of the questions needed to perform this experiment.

5.8 Experimental Methods

5.8.1 Transport vs. Tilt Angle experiments

The general protocol for these experiments is as follows. First I scouted the culture for regions of dense, coordinated cilia. Typically the goal was to find a region where endogenous material was being transported roughly along the axis of the channel for a distance of at least a millimeter. The location of the spot was recorded

using the micrometer stage and visual landmarks in the sample, and then the channel was taken to the laminar flow hood and the endogenous material was removed as detailed in chapter 4. The channel and stage were returned to and remounted to the microscope. The channel was oriented so that the previously identified region would transport uphill when the microscope was tilted. At this point I pulled up the region of interest on the microscope and tilted the system to 30 degrees. I started with 30 degrees so that I had accurate control over the spread of the liquid. Had I added the liquid to a horizontal system, the liquid would have had the opportunity to spread throughout the entire apical compartment before tilting. Knowing the volume of the channel and approximately where the region was located, I estimated the amount of fluid to add to the channel; the objective was to make sure that the meniscus spanned the region of transport. I used a pipette to add fluid (with microbeads) to the lower apical port. For each field of view I took several videos and then I translated uphill to the next field of view. After traversing several fields of view, I returned to the initial field of view and tilted the microscope to the next angle. For these experiments the angle progression went 30,45,60,90 followed by a return to horizontal.

5.8.2 Clearance Assay Experiment Protocol

My general procedure for performing clearance assay experiments stayed pretty close to the protocol that I used in tilt angle experiments. In short I identified a prospective area, recorded its location and then removed the endogenous material from the system. When returning the device to the microscope, I only used a 60-degree tilt. I chose to do the 60-degree angle because it still maintained a strong

drainage component (50% of the vertical conformation) while avoiding the focus drifting issues that I had at 90 degrees with the tilting microscope. Once the device was in place on the scope I added the buffer/bead solution, which had been warmed to 37C, to the bottom apical port until it reached my predetermined region of interest. Initially this step was to serve as a negative control, but as I learned later it acted as an extension of the washing step. I recorded video at that region, and at the field of views uphill of that spot. At the conclusion of the experiment I withdrew the fluid from the top apical port, performed a rinsing step by administering buffer at the bottom apical port while simultaneously withdrawing it from the top apical port, and then administered the heated simulant to the bottom apical port. I repeated the preceding steps, however, on removing the simulant I pulled it from the bottom port if it didn't successfully transport. I performed rinsing steps and then added heated 2.5% reconstituted mucus to the bottom apical port to perform the positive control.

References

- Adam, E. C., Mitchell, B. S., Schumacher, D. U., Grant, G., & Schumacher, U. (1997). Pseudomonas aeruginosa II lectin stops human ciliary beating: therapeutic implications of fucose. *American Journal of Respiratory and Critical Care Medicine*, 155(6), 2102.
- Alexander, I., Ritchie, B. C., Maloney, J. E., & Hunter, C. R. (1975). Epithelial surfaces of the trachea and principal bronchi in the rat. *Thorax*, 30(2), 171–177. doi:10.1136/thx.30.2.171
- Allahverdian, S., Wojcik, K. R., & Dorscheid, D. R. (2006). Airway epithelial wound repair: role of carbohydrate sialyl Lewisx. *American Journal of Physiology- Lung Cellular and Molecular Physiology*, 291(4), 828–836. doi:10.1152/ajplung.00120.2006
- Ayers, M. M., & Jeffery, P. K. (1988). Proliferation and differentiation in mammalian airway epithelium. *European Respiratory Journal*, 1(1), 58–80.
- Basbaum, C. B., Jany, B., & Finkbeiner, W. E. (1990). The Serous Cell. *Annual Review of Physiology*, 52(1), 97–113. doi:10.1146/annurev.ph.52.030190.000525
- Batchelor, G. K. (2000). *An Introduction to Fluid Dynamics*. Cambridge University Press.
- Berry, M., McMaster, T. J., Corfield, A. P., & Miles, M. J. (2001). Exploring the Molecular Adhesion of Ocular Mucins. *Biomacromolecules*, 2(2), 498–503. doi:10.1021/bm000145y
- Blake, J. (1973). Mucus flows. *Mathematical Biosciences*, 17(3-4), 301–313. doi:10.1016/0025-5564(73)90073-4
- Blake, J. (1975). On the movement of mucus in the lung. *Journal of Biomechanics*, 8(3-4), 179–190.
- Blake, J. R. (1972). A model for the micro-structure in ciliated organisms. *J Fluid Mech*, 55(1), 1–23.
- Bloodgood, R. A. (1990). *Ciliary and flagellar membranes*. Plenum Press.
- Boucher, R. C., Stutts, M. J., Bromberg, P. A., & Gatzky, J. T. (1981). Regional differences in airway surface liquid composition.
- Breatnach, E., Abbott, G. C., & Fraser, R. G. (1984). Dimensions of the normal human trachea. *AJR. American Journal of Roentgenology*, 142(5), 903–906.
- Burdick, G., & Berman, N. (2001). Journal of Nanoparticle Research, Volume 3, Numbers 5-6 - SpringerLink. *Journal of Nanoparticle*
- Button, B., & Boucher, R. (2008). Role of mechanical stress in regulating airway surface hydration and mucus clearance rates. *Respiratory Physiology & Neurobiology*.
- Button, B., Cai, L. H., Ehre, C., Kesimer, M., Hill, D. B., Sheehan, J. K., et al. (2012). A Periciliary Brush Promotes the Lung Health by Separating the Mucus Layer from Airway Epithelia. *Science*, 337(6097), 937–941. doi:10.1126/science.1223012
- Button, B., Picher, M., & Boucher, R. (2007a). Differential effects of cyclic and constant stress on ATP release and mucociliary transport by human airway

- epithelia. *The Journal of Physiology*.
- Button, B., Picher, M., & Boucher, R. (2007b). Differential effects of cyclic and constant stress on ATP release and mucociliary transport by human airway epithelia. *The Journal of Physiology*.
- Carnoy, C., Scharfman, A., Van Brussel, E., LAMBLIN, G., Ramphal, R., & Roussel, P. (1994). Pseudomonas aeruginosa outer membrane adhesins for human respiratory mucus glycoproteins.
- Chen, T. M., & Dulfano, M. J. (1978). Mucus viscoelasticity and mucociliary transport rate. *The Journal of Laboratory and Clinical Medicine*, 91(3), 423–431.
- Christophis, C., Grunze, M., & Rosenhahn, A. (2010). Quantification of the adhesion strength of fibroblast cells on ethylene glycol terminated self-assembled monolayers by a microfluidic shear force assay. *Physical Chemistry Chemical Physics : PCCP*, 12(17), 4498–4504. doi:10.1039/b924304f
- Clary-Meinesz, C., Cosson, J., & Huitorel, P. (1992). ScienceDirect - Biology of the Cell : Temperature effect on the ciliary beat frequency of human nasal and tracheal ciliated cells. *Biology of the Cell*.
- Crapo, J. D., Barry, B. E., Gehr, P., Bachofen, M., & WEIBEL, E. R. (1982). Cell number and cell characteristics of the normal human lung. *The American Review of Respiratory Disease*, 126(2), 332–337.
- Crouch, E., Parghi, D., Kuan, S. F., & Persson, A. (1992). Surfactant protein D: subcellular localization in nonciliated bronchiolar epithelial cells.
- Demir, M., Yilgor, I., Yilgor, E., & Erman, B. (2002). Electrospinning of polyurethane fibers. *Polymer*.
- Devereux, T. R., Serabjit-Singh, C. J., Slaughter, S. R., Wolf, C. R., Philpot, R. M., & Fouts, J. R. (1981). Identification of cytochrome P-450 isozymes in nonciliated bronchiolar epithelial (Clara) and alveolar type II cells isolated from rabbit lung. *Experimental Lung Research*, 2(3), 221–230.
- Ellefsen, P., & Tos, M. (1972). Goblet cells in the human trachea. Quantitative studies of a pathological biopsy material. *Archives of Otolaryngology (Chicago, Ill. : 1960)*, 95(6), 547–555.
- Engler, A. J., Sen, S., Sweeney, H. L., & Discher, D. E. (2006). Matrix elasticity directs stem cell lineage specification. *Cell*, 126(4), 677–689. doi:10.1016/j.cell.2006.06.044
- Espinosa, F. F., & Kamm, R. D. (1997). Thin layer flows due to surface tension gradients over a membrane undergoing nonuniform, periodic strain. *Annals of Biomedical Engineering*, 25(6), 913–925.
- Even-Tzur, N., Elad, D., Zaretsky, U., & Randell, S. (2006). Custom-Designed Wells and Flow Chamber for Exposing Air–Liquid Interface Cultures to Wall Shear *Annals of Biomedical Engineering*.
- Even-Tzur, N., Jaffa, A., Gordon, Z., Gottlieb, R., Kloog, Y., Einav, S., et al. (2010). Air–Liquid Interface Culture of Nasal Epithelial Cells on Denuded Amniotic Membranes. *Cellular and Molecular Bioengineering*, 3(3), 307–318. doi:10.1007/s12195-010-0118-y
- Finkbeiner, W. E., Zlock, L. T., Mehdi, I., & Widdicombe, J. H. (2009). Cultures of human tracheal gland cells of mucous or serous phenotype. *In Vitro Cellular & Developmental Biology-Animal*, 46(5), 450–456. doi:10.1007/s11626-009-9262-x

- Fulcher, M., Gabriel, S., Burns, K., Yankaskas, J., & Randell, S. (2005). Well-differentiated human airway epithelial cell cultures. *Methods Mol Med*, *107*, 183–206.
- Ganz, T. (2002). Antimicrobial polypeptides in host defense of the respiratory tract. *Journal of Clinical Investigation*, *109*(6), 693–697. doi:10.1172/JCI15218
- Gelman, R. A., & Meyer, F. A. (1979). Mucociliary transference rate and mucus viscoelasticity dependence on dynamic storage and loss modulus. *The American Review of Respiratory Disease*, *120*(3), 553–557.
- Gheber, L., & Priel, Z. (1989). Synchronization between beating cilia. *Biophysical Journal*.
- Goldman, M. J., Anderson, G. M., Stolzenberg, E. D., Kari, U. P., Zasloff, M., & Wilson, J. M. (1997). Human beta-defensin-1 is a salt-sensitive antibiotic in lung that is inactivated in cystic fibrosis. *Cell*, *88*(4), 553–560.
- Gray, T. E., Guzman, K., Davis, C. W., Abdullah, L. H., & Nettesheim, P. (1996). Mucociliary differentiation of serially passaged normal human tracheobronchial epithelial cells. *American Journal of Respiratory Cell and Molecular Biology*, *14*(1), 104–112.
- Guirao, B., & Joanny, J. (2007). Spontaneous creation of macroscopic flow and metachronal waves in an array of cilia. *Biophysical Journal*, *92*(6), 1900–1917.
- Guirao, B., Meunier, A., Mortaud, S., Aguilar, A., Corsi, J., Strehl, L., et al. (2010). Coupling between hydrodynamic forces and planar cell polarity orients mammalian motile cilia. *Nature Cell Biology*, *12*(4), 341–350.
- Gum, J. R., Hicks, J. W., Toribara, N. W., Siddiki, B., & Kim, Y. S. (1994). Molecular cloning of human intestinal mucin (MUC2) cDNA. Identification of the amino terminus and overall sequence similarity to prepro-von Willebrand factor. *Journal of Biological Chemistry*, *269*(4), 2440–2446.
- Gump, A., Haughney, L., & Fredberg, J. (2001). Relaxation of activated airway smooth muscle: relative potency of isoproterenol vs. tidal stretch. *Journal of Applied Physiology*, *90*(6), 2306–2310.
- Gutierrez, E., & Groisman, A. (2007). Quantitative measurements of the strength of adhesion of human neutrophils to a substratum in a microfluidic device. *Analytical Chemistry*, *79*(6), 2249–2258. doi:10.1021/ac061703n
- Haies, D. M., GIL, J., & WEIBEL, E. R. (1981). Morphometric study of rat lung cells. I. Numerical and dimensional characteristics of parenchymal cell population. *The American Review of Respiratory Disease*, *123*(5), 533–541.
- Hasleton, P. S. (1972). The internal surface area of the adult human lung. *Journal of Anatomy*, *112*(Pt 3), 391–400.
- Hatrup, C. L., & Gendler, S. J. (2008). Structure and Function of the Cell Surface (Tethered) Mucins. *Annual Review of Physiology*, *70*(1), 431–457. doi:10.1146/annurev.physiol.70.113006.100659
- Huh, D., Fujioka, H., Tung, Y., Futai, N., & Paine, R. (2007). Acoustically detectable cellular-level lung injury induced by fluid mechanical stresses in *Proceedings of the National Academy of Sciences*.
- Hwang, S. Y., Kwon, K. W., Jang, K.-J., Park, M. C., Lee, J. S., & Suh, K. Y. (2010). Adhesion assays of endothelial cells on nanopatterned surfaces within a microfluidic channel. *Analytical Chemistry*, *82*(7), 3016–3022.

doi:10.1021/ac100107z

- Irvin, C., & Bates, J. (2003). Measuring the lung function in the mouse: the challenge of size. *Respir Res.*
- Jang, K., & Suh, K. (2010). A multi-layer microfluidic device for efficient culture and analysis of renal tubular cells. *Lab on a Chip*, *10*(1), 36–42.
- Janmey, P. A., Winer, J. P., Murray, M. E., & Wen, Q. (2009). The hard life of soft cells. *Cell Motility and the Cytoskeleton*, *66*(8), 597–605. doi:10.1002/cm.20382
- Javanmard, M., Babrzadeh, F., & Davis, R. W. (2010). Microfluidic force spectroscopy for characterization of biomolecular interactions with piconewton resolution. *Applied Physics Letters*, *97*(17), 173704. doi:10.1063/1.3491547
- Jeffery, P., & Li, D. (1997). Airway mucosa: secretory cells, mucus and mucin genes. *European Respiratory Journal*.
- Jentoft, N. (1990). Why are proteins O-glycosylated? *Trends in Biochemical Sciences*, *15*(8), 291.
- Keller, S., & Wu, T. (1975). A Traction-Layer Model for Ciliary Propulsion - CaltechAUTHORS.
- Kesimer, M., Kirkham, S., Pickles, R. J., Henderson, A. G., Alexis, N. E., DeMaria, G., et al. (2008). Tracheobronchial air-liquid interface cell culture: a model for innate mucosal defense of the upper airways? *AJP: Lung Cellular and Molecular Physiology*, *296*(1), L92–L100. doi:10.1152/ajplung.90388.2008
- Kesimer, M., Kirkham, S., Pickles, R. J., Henderson, A. G., Alexis, N. E., DeMaria, G., et al. (2009). Tracheobronchial air-liquid interface cell culture: a model for innate mucosal defense of the upper airways?
- Kimura, H., Yamamoto, T., Sakai, H., Sakai, Y., & Fujii, T. (2008). An integrated microfluidic system for long-term perfusion culture and on-line monitoring of intestinal tissue models. *Lab on a Chip*, *8*(5), 741–746.
- King, M. (1980). Relationship between mucus viscoelasticity and ciliary transport in guaran gel/frog palate model system. *Biorheology*, *17*(3), 249–254.
- King, M. (1998). Experimental models for studying mucociliary clearance. *European Respiratory Journal*, *11*(1), 222–228.
- King, M., Brock, G., & Lundell, C. (1985). Clearance of mucus by simulated cough. *Journal of Applied Physiology*, *58*(6), 1776–1782.
- Knowles, M., & Boucher, R. (2002). Mucus clearance as a primary innate defense mechanism for mammalian airways. *Journal of Clinical Investigation*.
- La Fuente, De, L., Montanes, E., Meng, Y., Li, Y., Burr, T. J., Hoch, H. C., & Wu, M. (2007). Assessing Adhesion Forces of Type I and Type IV Pili of *Xylella fastidiosa* Bacteria by Use of a Microfluidic Flow Chamber.
- LAMBLIN, G., Aubert, J., Perini, J., KLEIN, A., Porchet, N., Degand, P., & Roussel, P. (1992). Human respiratory mucins.
- LAMBLIN, G., LHERMITTE, M., KLEIN, A., Houdret, N., Scharfman, A., Ramphal, R., & Roussel, P. (1991). The carbohydrate diversity of human respiratory mucins: a protection of the underlying mucosa? *The American Review of Respiratory Disease*, *144*(3 Pt 2), S19–24.
- Lansley, A. B., & Sanderson, M. J. (1999). Regulation of airway ciliary activity by Ca²⁺: simultaneous measurement of beat frequency and intracellular Ca²⁺. *Biophysj*, *77*(1), 629–638. doi:10.1016/S0006-3495(99)76919-5

- Lawrence, M., & Springer, T. (1991). ScienceDirect.com - Cell - Leukocytes roll on a selectin at physiologic flow rates: Distinction from and prerequisite for adhesion through integrins. *Cell*.
- Lemullois, M., Klotz, C., & Sandoz, D. (1987). Immunocytochemical localization of myosin during ciliogenesis of quail oviduct. *European Journal of Cell Biology*, 43(3), 429–437.
- Liu, T., & Moiseeva, E. (2008). *Liu: Chips & Tips: Integrated reservoirs for PDMS...* - Google Scholar. Lab Chip.
- Lo, C. M., Wang, H. B., Dembo, M., & Wang, Y. L. (2000). Cell movement is guided by the rigidity of the substrate. *Biophysj*, 79(1), 144–152. doi:10.1016/S0006-3495(00)76279-5
- Lu, H., Koo, L. Y., Wang, W. M., Lauffenburger, D. A., Griffith, L. G., & Jensen, K. F. (2004). Microfluidic Shear Devices for Quantitative Analysis of Cell Adhesion. *Analytical Chemistry*, 76(18), 5257–5264. doi:10.1021/ac049837t
- Luk, C. K., & Dulfano, M. J. (1983). Effect of pH, viscosity and ionic-strength changes on ciliary beating frequency of human bronchial explants. *Clinical Science (London, England : 1979)*, 64(4), 449–451.
- Macchione, M. M., King, M. M., Lorenzi-Filho, G. G., Guimarães, E. T. E., Zin, W. A. W., Böhm, G. M. G., & Saldiva, P. H. P. (1995). Rheological determinants of mucociliary transport in the nose of the rat. *Respiration Physiology*, 99(1), 165–172.
- Madsen, J., Kliem, A., Tornøe, I., Skjødt, K., Koch, C., & Holmskov, U. (2000). Localization of Lung Surfactant Protein D on Mucosal Surfaces in Human Tissues. *The Journal of*
- Majima, Y., Sakakura, Y., Matsubara, T., Hamaguchi, Y., Hirata, K., Takeuchi, K., & Miyoshi, Y. (1986). Rheological properties of middle ear effusions from children with otitis media with effusion. *The Annals of Otolaryngology, Rhinology & Laryngology. Supplement*, 124, 1–4.
- Mall, M., Grubb, B., Harkema, J., & O'Neal, W. (2004). Increased airway epithelial Na⁺ absorption produces cystic fibrosis-like lung disease in mice - Nature Medicine. *Nature Medicine*.
- Mammoto, A., Montoya-Zavala, M., Hsin, H., & Ingber, D. (2010). Reconstituting Organ-Level Lung Functions on a Chip. *Science*.
- Manawadu, B. R., Mostow, S. R., & LaForce, F. M. (1979). Impairment of Tracheal Ring Ciliary Activity by Halothane. *Anesthesia & Analgesia*, 58(6), 500–504.
- Marino, M. (1982). Cinemicrographic analysis of beat dynamics of human respiratory cilia - Marino - 2005 - Cell Motility - Wiley Online Library. *Cell Motility*.
- Martins, M. de F., & Bairos, V. A. (2002). Glycocalyx of lung epithelial cells. *International Review of Cytology*, 216, 131–173.
- Mathers, C., Fat, D. M., World Health Organization, & Boerma, J. T. (2008). The global burden of disease: 2004 update. (World Health Organization, Ed.), 1–160.
- Matsui, H., Davis, C. W., Tarran, R., & Boucher, R. C. (2000). Osmotic water permeabilities of cultured, well-differentiated normal and cystic fibrosis airway epithelia. *Journal of Clinical Investigation*, 105(10), 1419–1427. doi:10.1172/JCI4546
- Matsui, H., Grubb, B. R., Tarran, R., Randell, S. H., Gatzky, J. T., Davis, C. W., &

- Boucher, R. C. (1998a). Evidence for periciliary liquid layer depletion, not abnormal ion composition, in the pathogenesis of cystic fibrosis airways disease. *Cell*, 95(7), 1005–1015.
- Matsui, H., Randell, S. H., Peretti, S. W., Davis, C. W., & Boucher, R. C. (1998b). Coordinated clearance of periciliary liquid and mucus from airway surfaces. *Journal of Clinical Investigation*, 102(6), 1125–1131. doi:10.1172/JCI2687
- Matsui, H., Randell, S., Peretti, S., & William Davis, C. (1998c). Coordinated clearance of periciliary liquid and mucus from airway surfaces. *Journal of Clinical Investigation*.
- McDonald, J., Duffy, D., Anderson, J., Chiu, D., & Wu, H. (2000). Fabrication of microfluidic systems in poly (dimethylsiloxane). *Electrophoresis*.
- McEver, R. P. (2005). A sulfated address for lymphocyte homing. *Nature Immunology*, 6(11), 1067–1069. doi:10.1038/ni1105-1067
- MCSP, L. J. F. B., DMS, P. A. M., & FRCP, D. B. M. (2012). Chest Physiotherapy Techniques in Bronchiectasis. *Clinics in Chest Medicine*, 33(2), 351–361. doi:10.1016/j.ccm.2012.02.009
- Mesland, D. A. M., & Ende, H. (1979). The role of flagellar adhesion in sexual activation of *Chlamydomonas eugametos*. *Protoplasma*, 98(1-2), 115–129. doi:10.1007/BF01676665
- Mitchell, B., Jacobs, R., Li, J., Chien, S., & Kintner, C. (2007). A positive feedback mechanism governs the polarity and motion of motile cilia. *Nature*.
- Moller, P. C., Partridge, L. R., Cox, R., Pellegrini, V., & Ritchie, D. G. (1987). An in vitro system for the study of tracheal epithelial cells. *Tissue & Cell*, 19(6), 783–791.
- O'Neill, M. E. (1968). A sphere in contact with a plane wall in a slow linear shear flow. *Chemical Engineering Science*, 23(11), 1293–1298. doi:doi: 10.1016/0009-2509(68)89039-6
- Patton, J. S., & Byron, P. R. (2007). Inhaling medicines: delivering drugs to the body through the lungs. *Nature Reviews. Drug Discovery*, 6(1), 67–74. doi:10.1038/nrd2153
- Pazour, G. (2008). Chapter 5 Targeting Proteins to the Ciliary Membrane 10.1016/S0070-2153(08)00805-3 : Current Topics in Developmental Biology | ScienceDirect.com. *Current Topics in Developmental Biology*.
- Puchelle, E. E., & Zahm, J. M. J. (1984). Influence of rheological properties of human bronchial secretions on the ciliary beat frequency. *Biorheology*, 21(1-2), 265–272.
- Puchelle, E. E., Zahm, J. M. J., & Duvivier, C. C. (1983). Spinability of bronchial mucus. Relationship with viscoelasticity and mucous transport properties. *Biorheology*, 20(2), 239–249.
- Puchelle, E., Zahm, J. M., & Quemada, D. (1987). Rheological properties controlling mucociliary frequency and respiratory mucus transport. *Biorheology*, 24(6), 557–563.
- Ramrattan, N. N., Heijkants, R. G. J. C., van Tienen, T. G., Schouten, A. J., Veth, R. P. H., & Buma, P. (2005). Assessment of tissue ingrowth rates in polyurethane scaffolds for tissue engineering. *Tissue Engineering*, 11(7-8), 1212–1223. doi:10.1089/ten.2005.11.1212

- Randell, S. H. (2006). Effective Mucus Clearance Is Essential for Respiratory Health. *American Journal of Respiratory Cell and Molecular Biology*, 35(1), 20–28. doi:10.1165/rcmb.2006-0082SF
- Rautiainen, M., Matsune, S., Shima, S., Sakamoto, K., Hanamura, Y., & Ohyama, M. (1992). Ciliary beat of cultured human respiratory cells studied with differential interference microscope and high speed video system. *Acta Oto-Laryngologica*, 112(5), 845–851.
- Regehr, K. J., Domenech, M., Koepsel, J. T., Carver, K. C., Ellison-Zelski, S. J., Murphy, W. L., et al. (2009). Biological implications of polydimethylsiloxane-based microfluidic cell culture. *Lab on a Chip*, 9(15), 2132–2139. doi:10.1039/b903043c
- Reid, L. (1965). NATURAL HISTORY OF MUCUS IN THE BRONCHIAL TREE. *Archives of Environmental Health*, 10, 265–273.
- Reid, L., Meyrick, B., Antony, V. B., Chang, L.-Y., Crapo, J. D., & Reynolds, H. Y. (2005). The mysterious pulmonary brush cell: a cell in search of a function. *American Journal of Respiratory and Critical Care Medicine*, 172(1), 136–139. doi:10.1164/rccm.200502-203WS
- Rhodin, J. (1966). The ciliated cell. Ultrastructure and function of the human tracheal mucosa. *The American Review of Respiratory Disease*, 93(3), Suppl: 1.
- Riordan, Rommens, J., Kerem, B., Alon, N., Rozmahel, R., Grzelczak, Z., et al. (1989). Identification of the cystic fibrosis gene: cloning and characterization of complementary DNA. *Science*, 245(4922), 1066–1073. doi:10.1126/science.2475911
- Roberts, R. B., & Rendell-Baker, L. (1972). Ethylene-Oxide Sterilization. *Hospital Topics*, 50(5), 60–60. doi:10.1080/00185868.1972.9947915
- Rossi, M., Lindken, R., Hierck, B. P., & Westerweel, J. (2009). Tapered microfluidic chip for the study of biochemical and mechanical response at subcellular level of endothelial cells to shear flow. *Lab on a Chip*, 9(10), 1403–1411. doi:10.1039/b822270n
- Rutland, J., Griffin, W. M., & Cole, P. J. (1982). Human ciliary beat frequency in epithelium from intrathoracic and extrathoracic airways. *The American Review of Respiratory Disease*, 125(1), 100–105.
- Sanderson, M. (1981). Ciliary activity of cultured rabbit tracheal epithelium: beat pattern and metachrony. *Journal of Cell Science*.
- Scotton, C. J. (2011). A breath of fresh air for tissue engineering? *Materials Today*, 14(5), 212–216. doi:10.1016/S1369-7021(11)70116-X
- Sears, P. R., Davis, C. W., Chua, M., & Sheehan, J. K. (2011). Mucociliary interactions and mucus dynamics in ciliated human bronchial epithelial cell cultures. *American Journal of Physiology- Lung Cellular and Molecular Physiology*, 301(2), 181–186. doi:10.1152/ajplung.00321.2010
- Shah, A. J., & Donovan, M. D. (2007). Rheological characterization of neutral and anionic polysaccharides with reduced mucociliary transport rates. *AAPS PharmSciTech*, 8(2), E40–E47. doi:10.1208/pt0802032
- Sheehan, J. K., Kirkham, S., Howard, M., Woodman, P., Kutay, S., Brazeau, C., et al. (2004). Identification of molecular intermediates in the assembly pathway of the MUC5AC mucin. *Journal of Biological Chemistry*, 279(15), 15698–15705.

doi:10.1074/jbc.M313241200

- Shields, A., Fiser, B., Evans, B., Falvo, M., Washburn, S., & Superfine, R. (2010). Biomimetic cilia arrays generate simultaneous pumping and mixing regimes. *Proceedings of the National Academy of Sciences*, *107*(36), 15670–15675.
- Shih, C. K., Litt, M., Khan, M. A., & Wolf, D. P. (1977). Effect of nondialyzable solids concentration and viscoelasticity on ciliary transport of tracheal mucus. *The American Review of Respiratory Disease*, *115*(6), 989–995.
- Sia, S., & Whitesides, G. (2003). Microfluidic devices fabricated in poly (dimethylsiloxane) for biological studies. *Electrophoresis*.
- Sisson, J., Stoner, J., & Ammons, B. (2003). All-digital image capture and whole-field analysis of ciliary beat frequency. *Journal of*
- Smith, D. J., Lubkin, D. J., Gaffney, E. A., & Blake, J. R. (2007). A viscoelastic traction layer model of muco-ciliary transport. *Bulletin of Mathematical Biology*, *69*(1), 289–327. doi:10.1007/s11538-005-9036-x
- Smith, J., Travis, S., & Greenberg, E. (1996). ScienceDirect.com - Cell - Cystic Fibrosis Airway Epithelia Fail to Kill Bacteria Because of Abnormal Airway Surface Fluid. *Cell*.
- Snyder, J. C., Reynolds, S. D., Hollingsworth, J. W., Li, Z., Kaminski, N., & Stripp, B. R. (2010). Clara Cells Attenuate the Inflammatory Response through Regulation of Macrophage Behavior. *American Journal of Respiratory Cell and Molecular Biology*, *42*(2), 161–171. doi:10.1165/rcmb.2008-0353OC
- Spungin, B., & Silberberg, A. (1984). Stimulation of mucus secretion, ciliary activity, and transport in frog palate epithelium. *American Journal of Physiology- Cell Physiology*, *247*(5), 299–308.
- Stonebraker, J. R., Wagner, D., Lefensty, R. W., Burns, K., Gendler, S. J., Bergelson, J. M., et al. (2004). Glycocalyx Restricts Adenoviral Vector Access to Apical Receptors Expressed on Respiratory Epithelium In Vitro and In Vivo: Role for Tethered Mucins as Barriers to Luminal Infection. *Journal of Virology*, *78*(24), 13755–13768. doi:10.1128/JVI.78.24.13755-13768.2004
- Suk, J., Pace, A., Cone, R., & Hanes, J. (2008). Addressing the PEG mucoadhesivity paradox to engineer nanoparticles that “slip” through the human mucus barrier. *Angewandte Chemie*
- Takadoun, J. (2010). *Materials and Surface Engineering in Tribology*. Wiley.
- Takizawa, T., & Thurlbeck, W. M. (1971). A comparative study of four methods of assessing the morphologic changes in chronic bronchitis. *The American Review of Respiratory Disease*, *103*(6), 774–783.
- Talbot, P., Shur, B. D., & Myles, D. G. (2003). Cell Adhesion and Fertilization: Steps in Oocyte Transport, Sperm-Zona Pellucida Interactions, and Sperm-Egg Fusion.
- Tarran, R., & Button, B. (2006). Regulation of normal and cystic fibrosis airway surface liquid volume by phasic shear stress. *Annu Rev Physiol*.
- Tarran, R., Button, B., Picher, M., Paradiso, A. M., Ribeiro, C. M., Lazarowski, E. R., et al. (2005). Normal and cystic fibrosis airway surface liquid homeostasis. The effects of phasic shear stress and viral infections. *Journal of Biological Chemistry*, *280*(42), 35751–35759. doi:10.1074/jbc.M505832200
- Tarran, R., Grubb, B. R., Parsons, D., Picher, M., Hirsh, A. J., Davis, C. W., & Boucher, R. C. (2001). The CF salt controversy: in vivo observations and

- therapeutic approaches. *Molecular Cell*, 8(1), 149–158.
- Thornton, D. J. (2004). From Mucins to Mucus: Toward a More Coherent Understanding of This Essential Barrier. *Proceedings of the American Thoracic Society*, 1(1), 54–61. doi:10.1513/pats.2306016
- Thornton, D. J., Rousseau, K., & McGuckin, M. A. (2008). Structure and Function of the Polymeric Mucins in Airways Mucus. *Annual Review of Physiology*, 70(1), 459–486. doi:10.1146/annurev.physiol.70.113006.100702
- Tos, M. (1966). *Development of the tracheal glands in man: Number, density, structure, shape, and distribution of mucous glands elucidated by quantitative studies of ... Scandinavica. v. 68. Supplementum*. Munksgaard.
- Varki, A. (1999). *Essentials of Glycobiology*, 653.
- Verdugo, P. (1991). Mucin Exocytosis.
- Vladar, E. K., Bayly, R. D., Sangoram, A. M., Scott, M. P., & Axelrod, J. D. (2012). Microtubules Enable the Planar Cell Polarity of Airway Cilia. *Current Biology*, 22(23), 2203–2212. doi:10.1016/j.cub.2012.09.046
- Voorhout, W. F., Weaver, T. E., Haagsman, H. P., Geuze, H. J., & Van Golde, L. M. (1993). Biosynthetic routing of pulmonary surfactant proteins in alveolar type II cells. *Microscopy Research and Technique*, 26(5), 366–373. doi:10.1002/jemt.1070260504
- Wanner, A., Salathe, M., & O'Riordan, T. G. (1996). Mucociliary clearance in the airways. *American Journal of Respiratory and Critical Care Medicine*, 154(6), 1868–1902.
- WEIBEL, E. R., & GOMEZ, D. M. (1962). Architecture of the human lung. Use of quantitative methods establishes fundamental relations between size and number of lung structures. *Science*, 137(3530), 577–585.
- Weibel, E., Gehr, P., Haies, D., & GIL, J. (1976). *Weibel: The cell population of the normal lung - Google Scholar*. Lung cells in
- Werner, M. E., Hwang, P., Huisman, F., Taborek, P., Yu, C. C., & Mitchell, B. J. (2011). Actin and microtubules drive differential aspects of planar cell polarity in multiciliated cells. *The Journal of Cell Biology*, 195(1), 19–26. doi:10.1083/jcb.201106110
- Whimster, W. (1986). Number and mean volume of individual submucous g... [Appl Pathol. 1986] - PubMed - NCBI. *Applied Pathology*.
- Whitcutt, M., Adler, K., & Wu, R. (1988). A biphasic chamber system for maintaining polarity of differentiation of culture respiratory tract epithelial cells. *In Vitro Cellular & Developmental Biology*-
- Widdicombe, J. H. (2002). Regulation of the depth and composition of airway surface liquid. *Journal of Anatomy*, 201(4), 313–318. doi:10.1046/j.1469-7580.2002.00098.x
- Widdicombe, J., Bastacky, S., & Wu, D. (1997). Regulation of depth and composition of airway surface liquid. *European Respiratory*
- Wilson, G. B., Jahn, T. L., & Fonseca, J. R. (1975). Studies on Ciliary Beating of Frog Pharyngeal Epithelium in vitro: I. Isolation and Ciliary Beat of Single Cells. *Transactions of the American Microscopical Society*, 94(1), 43. doi:10.2307/3225531
- Winters, S. L., Davis, C. W., & Boucher, R. C. (2007). Mechanosensitivity of mouse

- tracheal ciliary beat frequency: roles for Ca²⁺, purinergic signaling, tonicity, and viscosity. *American Journal of Physiology- Lung Cellular and Molecular Physiology*, 292(3), L614–L624. doi:10.1152/ajplung.00288.2005
- Yi, S. M., Harson, R. E., Zabner, J., & Welsh, M. J. (2001). Lectin binding and endocytosis at the apical surface of human airway epithelia. *Gene Therapy*, 8(24), 1826–1832. doi:10.1038/sj.gt.3301598
- Young, E., & Beebe, D. (2010). Fundamentals of microfluidic cell culture in controlled microenvironments. *Chemical Society Reviews*, 39(3), 1036–1048.